

# **3D MODELLING OF SHEET PILE CORNER IN DIFFICULT GROUND CONDITIONS**

**JOSÉ BENEDITO GONÇALVES ARÊDE CALEJO**

Dissertação submetida para satisfação parcial dos requisitos do grau de  
**MESTRE EM ENGENHARIA CIVIL — ESPECIALIZAÇÃO EM GEOTECNIA**

---

Orientador: Professor Doutor António Milton Topa Gomes

---

Coorientador: Professor Doutor Ole Hededal

JULHO DE 2015

## **MESTRADO INTEGRADO EM ENGENHARIA CIVIL 2014/2015**

DEPARTAMENTO DE ENGENHARIA CIVIL

Tel. +351-22-508 1901

Fax +351-22-508 1446

✉ [miec@fe.up.pt](mailto:miec@fe.up.pt)

*Editado por*

FACULDADE DE ENGENHARIA DA UNIVERSIDADE DO PORTO

Rua Dr. Roberto Frias

4200-465 PORTO

Portugal

Tel. +351-22-508 1400

Fax +351-22-508 1440

✉ [feup@fe.up.pt](mailto:feup@fe.up.pt)

🌐 <http://www.fe.up.pt>

Reproduções parciais deste documento serão autorizadas na condição que seja mencionado o Autor e feita referência a *Mestrado Integrado em Engenharia Civil - 2014/2015 - Departamento de Engenharia Civil, Faculdade de Engenharia da Universidade do Porto, Porto, Portugal, 2015.*

As opiniões e informações incluídas neste documento representam unicamente o ponto de vista do respetivo Autor, não podendo o Editor aceitar qualquer responsabilidade legal ou outra em relação a erros ou omissões que possam existir.

Este documento foi produzido a partir de versão eletrónica fornecida pelo respetivo Autor.

Aos meus pais, irmãs, amigos e avô

*Life is not the number of days you live, is the number of days you remember*

*Pasha*



## ACKNOWLEDGMENTS

This project is the climax of an unforgettable phase of my life that defined me as a civil engineer and as a citizen of the world. During the five years of my degree, and especially in the last 4 months, I had the support from many people, to whom I would like to express my gratitude:

- To my supervisor in Portugal, Professor António Topa Gomes, for all the recommendations, guidance, motivation and feedback;
- To my supervisor at COWI, Professor Ole Hededal, for the theoretical support, recommendations and especially for providing me this amazing opportunity of developing my thesis in such a recognized company;
- To all the staff of COWI, who provided me with the necessary knowledge to conclude my project successfully and also for the advice given to thrive in the engineering world;
- To António Fonseca, for the companionship and laugh in every day we spent together at COWI, and for all the critics, suggestions and discussion of the problems I was facing day by day;
- To Diana Abrunhosa, for being an awesome adventure partner, keeping me inspired and motivated to accomplish my objectives as an engineer and as a person;
- To my dearest friend João Nogueira, for being my University companion and, for sure, a friend for life;
- To all the people that shared with me these 5 years of knowledge gain, personal development and increase of life profit;
- To my parents and sisters, regardless of the continent they are, the support never fades.



## **ABSTRACT**

Anchored sheet piles are used as perimeter bunds for a reclamation area. Example of such use is the Värtahamnen Port, in Stockholm. In this case, soil conditions are relatively poor consisting of soft clay/sediments overlaying a thin layer of till and, under that, very competent bedrock. The soft sediments are improved by means of either lime-cement columns or rigid inclusions consisting of grout piles installed by high-pressure jetting.

A key element in the design is the corner layout where the sheet piles are mutually supporting each other by ties instead of anchor plates. The backfilling construction method, the complex ground conditions and the kinematics of the retaining system are difficult to analyse analytically or by simple design methods. Hence, a three dimensional finite element method model is developed using PLAXIS 3D to investigate the performance of the corner in terms of global deformations and stability, earth pressure distribution as well as forces in structural elements.

The author opted to focus on three scenarios related to different conditions of soil reinforcement (by jet grouting or lime-cement piles) to study changes in wall behaviour and global stability.

Results obtained are according to expected. The application of soil reinforcement reduces earth pressures acting on the wall. Moreover, soil reinforcement reduces maximum deformations of the retaining wall and maximum structural forces. Jet grouting reveals to be a conservative and necessary solution for the stability of the sheet pile wall. Also, a sensitivity analysis to evaluate the influence of surface roughness of the sheet pile wall is provided.

**KEYWORDS:** multi-anchored sheet pile wall, soil improvement, lime-cement piles, jet grouting, numerical analysis, finite element method, mutually supported corner, backfilling.



## RESUMO

Cortinas de estaca-prancha são usadas como paredes de retenção para efeitos de reclamação de terreno. Um caso tipo é o porto *Värtahamnen*, em Estocolmo. Nesta situação, as condições do solo são fracas consistindo numa camada de argila mole normalmente consolidada (sedimentos) sobre uma fina camada competente de *till* (depósitos glaciares), sob a qual está presente uma camada bastante competente de maciço rochoso. A camada de sedimentos é reforçada tanto por colunas de cal-cimento ou blocos rígidos constituídos por estacas instaladas via *jet grouting* a alta pressão.

Um elemento chave no dimensionamento é a forma do canto onde as cortinas de estaca-prancha se suportam mutuamente por tirantes em vez de ancoragens de placa. O método construtivo por enchimento, as complexas condições do solo e a cinemática do sistema de retenção tornam-se de difícil análise pela via analítica ou métodos simples de dimensionamento. Assim, na presente dissertação é desenvolvido um modelo tri-dimensional pelo método dos elementos finitos usando o PLAXIS 3D para investigar a performance do canto em termos de deformações e estabilidade global, distribuição de pressões de terras assim como os esforços nos elementos estruturais.

O autor optou por se focar em três cenários relacionados com diferentes condições de melhoramento do solo (*jet grouting* ou colunas de cal-cimento) de modo a estudar alterações no comportamento da estrutura e estabilidade global.

Os resultados obtidos são de acordo com esperado. A aplicação de técnicas de reforço do solo reduz as pressões de terra a atuar na cortina. Além disso, o solo reforçado reduz as deformações máximas da cortina e os máximos esforços na estrutura. A aplicação de *jet grouting* revelou ser uma solução conservadora e necessária para a estabilidade da cortina. Na presente tese é também apresentada uma análise de sensibilidade para avaliar a influência da rugosidade da cortina metálica.

**PALAVRAS-CHAVE:** cortinas estaca-prancha pluri-ancoradas, melhoramento de solo, colunas de cal-cimento, *Jet Grouting*, análise número, método elementos finitos, canto com suporte mútuo, enchimento.



## ABSTRAKT

Forankrede spunsvægge bliver ofte brugt som afgrænsning for en arealudnyttelse. Et eksempel på en sådan situation er Värtahamnen i Stockholm. I dette tilfælde er jordforholdene relativt dårlige, bestående af bløde sedimenter og ler, lejret på et tyndt lag af moræne ler, hvor under der er solidt fjeld. De bløde sedimenter er blevet forstærket enten gennem brugen af kalk-cement søjler eller injicering bestående af cementpæle installeret ved højtryksinjicering.

Et væsentligt element i designet er hjørnesamlingen, hvor spunsvæggene støtter hinanden gennem trækbjælker i stedet for ankerplader. Påfyldningsprocessen, de besværlige jord forhold og kinematikken i støttesystemet gør en analytisk analyse eller simpel design metode besværlig. Derfor er en tredimensionel finite element model udviklet i PLAXIS 3D til at undersøge opførslen i hjørnesamlingen i forhold til globale deformationer, stabilitet, jordtryksfordeling og kræfterne i strukturelle elementer.

Forfatteren har valgt at fokusere på tre scenarier relateret til forskellige jordforstærkningsforhold (trykcementering eller kalk-cement pæle) for at studere ændringerne i vægopførsel og den globale stabilitet.

De opnåede resultater er som forventede. Brugen af jordforstærkninger reducerer jordtrykket på væggen. Derudover reducerer jordforstærkninger de maksimale deformationer i støttevæggen samt de maksimale strukturelle kræfter. Trykcementering viser sig at være en konservativ og nødvendig løsning for stabiliteten i spunsvæggen. Desuden er en sensitivitets analyse til at vurdere indflydelsen af overfladerughed på spunsvæggene udført.

**NØGLEORD:** multipelt forankrede spunsvægge, jordforstærkning, kalk-cement søjler, trykcementering, numerisk analyse, finite element method, gensidigt støttet hjørne, fyld.



## TABLE OF CONTENTS

<b>ACKNOWLEDGEMENTS</b> .....	i
<b>ABSTRACT</b> .....	iii
<b>RESUMO</b> .....	v
<b>ABSTRAKT</b> .....	vii
<b>1. INTRODUCTION</b> .....	<b>1</b>
1.1. BACKGROUND .....	1
1.2. OBJECTIVES.....	2
1.3. STRUCTURE OF THESIS.....	2
<b>2. CASE STUDY: ANCHORED SHEET PILE CORNER</b> .....	<b>3</b>
2.1. INSPIRATION: STOCKHOLM PORT.....	3
2.1.1. PROJECT BACKGROUND .....	3
2.1.2. CONSTRUCTION PROCEDURE.....	4
2.1.3. BACKFILLED MUTUALLY SUPPORTED SHEET PILE CORNER .....	5
2.1.3.1. Corner Effects .....	7
2.1.3.2. Corner Tie Rods .....	9
2.1.3.3. Failure Mechanisms .....	11
2.1.3.4. Soil Reinforcement .....	11
<b>2.2. GROUND CONDITIONS</b> .....	<b>13</b>
2.2.1. CLAYEY SEABED.....	13
2.2.2. GLACIAL TILL.....	13
<b>2.3. BACKFILL CONDITIONS</b> .....	<b>14</b>
2.3.1. CONSIDERATIONS IN BACKFILLING .....	14
2.3.2. BACKFILL MATERIAL.....	14
<b>2.4. ELEMENTS OF ANCHORED SHEET PILE WALL</b> .....	<b>15</b>
2.4.1. SHEET PILE WALL.....	15
2.4.2. ANCHOR RODS.....	18
2.4.3. "DEADMAN" ANCHOR .....	19
2.4.4. WALING AND CAPPING BEAM .....	22
<b>2.5. SOIL IMPROVEMENT</b> .....	<b>22</b>
2.5.1. KC PILES.....	22

2.5.2. JET GROUTING PILES.....	25
<b>3. ANALYTICAL ANALYSIS .....</b>	<b>29</b>
3.1. INTRODUCTION TO ANALYTICAL ANALYSIS .....	29
3.2. TERZAGHI & PECK DIAGRAMS .....	29
3.3. EQUIVALENT TIE SUPPORT METHOD.....	30
3.3.1. CLASSICAL DESIGN METHODS .....	30
3.3.2. EQUIVALENT TIE SUPPORT METHOD PROCEDURES .....	31
3.4. SUB-GRADE REACTION METHOD.....	33
3.5. STABILITY ANALYSIS OF SHEET PILE WALL.....	34
3.5.1. LATERAL EARTH PRESSURES CALCULATION .....	34
3.5.2. SOIL CHARACTERISTICS .....	36
3.5.3. SHEET PILE WALL SYSTEM.....	38
3.5.3. ANALYSIS OF THE RESULTS .....	39
<b>4. THREE-DIMENSIONAL MODELLING IN PLAXIS 3D .....</b>	<b>45</b>
4.1. NUMERICAL ANALYSIS.....	45
4.1.1. 3D ANALYSIS .....	45
4.1.2. FINITE ELEMENT METHOD .....	46
4.1.3. PLAXIS 3D .....	46
4.2. INPUT INFORMATION.....	47
4.2.1. SOIL LAYERS.....	47
4.2.2. GEOMETRY .....	49
4.2.3. STUDY SCENARIOS .....	51
4.2.4. BOUNDARY CONDITIONS.....	54
4.2.5. SOIL MODELS AND PARAMETERS.....	56
4.2.6. STRUCTURES AND INTERFACES.....	58
4.2.7. LOADING AND STAGES OF CONSTRUCTION .....	60
<b>5. ANALYSIS OF RESULTS .....</b>	<b>63</b>
5.1. METHODOLOGY .....	63
5.1.1. CROSS SECTIONS.....	63
5.1.2. EXTRACTION OF EARTH PRESSURES .....	64
5.2. VERIFICATION OF THREE DIMENSIONAL EFFECTS .....	65
5.3. NO SOIL REINFORCEMENT (NR) .....	67
5.3.1. EARTH PRESSURES .....	67

5.3.2. WALL DEFORMATION MODE .....	71
5.3.3. DEFORMATION OF CORNER.....	74
5.3.4. STRUCTURAL FORCES.....	77
5.3.4.1 Anchors and Ties .....	77
5.3.4.2 Waling and Capping Beam .....	78
5.3.4.3 Sheet Pile Wall.....	80
<b>5.4. KC PILES (KC).....</b>	<b>83</b>
5.4.1. EARTH PRESSURE .....	83
5.4.1.1 Coefficient of Earth Pressure .....	83
5.4.1.2 Transfer of Loads through the Monolith.....	86
5.4.2. WALL DEFORMATION MODE .....	87
5.4.3. DEFORMATION OF CORNER.....	89
5.4.4. STRUCTURAL FORCES.....	91
5.4.4.1 Anchors and Ties .....	91
5.4.4.2 Waling and Capping Beam .....	91
5.4.4.3 Sheet Pile Wall.....	93
<b>5.5. KC PILES AND JET GROUTING (KC&amp;JG) .....</b>	<b>96</b>
5.5.1. EARTH PRESSURES .....	96
5.5.1.1. Coefficient of Earth Pressure .....	97
5.5.1.2. Transfer of Loads through the Monolith.....	98
5.5.2. WALL DEFORMATION MODE .....	99
5.5.3. DEFORMATION OF CORNER.....	101
5.5.4. STRUCTURAL FORCES.....	103
5.5.4.1 Anchors and Ties .....	103
5.5.4.2 Waling and Capping Beam .....	104
5.5.4.3 Sheet Pile Wall.....	106
<b>5.6. COMPARISON BETWEEN KC AND KC&amp;JG .....</b>	<b>107</b>
5.6.1. COEFFICIENT OF EARTH PRESSURE .....	107
5.6.2. WALL DEFORMATION MODE .....	109
5.6.3. STRUCTURAL FORCES.....	110
<b>5.7. SURFACE ROUGHNESS BETWEEN SHEET PILE WALL AND SOIL.....</b>	<b>112</b>
<b>6. CONCLUSIONS .....</b>	<b>115</b>
<b>6.1. CONCLUSIONS.....</b>	<b>115</b>

**6.2. SUGGESTIONS FOR FUTURE RESEARCH..... 117**

## TABLE OF FIGURES

Figure 2.1 - Värtahamnen port: a) Construction of pile deck (Stockholm Royal Seaport) and b) render of final shape of the port (Aarsleff 2014) .....	3
Figure 2.2 - Geometry of the port and phases of construction (Aarsleff 2014) .....	4
Figure 2.3 - Lifting of a gravity L-wall for positioning on-site .....	5
Figure 2.4 - Location of the corner in Värtahamnen Port (Aarsleff 2014) .....	5
Figure 2.5 - Plan of the Värtahamnen port with location of the corner (Aarsleff 2014).....	6
Figure 2.6 - 3D representation of the sheet pile corner: anchors, sheet pile wall (dark blue), gravity wall (dark grey), filling material (light blue) and soil reinforcement (grey).....	6
Figure 2.7 - Variation of PSR with distance from the corner and aspect of the site (Ou et al. 1996) .....	7
Figure 2.8 - Relation of vertical earth pressure with depth, revealing silo effect.....	9
Figure 2.9 - Detailed plan of sheet pile wall, anchors and corner tie rods (COWI 2015).....	9
Figure 2.10 - Example of double wall tie cofferdam (left) and cellular cofferdams (right) (C.J. Mahan)	10
Figure 2.11 - Scheme of the anchors in the corner .....	10
Figure 2.12 - Expected failure mechanisms in the corner: tilting around tip (left) and translation (right) .....	11
Figure 2.13 - Typical soil profile from Stockholm coastal area .....	12
Figure 2.14 - Disposal of the applied ground reinforcement .....	12
Figure 2.15 - Soil profile on-site with layers' thickness .....	13
Figure 2.16 - Samples of the <i>Sprängsten</i> material used as backfill.....	15
Figure 2.17 - Drainage system installed before applying top layer of filling material.....	15
Figure 2.18 - U (left) and Z (right) steel sheet pile sections and correspondent interlocks.....	16
Figure 2.19 - Hydraulic system used for pile driving pressing method (ThyssenKrupp 2010) .....	17
Figure 2.20 - Representations of impact (left) and vibration (right) pile driving methods (ThyssenKrupp 2010) .....	18
Figure 2.21 - Example of connections of the tie rods to the sheet pile wall: normal bolting with plate (left) and MACALLOY type rods (right) .....	19
Figure 2.22 - Example of different anchoring techniques (ThyssenKrupp 2010) .....	20
Figure 2.23 - Representation of a deadman anchor (side cut).....	20
Figure 2.24 - Admissible location of anchor blocks (ThyssenKrupp 2010) .....	21
Figure 2.25 - Admissible location of anchor blocks in cohesive soils (ThyssenKrupp 2010) .....	21
Figure 2.26 - Representation of waling beam (left) and concrete capping beam (right).....	22
Figure 2.27 - Execution of dry mixing lime, lime-cement or cement pile (Moseley & Kirsch 2004).....	23

Figure 2.28 - Representation of the failure modes assumed in a block of piles (Moseley & Kirsch 2004) .....23

Figure 2.29 - Example sheet pile wall with lime-cement piles used as soil reinforcement (Moseley & Kirsch 2004) .....24

Figure 2.30 - Steps of application of jet grouting (ArchiExpo).....25

Figure 2.31 - Three techniques of jet grouting: single, double (or twin) and triple. Top (Solentanche Bachy) and bottom (Moseley & Kirsch 2004) .....26

Figure 3.1 - Terzaghi and Peck Diagrams (Matos Fernandes 1990) .....30

Figure 3.2 - Free earth support method (Vieira & Matos Fernandes 2000) .....31

Figure 3.3 - Fixed earth support method (Vieira & Matos Fernandes 2000).....31

Figure 3.4 - Representation of ETM procedure (Carrubba & Colonna 2000) .....32

Figure 3.5 - Bilinear stress-displacement relationship (Carrubba & Colonna 2000) .....33

Figure 3.6 - Representation of wall deformations associated with active and passive limit states .....35

Figure 3.7 - Soil masses generating earth pressures on retaining wall.....36

Figure 3.8 - Sketch of the retaining wall system (left) and adopted representative structural model (right).....39

Figure 3.9 - Lateral earth pressures on the wall produced by the three scenarios .....40

Figure 3.10 - Bending moments (kN.m/m) on the wall for the three case scenarios: T&P,  $K_0$  and  $K_a$  (from left to right) .....41

Figure 3.11 - Shear forces (kN/m) on the wall for the three case scenarios: T&P,  $K_0$  and  $K_a$  (from left to right).....42

Figure 3.12 - Wall deformation (mm) for the three case scenarios: T&P,  $K_0$  and  $K_a$  (from left to right).43

Figure 4.1 - Plane Strain conditions.....45

Figure 4.2 - 10-node tetrahedral element used in PLAXIS 3D for soil discretisation (adapted from PLAXIS 2013a).....47

Figure 4.3 - 16-node element used for interfaces (left) and 6-node triangles used for plate elements (right) (adapted from PLAXIS 2013a) .....47

Figure 4.4 - Soil layers in three dimensional display using PLAXIS 3D.....48

Figure 4.5 - Borehole used to input soil layers in PLAXIS 3D (left) and soil-structure profile (right).....48

Figure 4.6 - Detailed drawing of wall 2, showing variation of till level.....49

Figure 4.7 - Plan of sheet pile wall and anchors distribution: upper level at -0.4m (left) and lower level at -9m (right) .....50

Figure 4.8 - Structural elements modelled in PLAXIS 3D: Sheet pile wall (blue), Gravity wall (grey), Waling (pink) and anchors (black), with highlighting of anchor on wall 2. ....50

Figure 4.9 - Scenario with no reinforcement: left - top view at depth -14m and right - general cross section.....51

Figure 4.10 - Scenario with KC Piles: left - top view at depth -14m and right - general cross section..52

Figure 4.11 - 3D representation of KC scenario, showing the KC Piles (brown).....	52
Figure 4.12 - Top view of the scenario with KC Piles with Jet Grouting reinforcement (KC&JG) at depth -14m and general cross section.....	53
Figure 4.13 - 3D representation of KC&JG scenario, showing the KC Piles (brown), jet grouting (dark grey) and spoil (light grey).....	54
Figure 4.14 - Horizontal plan describing the lengths of the model's borders .....	55
Figure 4.15 - Detail of the surface with fixed displacements in X- and Y-directions, simulating L gravity wall .....	55
Figure 4.16 - Diagram representative of perfectly elastic-plastic model (PLAXIS 2013b) .....	56
Figure 4.17 - Concept of dilation angle .....	57
Figure 4.18 - Critical State line .....	58
Figure 4.19 - Horizontal cross section of idealized sheet pile .....	60
Figure 4.20 - Loading phases 3 to 8 for the no reinforcement case (NR).....	62
Figure 5.1 - Location of selected cross sections .....	64
Figure 5.2 - Horizontal effective earth pressures extracted in three different locations: at the interface, at 0.05 m and at 0.5 m from the wall.....	65
Figure 5.4 - Wall deformation normalized to wall height, for NR (s/H).....	66
Figure 5.5 - Transverse displacement of capping beam (m).....	67
Figure 5.6 - Deformation of sheet pile wall in a 3D environment.....	67
Figure 5.7 - Effective vertical (left) and horizontal (right) earth pressures at CSB, PSD and "at rest" section, for NR .....	68
Figure 5.8 - Ratio of effective horizontal and vertical stresses at CSB and PSD .....	69
Figure 5.9 - Horizontal (Y-direction) earth pressures at -9 m .....	70
Figure 5.10 - Vertical effective stresses at depth -10m, revealing corner effect .....	70
Figure 5.11 - Effective Vertical Stresses at vertical sections L1 (25.5;19.5) and L2 (25.5;-5) .....	71
Figure 5.12 - Normalized wall deformation (s/H) at CSB along loading phases, in percentage of wall height.....	72
Figure 5.13 - Normalized wall deformation (s/H) at PSD along loading phases, in percentage of wall height.....	73
Figure 5.14 - Lateral displacement of wall in Y-direction at depths -0.4 m and -9 m.....	74
Figure 5.15 - Scheme of corner opening (left) and pulling of wall 2 (right) .....	74
Figure 5.16 - Wall displacement in Y-direction (Horizontal displacement).....	75
Figure 5.17 - Wall displacement in Z-direction (Vertical displacement) .....	75
Figure 5.18 - Displacement in Y-direction at CSC, showing outwards wall rotation.....	76
Figure 5.19 - Horizontal wall displacement at depth -0.4 m (left) and -9 m (right) .....	76

Figure 5.20 - Wall deformation at CSC, along loading phases .....77

Figure 5.21 - Axial forces (kN) in anchors and ties at upper (0.4 m) and lower (-9 m) levels.....78

Figure 5.22 - Axial force in waling at -9 m (kN) .....79

Figure 5.23 - Axial force in capping beam (kN).....79

Figure 5.24 - Bending moments in waling beam at -9m (kN.m).....80

Figure 5.25 - Bending moments in capping beam (kN.m) .....80

Figure 5.26 - Bending moment diagram at PSD, CSB and CSC (kN.m) .....81

Figure 5.27 - Vertical axial force in sheet pile wall (kN/m) .....82

Figure 5.28 - Vertical axial force in sheet pile wall at CSB (kN).....82

Figure 5.29 - Detail of the soil layer 1m thick, between sheet pile and monolith .....83

Figure 5.30 - Effective horizontal (left) and vertical (right) stresses at CSB and PSD.....84

Figure 5.31 - Coefficient of Reduction of lateral earth pressures .....85

Figure 5.32 - Effective vertical stresses in cross section at x=19.....86

Figure 5.33 - Effective vertical stresses at depth -11m, in a cross section at x=19 .....86

Figure 5.34 - Principal directions in a cross section at x=19.....87

Figure 5.35 - Normalized wall deformation (s/H) at CSB along loading phase for KC, in percentage of wall height .....88

Figure 5.36 - Lateral displacement of wall in Y-direction at depth -0.4 m and -9 m, for KC .....88

Figure 5.37 - Wall displacement in Y-direction (Horizontal displacement) for KC.....89

Figure 5.38 - Wall displacement in Z-direction (Vertical displacement) for KC.....89

Figure 5.39 - Horizontal wall displacement at depth -0.4 m (left) and -9 m (right) for KC.....90

Figure 5.40 - Normalized wall deformation (s/H) at CSC along loading phases for KC, in percentage of wall height .....90

Figure 5.41 - Axial forces in anchors and ties at upper (-0.4 m) and lower (-9 m) levels, for KC (kN) ..91

Figure 5.42 - Axial force in waling at -9m, for KC (kN) .....92

Figure 5.43 - Axial force in capping beam, for KC (kN) .....92

Figure 5.44 - Bending moments in waling beam at -9 m (kN.m).....93

Figure 5.45 - Bending moments in capping beam (kN.m) .....93

Figure 5.46 - Bending moment diagram at CSB and CSC, for KC (kN.m) .....94

Figure 5.47 - Effective horizontal stresses in front and back of the sheet pile wall (kPa).....95

Figure 5.48 - Vertical axial force in sheet pile wall at CSB, for KC (kN) .....95

Figure 5.49 - Effective horizontal (left) and vertical (right) stresses at CSB and PSD, for KC&JG .....96

Figure 5.50 - Coefficient of lateral earth pressures .....97

Figure 5.51 - Effective vertical stresses in cross section at x=19 m.....98

Figure 5.52 - Principal directions in a cross section at $x=19$ m .....	98
Figure 5.53 - Displacement in Y-direction of monolith composed by Jet grouting and KC Piles .....	99
Figure 5.54 - Normalized wall deformation ( $s/H$ ) at CSB along loading phases for KC&JG, in percentage of wall height .....	100
Figure 5.55 - Lateral displacement of wall in Y-direction at depth -0.4 m and -9 m .....	100
Figure 5.56 - Wall displacement in Y-direction (Horizontal displacement), for KC&JG .....	101
Figure 5.57 - Wall displacement in Z-direction (Vertical displacement), for KC&JG .....	101
Figure 5.58 - Horizontal wall displacement at depth -0.4 m (left) and -9 m (right), for KC&JG .....	102
Figure 5.59 - Normalized wall deformation ( $s/H$ ) at CSC along loading phases for KC&JG, in percentage of wall height .....	102
Figure 5.60 - Axial forces in anchors and ties at upper (-0.4 m) and lower (-9 m) levels, for KC&JG (kN) .....	103
Figure 5.61 - Axial force in waling at -9m, for KC&JG (kN).....	104
Figure 5.62 - Axial force in capping beam, for KC&JG (kN).....	104
Figure 5.63 - Bending moments in waling beam at -9 m (kN.m) .....	105
Figure 5.64 - Bending moments in capping beam (kN.m).....	105
Figure 5.65 - Bending moment diagram at CSB and CSC, for KC&JG (kN.m).....	106
Figure 5.66 - Vertical axial force in sheet pile wall at CSB, for KC&JG (kN).....	107
Figure 5.67 - Coefficient of reduction of lateral earth pressures at CSB, for KC and KC&JG.....	108
Figure 5.68 - Normalized wall deformation ( $s/H$ ) at CSB in last loading phase for KC and KC&JG, in percentage of wall height .....	109
Figure 5.69 - Lateral displacement of wall in Y-direction at depths -0.4 m and -9 m for KC and KC&JG .....	110
Figure 5.70 - Axial forces in anchors and ties at upper (-0.4 m) and lower (-9 m) levels, for KC and KC&JG .....	110
Figure 5.71 - Bending moment diagram at CSB for KC and KC&JG (kN.m) .....	111
Figure 5.72 - Normalized wall deformation ( $s/H$ ) at CSB in last loading phase for surface roughness 0.3, 0.5 and 2/3, in percentage of wall height.....	113
Figure 5.73 - Bending moment at CSB for surface roughness 0.3, 0.5 and 2/3 (kN.m) .....	113
Figure 5.74 - Vertical axial force in sheet pile wall at CSB for surface roughness 0.3, 0.5 and 2/3 (kN) .....	114



**TABLE OF TABLES**

Table 3.1 - Soil parameters used for lateral earth pressure calculation .....	37
Table 3.2 - Properties of structural elements.....	38
Table 3.3 - Reaction forces for the three case scenarios.....	42
Table 4.1 - Input soil parameters used initially in the model .....	57
Table 4.2 - Input undrained soil parameters.....	57
Table 4.3 - Description of structural elements used <i>in situ</i> .....	59
Table 4.4 - Input structural element parameters used in the model .....	59
Table 4.5 - Adapted input parameters for sheet pile.....	59
Table 4.6 - Description of phases of construction for each study scenario.....	61
Table 5.1 - Three cases (NR, KC and KC&JG) analysed with PLAXIS 3D.....	63
Table 5.2 - Comparative cases KC and KC&JG.....	107
Table 5.3 - Surface roughness chosen for the sensitivity analysis.....	112



## SYMBOLS, ACRONYMS AND ABBREVIATIONS

- $E$  - elastic modulus [kPa]
- KC Piles - lime-cement piles
- PSR - plane strain ratio
- T&P - Terzaghi and Peck
- ETM - equivalent tie support method
- $R_d$  - passive resistant force (kN)
- $R_i$  - equivalent force in step  $i$  (kN)
- $x_i$  - distance of equivalent force in step  $i$  (m)
- $T_i$  - force in anchor  $i$  (kN)
- $y_i$  - distance from the top of the wall to the anchor  $i$  (m)
- SRM - sub-grade reaction method
- $J$  - moment of inertia
- $K_h$  - horizontal sub-grade reaction modulus
- $w$  - horizontal wall displacement (m)
- $z$  - depth (m)
- $k$  - spring stiffness in SRM; anchor axial stiffness (kN/m)
- $a$  - non-dimensional coefficient
- $L$  - length (m)
- $A$  - area (m<sup>2</sup>)
- $F_d$  - driving force (kN)
- $m_u$  - mass weight (kg)
- $r_u$  - distance to point of rotation (m)
- $\Omega$  - frequency of excitation
- $D$  - diameter (m)
- $\sigma_z$  - vertical earth pressure (kPa)
- $K, K_0$  - at-rest earth pressure coefficient
- $K_a$  - active earth pressure coefficient
- $K_p$  - passive earth pressure coefficient
- $\varphi'$  - friction angle (°)
- $\delta$  - wall roughness
- $\beta$  - sloping of ground surface (°)

$\alpha$  - inclination of retaining wall ( $^{\circ}$ )

NR - no reinforcement scenario

KC - soil reinforcement with lime-cement piles scenario

KC&JG - soil reinforcement with lime-cement piles and jet grouting scenario

PSD - plane strain deformation cross section

CSB - cross section B

CSC - cross section C

CSD - cross section D

$\psi$  - dilation angle ( $^{\circ}$ )

$\Psi$  - dilation

$c'$  - cohesion (kPa)

$c_u$  - undrained shear strength (kPa)

$\gamma$  - unit weight ( $\text{kN/m}^3$ )

$\nu$  - *Poisson* ratio

MC - Mohr-Coulomb

$E_{oed}$  - oedometric modulus (kPa)

$E_{50}$  - modulus of deformability (kPa)

$R_{inter}$  - reduction of strength at the interface

$I_2, I_3$  - inertia ( $\text{m}^4$ )

# 1

## INTRODUCTION

### 1.1. BACKGROUND

With the growing of world population and consequent urban area, the need for more construction area has increased and is demanding for wiser and more innovative engineering solutions. In many coastal structures, such as ports and quays, the reclamation of sea area is one solution to be taken when the construction or expansion is necessary in order to avoid usage of valuable inland area. The main idea when doing such claims is to create a boundary structure that will be able to retain fill material, on which the desired construction may settle and have its foundations with the required level of safety.

At present time, among the available solutions in the market, the usage of steel sheet pile walls is a widespread used solution in marine and coastal constructions, especially as quay walls (Osório et al., 2010). This is mainly due to the fact that sheet pile walls are easily installed within short time, can produce a watertight wall (Eskandari & Kalantari, 2011) and the environmental impacts are minimum (Arcelor Mittal, 2014).

Although retaining walls are used frequently on excavations and thus their design approaches and methods are deeply studied, its behaviour in backfill construction is still not as much understood and predictable (Bilgin, 2010). Actually, the current design procedures used in sheet pile walls are based on limit equilibrium approaches that make use of active and passive earth pressures, related to the Mohr-Coulomb failure criterion. However, these do not take into account the construction procedures which may cause different loading conditions in the soil and consequently dissimilar behaviour of the structure. This way, conventional assumptions and tools, such as the Rowe moment reduction curves used to calculate design moment, might not be valid in backfilling conditions since they are based on tests simulating walls in excavation conditions (Bilgin, 2010) (Rowe, 1952).

Furthermore, specific details in steel sheet pile walls, such as waling system and self supporting walls in corners are highly influenced by three-dimensional effects, which are not taken into account in simple two dimension plain strain analysis.

Therefore, the existence of practical situations where backfilled sheet pile wall corners were built on difficult ground conditions impelled the necessity for a further study on the behaviour of these structures on a third dimension environment using numerical methods, such as the finite element method utilized in PLAXIS 3D.

## **1.2. OBJECTIVES**

The main objectives of this Master Thesis are modelling the corner of a backfilled sheet pile wall built in soil with poor conditions and studying its behaviour and deformation modes. Also, soil improvement techniques, such as KC Piles and Jet Grouting are modelled and compared.

All three dimensional analysis are done using the finite element program PLAXIS 3D and compared with reference plane strain sections.

The model is built in similarity to a case study suggested by COWI, company with which the author collaborated to develop this thesis.

## **1.3. STRUCTURE OF THESIS**

This thesis is structured in six main chapters.

Chapter one is the introduction where a background on usage and design of sheet pile walls is presented. Also, the main objectives and structures of the thesis are detailed.

The second chapter introduces the case study that basis the built model, describing construction details and ground conditions.

The following chapter presents a simple analytical analysis that will serve as comparison basis to the numerical results. Also, typical design methods of multi-supported walls are explained.

The fourth chapter contains an introduction to finite element method and relevant information regarding the modellation of the problem in PLAXIS 3D.

The fifth chapter includes observations, analysis and comparison of the results provided by PLAXIS 3D, regarding all considered scenarios. Besides it contains a sensitivity analysis.

The last chapter provides a conclusion of the obtained results, as well as recommendations for future research.

## 2

## CASE STUDY: ANCHORED SHEET PILE CORNER

### 2.1. INSPIRATION: STOCKHOLM PORT

#### 2.1.1. PROJECT BACKGROUND

Stockholm is the Swedish capital and is located in the coastal area bordered by the Baltic Sea. It is a city spread over twenty islands and is expected to have over one million inhabitants in 2022 (Stadsledningskontoret 2013). The fact that Stockholm is a city naturally surrounded by water and centrally located in the expanding Baltic Sea impels it to become the leading port city the region. In the past 2 years, it has been noticed that more shipping lines are choosing Stockholm as a cruise destination, shown by the increase of sixty-one per cent in the number of cruise ships arriving in this city. To respond to these figures, the city of Stockholm created a project of urban development in the Stockholm Royal Seaport area, where the renovation of old ports is planned (Stockholm Royal Seaport).

As part of the Stockholm Royal Seaport project, Värtahamnen, one of the main Stockholm ports, will be subject of expansion and renovation (Figure 2.1). At the moment, approximately 3.9 million passengers travel through the Värtahamnen, making it the port with higher amount of movement among all Stockholm's ports.

The expanded port is expected to have five quay-berths, a new passenger terminal and infrastructure developments. The construction is scheduled to end in 2016 and will have a calculated cost of 2.8 thousand Swedish kroner.

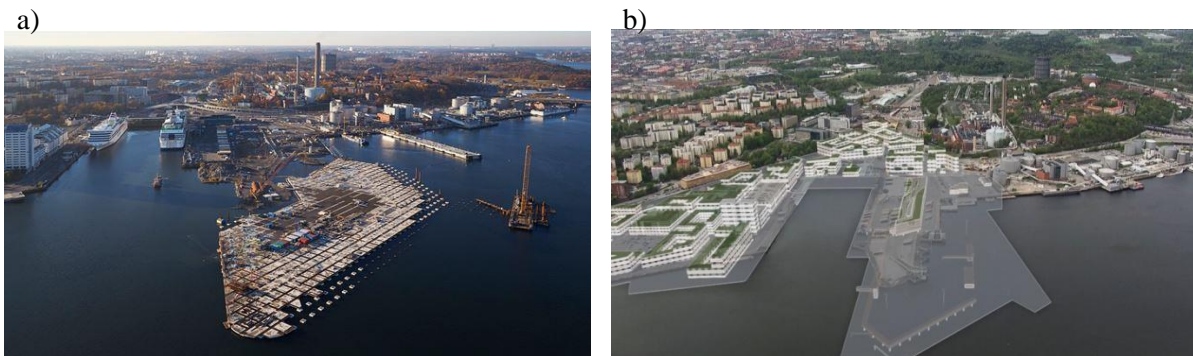


Figure 2.1 - Värtahamnen port: a) Construction of pile deck (Stockholm Royal Seaport) and b) render of final shape of the port (Aarsleff 2014)

### 2.1.2. CONSTRUCTION PROCEDURE

The extension of Värtahamnen port will consist of two main construction methods: 65,000 m<sup>2</sup> of pile decking and 20,000 m<sup>2</sup> of landfill. The pile deck is composed by a total of 1012 piles, 934 driven and 111 drilled, capped on top by a concrete slab.

Figure 2.2 shows the location of the two principal construction phases, which are expected to last 46 months, and the position where sheet pile walls and gravity L walls were initially planned to be placed. In the first phase of construction, the concrete piles are driven and cast in site, over which a prefabricated concrete capping is applied. At the same time, steel sheet pile walls and gravity walls are placed and stabilized. Following this stage, the final backfilling process will take place by placing frictional material in the bounded area, sustained by the retaining structures.

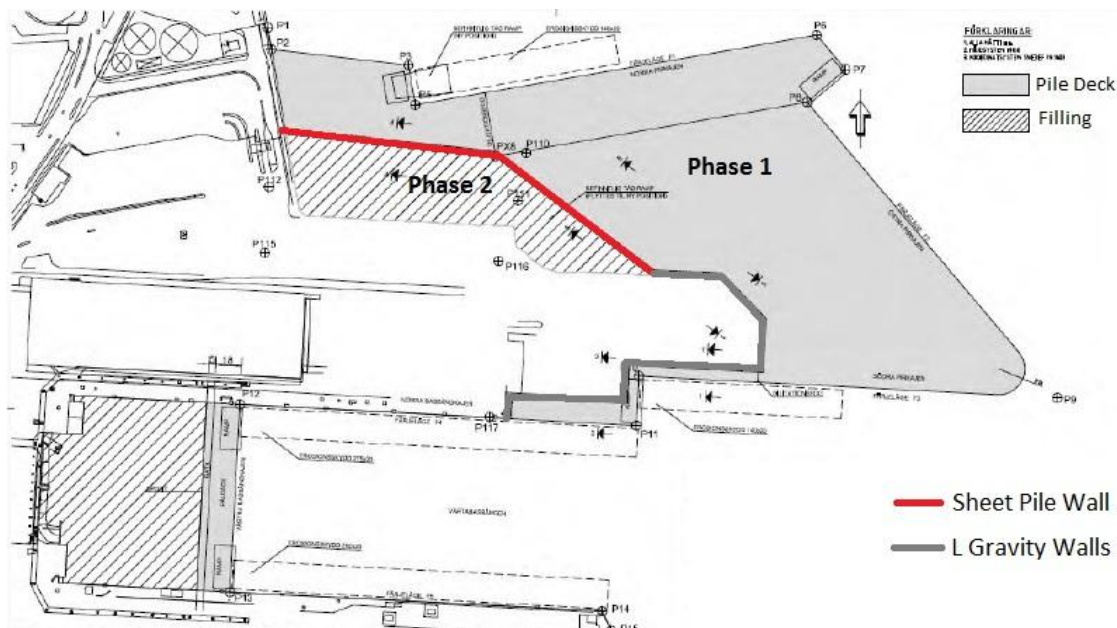


Figure 2.2 - Geometry of the port and phases of construction (Aarsleff 2014)

The landfill area provides the transition from the pile deck to the old port structure. It is a backfilled retaining structure constituted by gravity L walls (Figure 2.3) and steel sheet pile walls. The gravity walls are installed over a gravel bed and the sheet pile walls embedded in the ground. Both these elements are stabilized with anchors.

As the ground conditions revealed to be poor in some areas, it was necessary to reinforce the soil in the back of sheet pile walls. Therefore, the designer decided to implement dry mixed lime-cement piles, also called in Sweden as *KalkCementPelare* and in this work named KC Piles, as well as Jet Grouting in critical zones.



Figure 2.3 - Lifting of a gravity L-wall for positioning on-site

### 2.1.3. BACKFILLED MUTUALLY SUPPORTED SHEET PILE CORNER

The Värtahamnen project was chosen as a practical and existent example of a situation where there is a steel sheet pile wall with a mutually supported corner under backfill conditions. These cases are prompt to be cause of mistrust when going through the design process, possibly leading to over calculated structures with high costs. Such concerns arise from the fact that a simple two dimensional analysis might not be sufficient to fully understand the corner behaviour, to describe the deformation and failure mode, as well as the influence of soil improvement.

In Figure 2.4 and Figure 2.5 is detailed the location of the corner that is scope of study throughout the current thesis. Comparing with initial drawings outlined in Figure 2.2, this layout shows a different shape. In fact, after closer observation of the ground conditions on-site, some boulders with great dimensions were found on the seabed where the sheet piles should be placed, thus hampering the process of driving sheet piles. So, the solution was to drive the sheet piles around the area containing such blocks, resulting in the final corner layout in Figure 2.5.

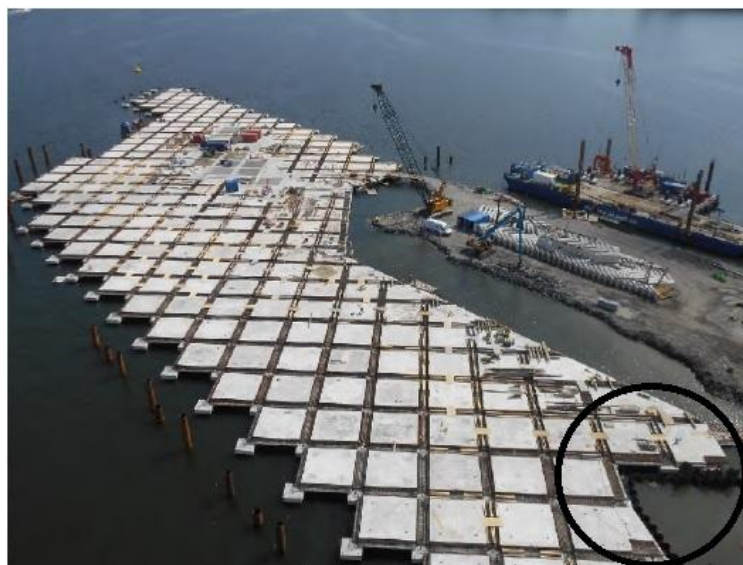


Figure 2.4 - Location of the corner in Värtahamnen Port (Aarsleff 2014)

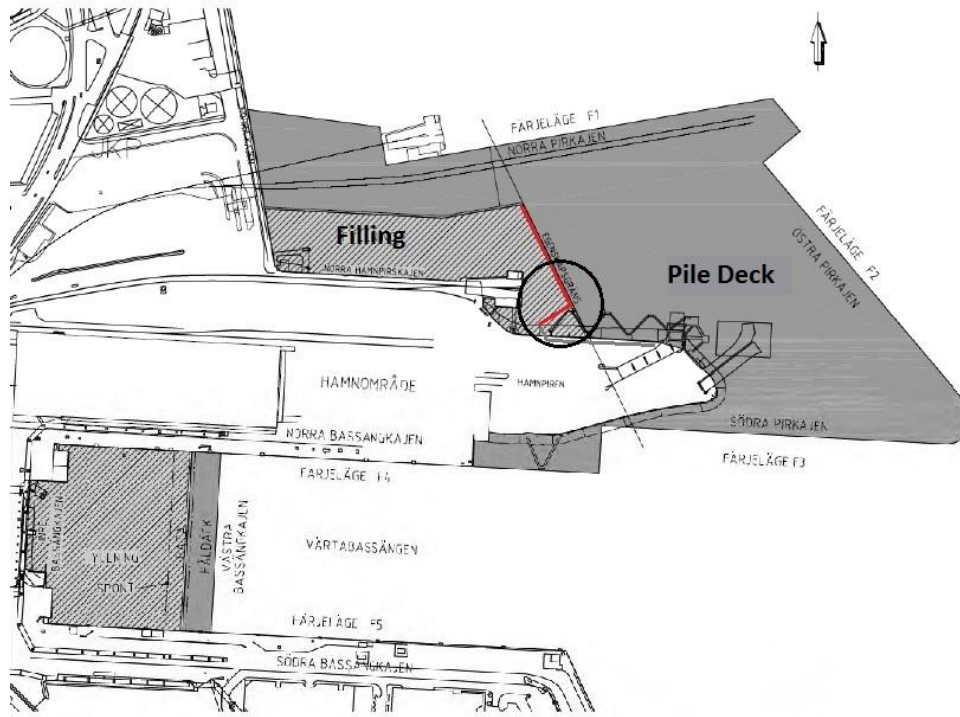


Figure 2.5 - Plan of the Värtahamnen port with location of the corner (Aarsleff 2014)

The corner is constituted by one main wall and a perpendicular smaller wall. The main wall develops parallel to the adjacent pile deck and is supported by two levels of anchors. On the other hand, the smaller wall is connected with tie rods to the main wall, supported in the top corner by an anchor and laterally prevented by neighbouring gravity L wall. Figure 2.6 shows a three dimensional model of the structure for better understanding the previous description. It is clear where the filling material (light blue) is deployed, the location of anchors, the layout of sheet pile wall (dark blue) and the gravity wall (grey).

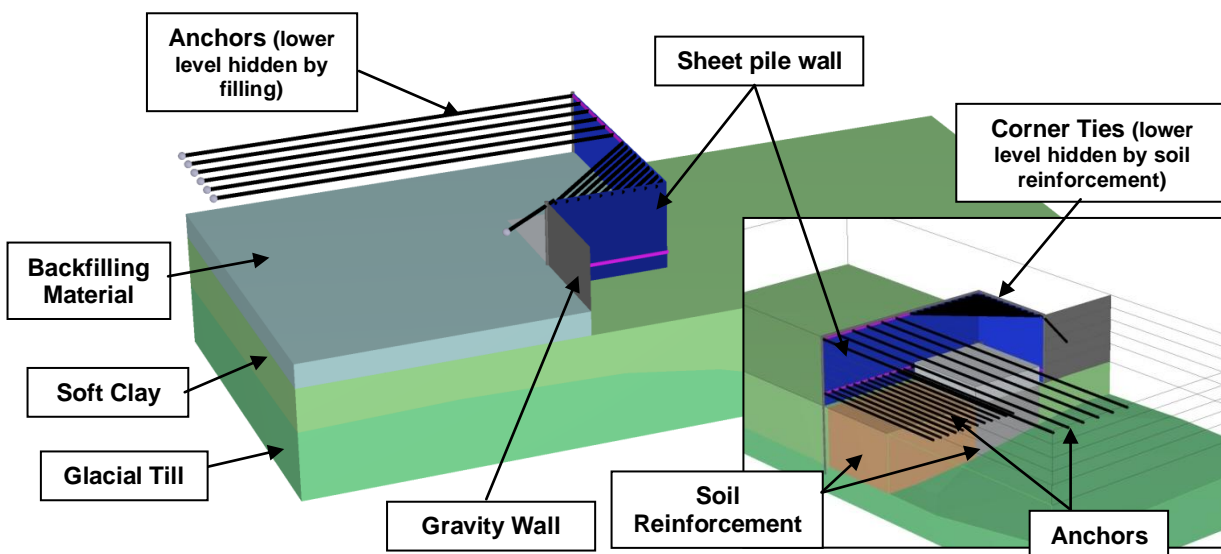


Figure 2.6 - 3D representation of the sheet pile corner: anchors, sheet pile wall (dark blue), gravity wall (dark grey), filling material (light blue) and soil reinforcement (grey)

The description of the entire system and adopted structural model are explained in detail in the following chapters, depending on the type of analysis (analytical or numerical).

Following, is presented a description of the particular aspects that make this special case an important subject of study, as well as some considerations that should be necessary to take into account when analysing and studying the present situation.

#### 2.1.3.1. Corner Effects

In excavations where corners exist it has been verified the occurrence of a phenomenon characterized by the restriction of wall deflection, which is here named as corner stiffening effect. In some situations, this corner effect has such influence on the behaviour of the retaining wall that can be taken into account to, for example, reduce costs in ground improvement (Ou et al. 2008).

The corner stiffening effect is normally observed in the displacement at the centre of retaining walls far from the corners, where the movement is generally higher than the values observed in areas near the corner. Furthermore, calculated values using plane strain analysis result in much higher deformations than the observed in construction sites at the central section of the retaining wall (Lee et al. 1998). This fact, among others, lead to increasing research by many authors in order to obtain a relationship between the wall displacement and the plain strain analysis calculated displacement. One of the parameters used to develop such studies is the plain strain ratio (PSR), which relates the maximum displacement of a wall in a certain section with the maximum displacement of the same cross section calculated using plain strain analysis. The PSR varies between zero and the unity, when the section in study is in a plain strain condition. Ou et al. (1996) developed a relationship between the PSR and the shape of excavation area, as well as with distance to corners for specific cases, described in Figure 2.7.

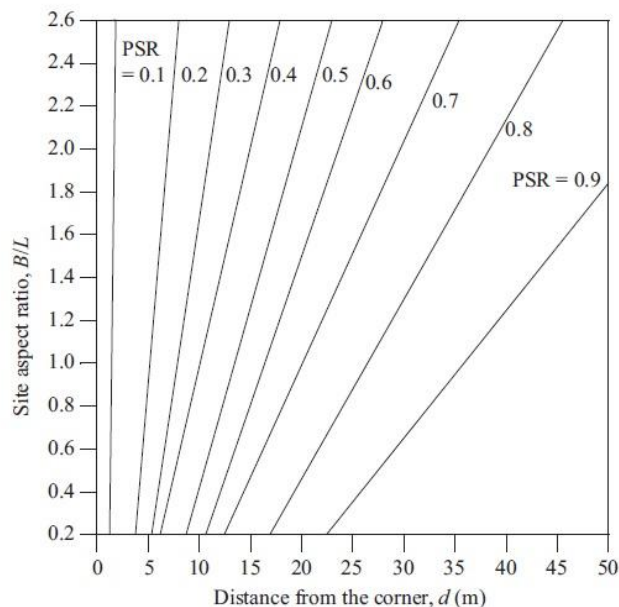


Figure 2.7 - Variation of PSR with distance from the corner and aspect of the site (Ou et al. 1996)

As the referred stiffening effect is very sensible to different parameters, such as stiffness of strutting system, depth of excavation, location of rigid layer and even by the horizontal geometry of the

excavation, it is not clearly evaluated using only two dimensional plain strain analysis. In fact, it has been verified by many authors that in excavation pits with corners the displacements in centre of excavation walls have higher values when calculated by plane strain finite element analysis than in three dimensional finite element analysis (Ou et al. 2008), (Finno et al. 2007).

The case study in the present thesis, a sheet pile corner under backfilling conditions, is a typical situation that had not been thoroughly studied before and a small amount of information is available on the literature. Therefore, the previously described corner effect might not be the same for excavation and backfill type of loadings on retaining walls, which adds up to the difficulties in predicting the behaviour of the structure.

Another possible consequence due to the existence of corners in the sheet pile system may be a similar effect to the known *silo effect*. This effect was described by Janssen in 1895 as a reduction of the earth pressure in the bottom of silos. Basically, in the top of the silos the vertical earth pressure develops similarly to the typical triangular distribution from Rankine's formulation, but tends to an asymptotic limit as it becomes deeper. Using the shear plane method, it is possible to analytically verify this fact, by simply calculating the static equilibrium of an infinitesimal horizontal layer, taking into account the weight of the soil mass and upwards friction from walls surface resultant of horizontal earth pressure (Widisinghe & Sivakugan 2012). According to the later confirmed Jáky's assumption (Pipatpongsa & Heng 2010), it is plausible to admit *at rest* pressure conditions and, therefore,  $K_0$  as the coefficient of earth pressure at rest using the horizontal and vertical stresses at centre of the section. By solving the static equilibrium, one obtains a function of vertical stress with the depth in equation (2.1), where  $D$  is the silo diameter,  $K$  the coefficient of earth pressure at rest,  $\gamma$  the soil weight and  $\delta$  the surface roughness.

$$\sigma_z = \frac{\gamma D}{4K \cdot \tan \delta} \left[ 1 - \exp\left(-\frac{4K \cdot \tan \delta \cdot z}{D}\right) \right] \quad (2.1)$$

Plotting the equation (2.1) with the depth  $z$ , obtains the diagram in Figure 2.8. The parameters used were 2 m as the diameter  $D$ , unit weight  $\gamma$  of 21 kN/m<sup>3</sup>. The surface roughness angle  $\delta$  corresponds to 2/3 of the friction angle, which was 40°. Earth pressure coefficient  $K$  was calculated using Jáky's formula and is dependent on the friction angle. The resultant graph clearly shows the asymptotic tendency of vertical stress as the depth increases. It is interesting to also note that the initial inclination is close to the unit weight of the soil, which indicates that close to the surface the arching effect and consequent silo effect is practically none.

The similarity of the silo shape to the corner shape makes it possible to assume that an analogous effect may occur.

Taking this fact into account, it is possible to expect some influence of the corner in the behaviour of the fill material, resulting in possible reduced earth pressures and increased vertical stresses in the sheet pile wall, among other consequences of this effect.

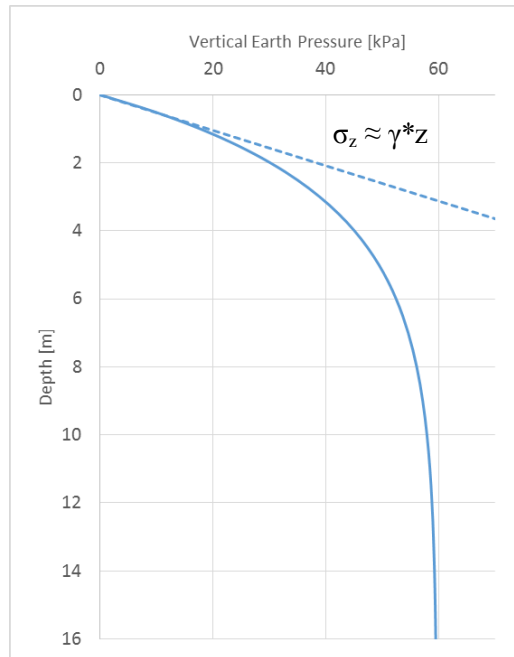


Figure 2.8 - Relation of vertical earth pressure with depth, revealing silo effect

### 2.1.3.2. Corner Tie Rods

Figure 2.9 shows a plan of the sheet pile wall and placement of anchors rods. On the right side, close to the corner, the walls are mutually supported by a group of 10 tie rods. These structural elements were used instead of anchors due to the difficulties that would be found in placing the anchor blocks of the smaller wall.

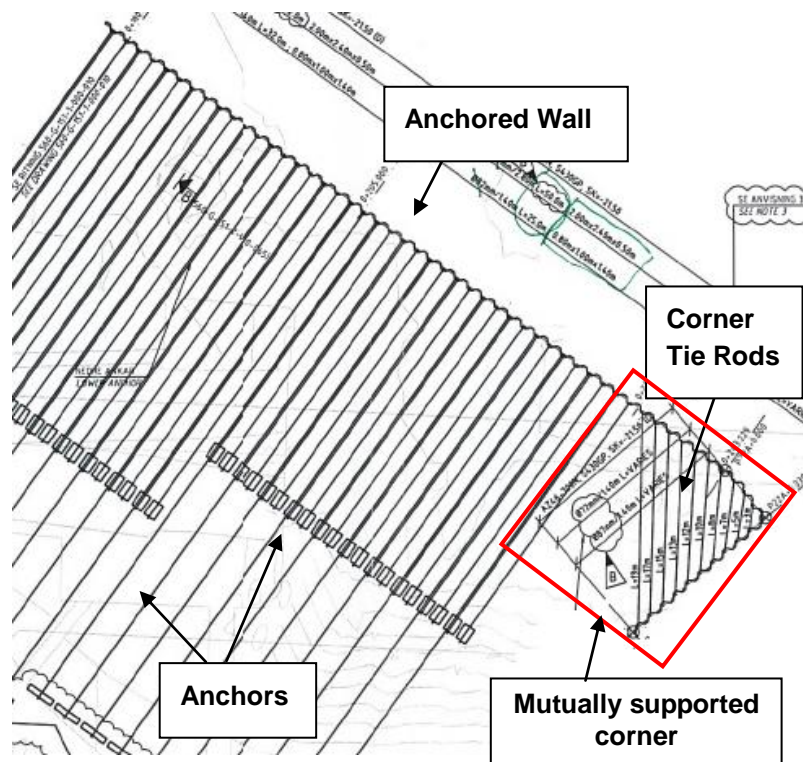


Figure 2.9 - Detailed plan of sheet pile wall, anchors and corner tie rods (COWI 2015)

In the back side of the wall, where the anchor blocks are located, the fill material will be placed. When the backfill material pushes the wall system outwards it is expected that in the mutually supported corner the group of tie rods work in tension as a response to the tendency of corner opening, resultant from the pushing of both walls. It is an intuitive prediction, but still the behaviour and distribution of stresses in these structures under such conditions is not totally known and predictable.

In fact, this situation has some similarities with double wall tied cofferdams, which are commonly used for waterfront structures and excavation enclosures (Figure 2.10). These structures consist in two parallel steel sheet pile walls connected by ties, creating a space in between that is filled with granular material, such as sand, gravel or even rock (Gui & Han 2009). Therefore, it is possible to admit that in both cases the wall, and consequently the tie rods are under the same backfill kind of loading.



Figure 2.10 - Example of double wall tie cofferdam (left) and cellular cofferdams (right) (C.J. Mahan)

However, in cofferdams the design is simply done by admitting a plane strain deformation analysis and calculation. In the assumed case of study this may not be correct and possibly is too conservative. Actually, the tie rods stiffness varies along the wall, due to different lengths, as represented in Figure 2.11. As the ties are connected to both walls, it appears to be difficult to calculate the correct stiffness to use in plane strain calculations.

In reality, the most common situation where a similar corner tie rod disposition is used is on cellular cofferdams, normally utilized to retain water and soil out of the excavation pit. Though, these are subjected to external earth pressure, and not to internal backfill pressure.

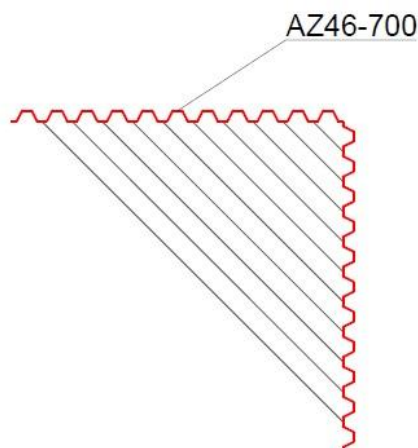


Figure 2.11 - Scheme of the anchors in the corner

### 2.1.3.3. Failure Mechanisms

As there is not enough knowledge on the behaviour of this specific structure, two main failure mechanisms were thought *a priori* when approaching any design of this detail. Translation of wall system and tilt around the longer wall are assumed to occur in the retaining system in the corner, as represented in Figure 2.12, and both are probable to occur simultaneously.

The translation of the corner is expected to occur in the direction perpendicular to the main long wall, named here as wall 1, and may be accompanied by a circular failure of the soil mass in front of the wall. Therefore, the stability is assumed to be assured by the passive resistance of the soil in front of wall 1 and by the anchor system.

The rotation of the structure occurs along the base of wall 1, pushing this wall outwards and the smaller wall, referred as wall 2, upwards. To assure the stability of the corner against rotation, it is thought to make use of the friction with the soil in the back of the wall 2, an anchor in the top of the same wall and passive resistance of soil in front of wall 1,

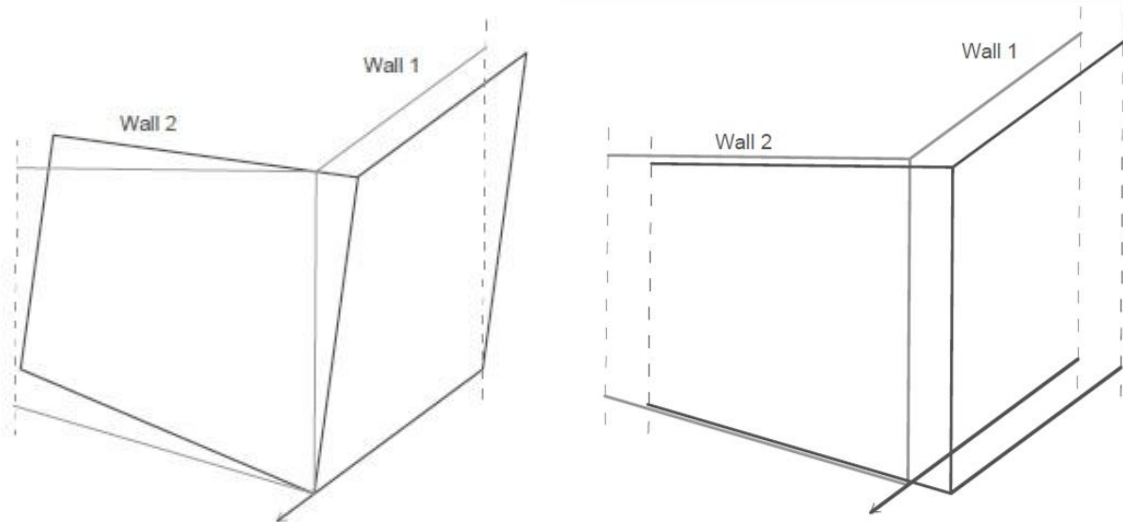


Figure 2.12 - Expected failure mechanisms in the corner: tilting around tip (left) and translation (right)

### 2.1.3.4. Soil Reinforcement

The ground in the construction area is mainly composed by a thick layer of soft sediment clay on top of glacial till and bedrock. This is the typical soil profile of the marine soil found in Scandinavia, detailed in Figure 2.13. The layer of till and bedrock prove normally to be competent structures capable of bearing high loads. However, the same cannot be said to the soft marine clay. In fact, the clay material in the region is resultant from the deposition of sediments that have been carried by the network of rivers that shore Stockholm. As the river flow keeps raking the seabed along the time, the clay does not suffer much consolidation. Therefore, it shows low strength parameters that rise up many concerns when building in such conditions.

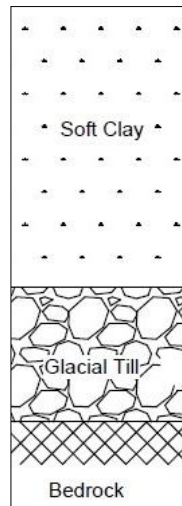


Figure 2.13 - Typical soil profile from Stockholm coastal area

When such soil conditions are present on site and it is necessary to achieve the required level of strength, techniques of soil reinforcement ought to be used.

Therefore, lime-cement piles (KC Piles) were applied to the clay seabed using a deep-mixing method all along the back of the sheet pile wall and jet grouting columns done in the critical areas next to the corner, as idealized in Figure 2.14.

It is possible that this improved ground would behave similarly to a monolith, especially in the corner, where a concrete block is likely to be created. This way, the reinforced soil would transmit earth pressures directly to bearing stratum, in this case the glacial till. However, the reduction in earth pressure is not certain, as the behaviour of the KC Piles and jet grouting is not surely known. It should be examined if there is any shear deformation that may induce earth pressures into the sheet pile wall and what is the failure mode of these systems.

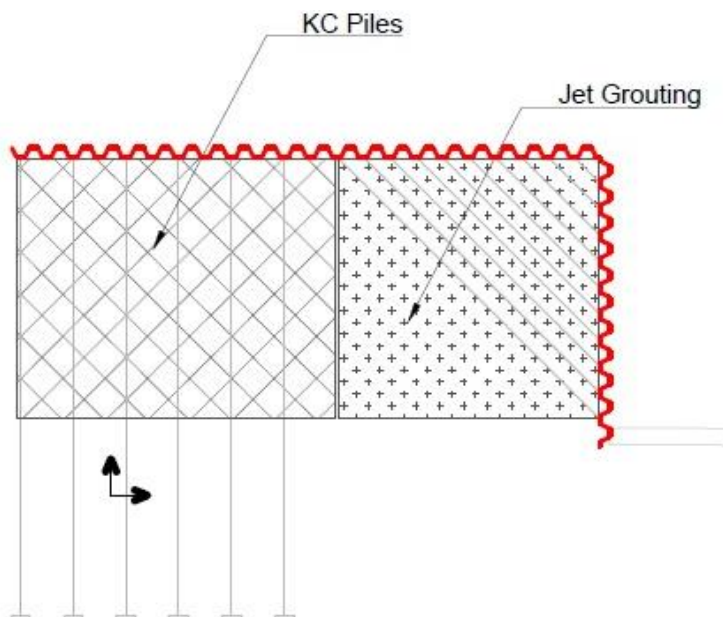


Figure 2.14 - Disposal of the applied ground reinforcement

## 2.2. GROUND CONDITIONS

The ground on site assumed in the analysis of the current work is a typical Scandinavian marine soil structure, composed of natural sediments, over a thin layer of natural glacial till, below which lies a very competent bedrock, as outlined in Figure 2.13. At this point, only introductory and geological considerations are done regarding the soil. Though, for each type of analysis in the following chapters the assumed ground profiles and geotechnical properties are provided in detail.

### 2.2.1. CLAYEY SEABED

The first particular aspect of the ground *in situ* is the seabed composed by soft clay. As detailed in Figure 2.15, it is a layer of clayey soil varying between 5 and 9 m of thickness, resultant from the deposition of river sediments in the coastal banks. It is a very fine and low permeable material, normally constituted by particles with less than 0.002 mm of diameter and with a plastic behaviour at the appropriate water content. Clay can be classified by the Atterberg limits which relates its behaviour with the water content and also by the plasticity index, liquidity index and activity level.

Normally consolidated clay is generally a problematic soil when it comes to design of geotechnical structures. Due to low cohesion, typical undrained behaviour and, in some situations, thixotropy, it is not considerable to completely assure stability of structures such as foundations and sheet pile walls.

In the region where the case study is placed, the appearing clay has relatively low values of undrained shear strength, down to 3 kPa.

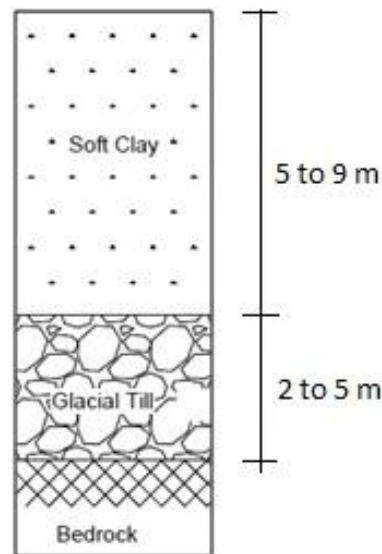


Figure 2.15 - Soil profile on-site with layers' thickness

### 2.2.2. GLACIAL TILL

The glacial till is a mix of a wide variety of granular particles, with varying sizes and shapes, from clay to boulders. It was formed by the movements of existing glacial ice in Scandinavia, which transported, eroded and deposited the rock fragments during advance and retreat of the ice mass (Strahler & Strahler 1973).

The granular composition goes from large boulders to fine clay. The smaller elements are formed due to erosion or abrasion between the elements of larger dimension and the bedrock underlying the glacier. Also, as it was deposited due to the melting of ice that contained the debris, it shows little stratification, thus has a less uniform arrangement of particles.

In general, glacial till is a competent and resistant material. In this specific case, the 2 to 5 m layer of till (Figure 2.15) shows a high value of friction angle and therefore has an adequate bearing capacity.

## 2.3. BACKFILL CONDITIONS

### 2.3.1. CONSIDERATIONS IN BACKFILLING

One of the peculiar aspects of the situation that is being investigated is the construction method and its design considerations.

As it was stated before, backfilling and excavation are generally two possible construction methods to use with retaining walls. Although in the end of the construction stage the shape is the same, i.e. there is a mass of soil being retained, the loading conditions in the wall and in the soil are different. Therefore, the expected behaviour is dissimilar (Bilgin 2010).

So, in order to calculate the earth pressures for the design of tied sheet pile walls under backfilling conditions some considerations that are taken into account in excavations cannot be assumed. For example, the Terzaghi-Peck diagrams, which are often used to design multi-tied excavations, were developed from results of many observations of excavations in constructions sites.

In reality, some authors that performed the few existing studies regarding backfill conditions concluded that the backfilling method has considerably higher wall deformations compared with excavation. Also, the wall tip deformations are even more affected by the construction method. Moreover, bending moments are significantly higher in backfilling than in excavations (Bilgin 2010). These conclusions lead to uncertainty about the design methods that should be applied to multi-tied sheet pile walls under backfilling conditions.

Regarding the procedures of construction, backfilling is done by layers that in the current situation, as the fill is submerged, will not be well compacted. In marine works, it is normally a dredge that spreads the material in layers. Though, the top layers, which will be used for infrastructure, are normally compacted and its application more controlled.

### 2.3.2. BACKFILL MATERIAL

The fill material is described as a frictional material, with high values of friction angle. It is composed of gravel and large sharp boulders (see Figure 2.16), retrieved normally from other ground works, resultant from blasting and excavation. The large elements sizes give the soil high levels of permeability, providing it with a drained behaviour.

The main function of the so called *Sprängsten* (translated to *blasted*) is to provide the base for the construction of infrastructures necessary for the port. While the lower layers serve solely as capable filling, the top layers will cover the underground service systems of the building, such as the drainage systems (Figure 2.17) and will be the contact layer with the structures above. Therefore, the material applied above water level has to be well compacted and its performance controlled.



Figure 2.16 - Samples of the *Sprängsten* material used as backfill

The interaction of the backfill material with the sheet pile wall is of main interest when analysing the behaviour of the structure. Actually, such interface characteristic should be studied to understand the effect of interface resistance (surface roughness) in lateral pressures on the wall and any disturbances in corner effects.



Figure 2.17 - Drainage system installed before applying top layer of filling material

## 2.4. ELEMENTS OF ANCHORED SHEET PILE WALL

### 2.4.1. SHEET PILE WALL

In order to retain the soil that will become the foundation ground for infrastructures of the port, sheet pile walls were used as the retaining system.

These types of retaining structures, commonly known as LARSSEN sheet piles, are applied in different situations that include excavations, waterfront structures, bridge abutments, cuttings, landfill,

flood protection and other ground enclosures. Therefore, it is a widely utilized system, with many advantages in engineering, such as:

- favourable ratio of cross-section to moment of resistance;
- suitability for a wide variety of soils;
- possibility to use in water conditions;
- fast implementation on site;
- possibility to reuse;
- Low permeability, with watertight interlocks.

In the actual market several types of sheet piling are available, varying mainly with section shape and material grade. In fact, it has been for many years that sheet piles made of wood were used in old constructions, as well as concrete jetted piles, aluminium and even vinyl (Eskandari & Kalantari 2011). However, steel is the most popular material used due to high strength and easy application. The generally used steel sheet pile sections are the U and Z sections shown in Figure 2.18, although exist also other types such as straight-web sections, normally used in cofferdams.

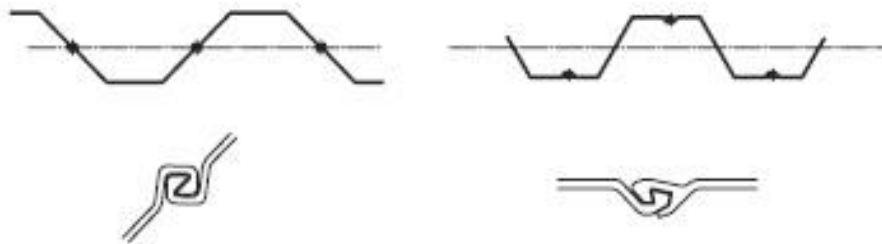


Figure 2.18 - U (left) and Z (right) steel sheet pile sections and correspondent interlocks

The main difference between these sections is focused on the position of the interlocks. Interlocks are elements responsible for joining together single piles to shape the complete sheet pile wall. They are normally mechanically crimped together to assure a good connection between the piles and, in some situations, welded as well. In U sections, interlocks coincide with the neutral axis, where the maximum shear stresses are located, whereas in Z sections they are located in the area with minimum shear stresses. Therefore, the efficiency of the section and section properties in U profiles is reduced in comparison with the Z profiles. In the present scenario, Z profiles are used with varying lengths depending on the location.

Normally, sheet piles are driven individually in the soil using existent methods that differ on the situation where the sheet pile is applied. Among the mostly used, it is possible to differentiate between threading, pressing, impact-driven and vibrated.

The first technique of driving the piles, threading, consists in simply drilling a hole or a excavating a trench where the sheet piles will be placed. Necessarily, the piles can be afterwards driven to their desired depth.

Pressing is, as threading, a low noise method for driving piles. It is mainly used in areas where low noise and vibration is a requirement, which is the case of constructions in urban residential areas or close to existing buildings, and even on embankments. As schemed in Figure 2.19, the technique

simply consists on a pressing plant which forces down the piles by means of a hydraulic system, using the self-weight of the equipment and the resistance of the already driven sheet piles as reaction force.

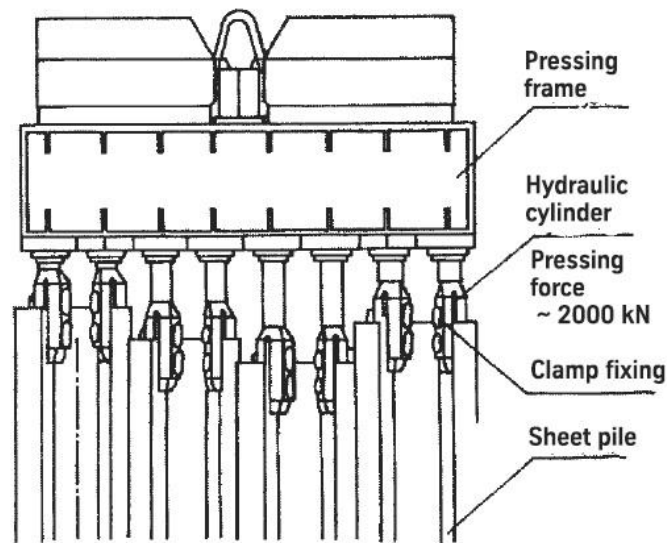


Figure 2.19 - Hydraulic system used for pile driving pressing method (ThyssenKrupp 2010)

Other two options of driving piles are the impact and vibratory driving, described in Figure 2.20. The first involves applying the piles into the ground with a series of strikes produced by a weight dropped from a certain height, lifted by hydraulic systems. The blows per minute required depend on the soil and on the type of hammer being used. In case of cohesive soils, low frequency hammering is applied to ensure dissipation of pore water pressure between blows. However, for light driving weight, rapid reaction hammers can be used.

Finally, vibratory driving is based on the harmonic loading of the sheet pile. Consequently, the soil is redistributed and reduction of toe resistance occurs, as well as decrease of friction between soil and sheet pile, associated with a local liquefaction of the soil in this interface. The applied force  $F_d$  is related to the static moment, the product of mass weight  $m_u$  and distance to the point of rotation  $r_u$ , and to the frequency of excitation  $\Omega$ , as described in equation (2.2). By adjusting the frequency of the harmonic excitation it is possible to adapt the applied force to the soil properties in order to achieve optimal driving evolution. However, when operating these equipment, it is necessary to take into account the passage through low frequencies, which can excite natural frequencies of nearby buildings (1-5 Hz).

$$F_d = m_u r_u \Omega^2 \quad (2.2)$$

Also, when using the impact or vibration method to drive sheet piles it is important to take into account ground vibrations that propagate in the subsoil, that can not only cause damage to close building due to vibration but also cause compaction of soil, and consequently not predicted settlement.

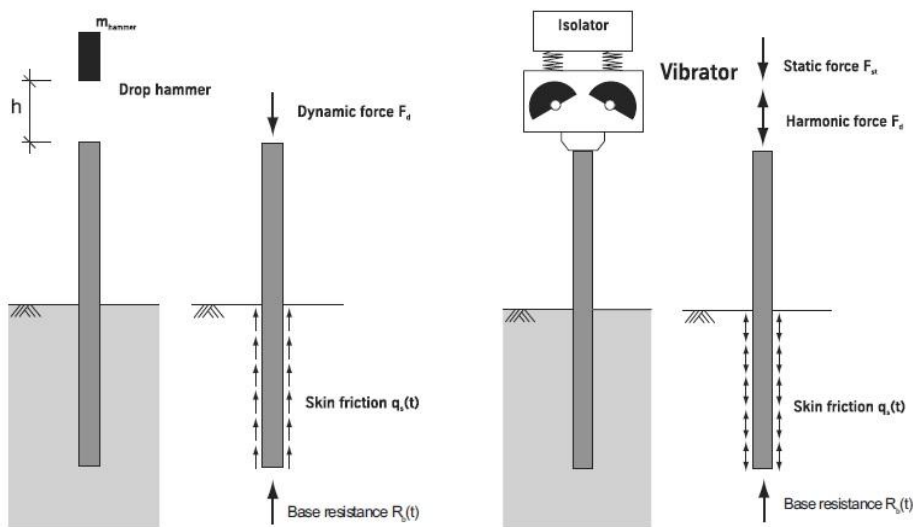


Figure 2.20 - Representations of impact (left) and vibration (right) pile driving methods (ThyssenKrupp 2010)

#### 2.4.2. ANCHOR RODS

The system used to support the sheet pile walls is an anchorage system, as detailed in Figure 2.9. The anchor rods transmit the horizontal earth stresses applied on the sheet pile wall to the anchor plates. Therefore, anchor rods are important and critical elements that will carry high loads and assure the stability of the wall.

For anchorage systems to be effective, one important aspect to keep in mind is that anchorages have to be situated outside the active failure zone that will exist behind the sheet pile wall. This means that anchor rods will most of the times have long lengths. In the assumed situation, as the back of the sheet pile wall will be filled after the installation of the piles, the anchorages need to be placed previously in the existent soil mass, far from the wall. Therefore, the anchor rods will have lengths varying from 25 to 50 m.

In simply tied walls, the calculation of anchor forces is relatively simple and direct, as it is not an indeterminate system. However, in the case of multi-tied walls the system becomes highly indeterminate due to the existence of various anchor levels. Though, in both situations an accurate value of the load in the tie rod can be difficult to determinate due to factors such as the variability of the retained mass and the arch effect in the soil. An approach on the design methods of anchors is presented in the following chapter.

When designing the tie rods, it should be taken into account the possible situation of failure of one rod and consequent redistribution of load from the missing tie to both neighbouring ties. This may require increased resistance of tie rods. Moreover, for permanent anchors, it is necessary to satisfy demands regarding corrosion protection and long term resistance.

Also, it is necessary to check axial deformation of tie rods under service load, to assure the wall deformations are below the adopted limit. However, such movements can be reduced in many cases by pre-loading the tie rods while being installed. Furthermore, bending and shear stresses caused by settlement of the fill should be considered when designing the rods, though this can be overcome by introduction of articulated joints.

The general technique used to connect the tie rods is by bolting in the opposite side of the wall, with a plate in between to avoid punching (Figure 2.21). However, in some situations where it is not so easy to do this way, such as a corner situation, it is possible to use, for example, the MACALLOY type rods. These are connected to a part called "eye piece" bolted to the wall, allowing an oblique connection and lateral movement.

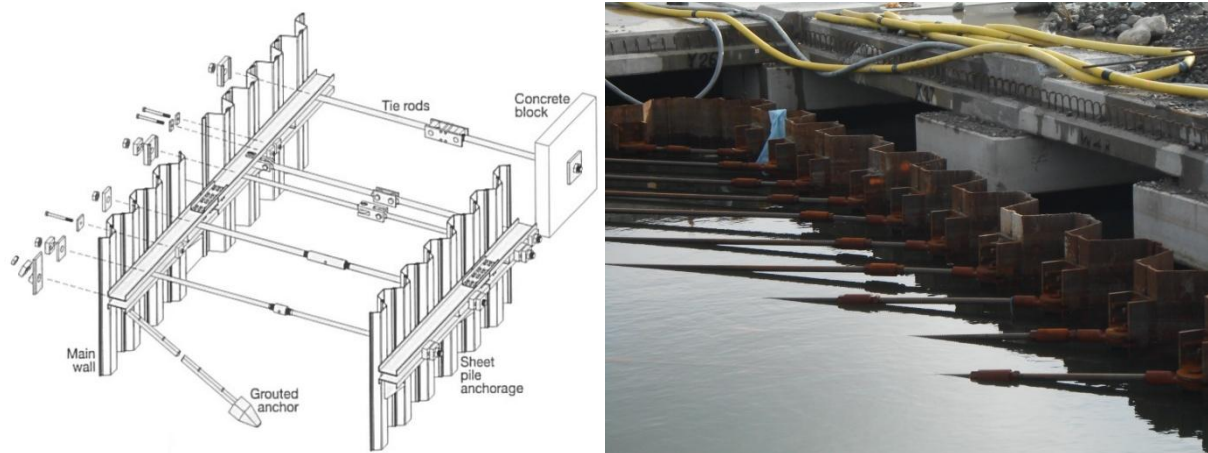


Figure 2.21 - Example of connections of the tie rods to the sheet pile wall: normal bolting with plate (left) and MACALLOY type rods (right)

#### 2.4.3. "DEADMAN" ANCHOR

The most important element of the anchorage system is the anchor itself. This component is responsible for transmitting the earth loads imposed on the sheet pile wall to the resistant soil behind the wall. As they are dependent on the soil resistant properties, anchors are critical parts of the anchorage system.

The ground anchor types differ mainly on the form of construction. It is possible to admit the following types, also shown in Figure 2.22:

- Anchor wall/plate;
- Grouted Anchors;
- Driven Anchor Piles;
- Driven grouted Pile;
- Raking Piles.

For cases where the sheet pile wall is backfilled, such as in quay walls, mainly anchor plates or deadman anchors can be used (Figure 2.23). The resistance of these constructions is activated upon backfilling the wall and is composed of the horizontal passive earth pressure plus the vertical weight acting on the anchor, which can actually be made of another sheet pile wall that reacts when the rod is tensioned. In such situation, the design might be similar to the design approach used in cofferdams.

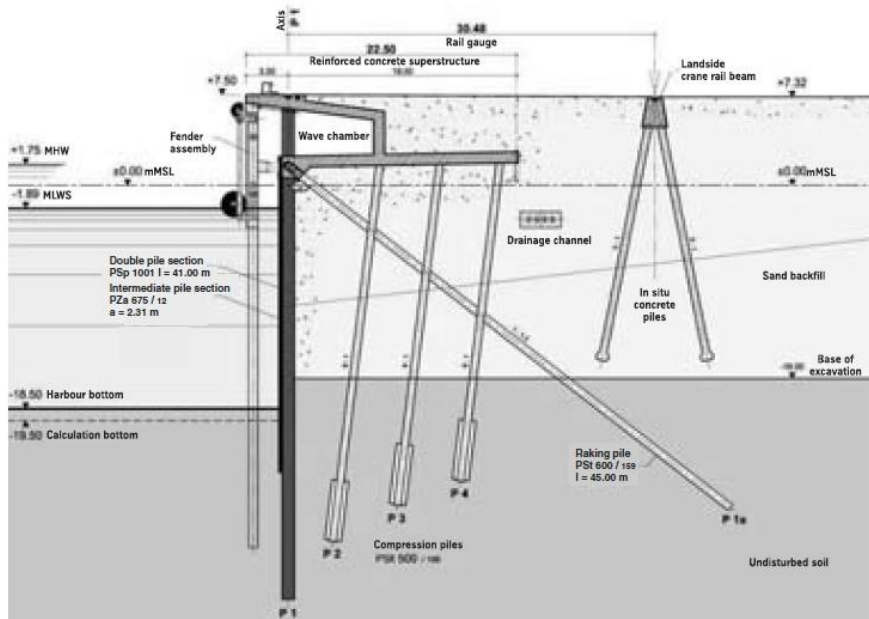


Figure 2.22 - Example of different anchoring techniques (ThyssenKrupp 2010)

In the exposed situation, deadman anchors were applied. The main characteristic of these is that they are generally a large block of concrete that is simply laid on the fill. Also, its weight has a greater consideration in the stability of the anchorage system. The shape of these anchors can vary, from the classical thin plate shape, to the longer pile shape. This last also has an important resistant component associated with skin friction between the anchor and the soil.

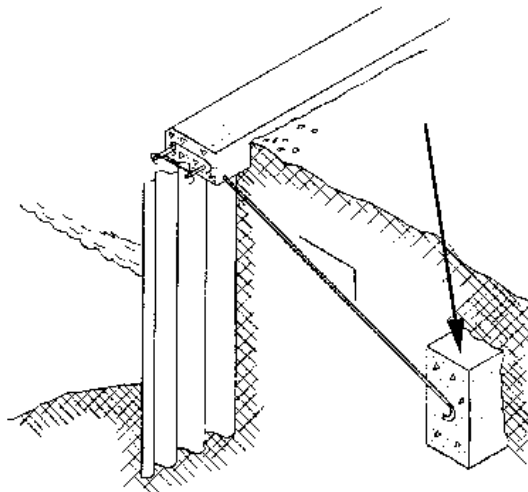


Figure 2.23 - Representation of a deadman anchor (side cut)

When designing the anchors, it is necessary to take into account the following aspects regarding the location of the blocks:

- Locate the anchor block behind the potential active failure zone;

- Assure that in the location chosen the passive failure wedge from the toe of the anchor does not coincide with active failure zone (Figure 2.24);
- In the case of cohesive soils, it should be located outside the slip circle. Also, it must be in such a distance so that it has enough shear resistance from the soil wedge in front of the anchorage (Figure 2.25).

To design the size and shape of the blocks, related to the resistance of the anchors, the following should be kept in mind:

- Limit deformations of wall under serviceability limit state conditions;
- Prevent the movement between the block and surrounding soil.
- Internal stability of the block, due to punching.

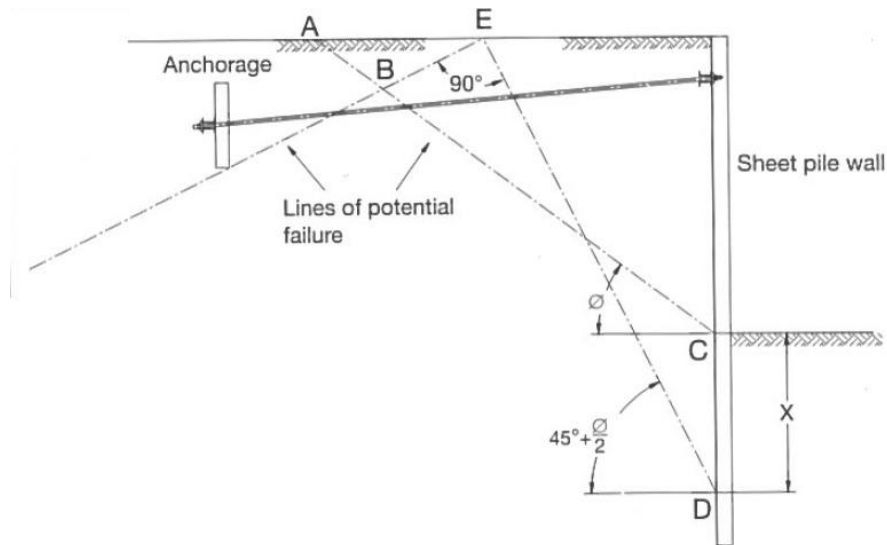


Figure 2.24 - Admissible location of anchor blocks (ThyssenKrupp 2010)

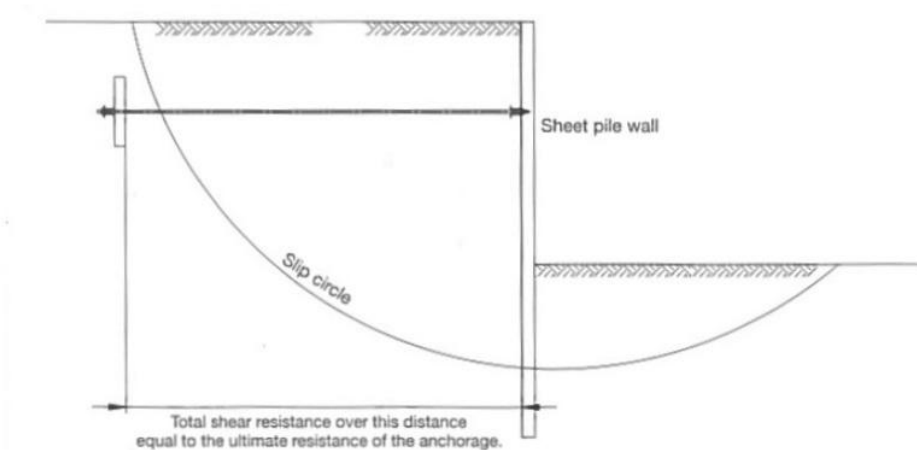


Figure 2.25 - Admissible location of anchor blocks in cohesive soils (ThyssenKrupp 2010)

#### 2.4.4. WALING AND CAPPING BEAM

The waling and capping beam are two elements of the sheet pile wall responsible for redistributing the reaction forces between the sheet pile wall and the anchors. Also, both provide higher stiffness to the wall, as well as connection between piles to prevent vertical shear and consequent relative vertical movement. However, typically the waling beam is made of steel and located in intermediate heights of the sheet pile wall, whereas the capping beam is built on top of the wall, working as a cap (Chu 2010).

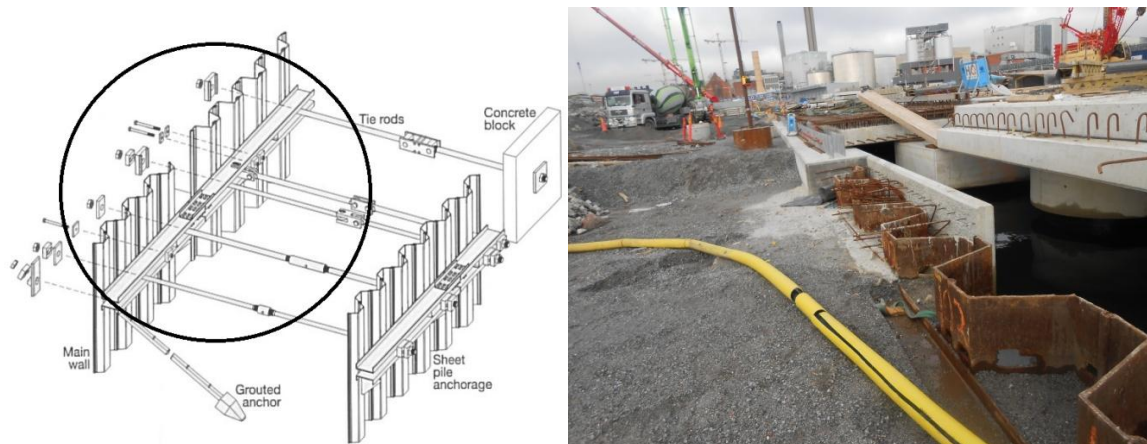


Figure 2.26 - Representation of waling beam (left) and concrete capping beam (right)

When designing these structures, the structural model of the beams should be considered simple supported with point loads applied by the anchor loads. Still, beams can alternatively be considered continuous and thus with fixed supports. Yet, this procedure is less conservative than the first option. Also, during the design, the possible loss of a tie rod has to be checked and a waling length of two times the single length should be considered.

The capping beam should in addition be designed to resist shear stresses due to relative vertical wall movement resultant of differential settlements or lateral bending. Besides, in the case of quays where the capping beam is the mooring zone, the stresses caused by the contact with mooring ships should be taken into account and additional safety measures should be considered.

## 2.5. SOIL IMPROVEMENT

### 2.5.1. KC PILES

Lime-cement piles, or in Swedish, *Kalkcementpelare* (KC Piles), are result of a soil stabilization technique where quicklime or cement are mixed *in situ* with soft soil, which can be constituted by soft clay or silt as well as organic soils. In the application of this method, a mixing tool ("egg beater") rotates as it goes deeper in the ground, remoulding the soil. When the required depth is reached, the required mix of lime, lime-cement or cement is supplied and mixed with the stabilizing soil, as the mixing tool rotates and returns to the surface (see Figure 2.27).

The use of lime-cement columns has been increasing since their development in the 1970's (Broms & Boman 1975). The method has been used in situations where soft marine deposits are existent, such as in ports and harbour areas, with the main purposes of increasing load bearing and reducing ground settlements. Application of such techniques has also extended to embankments, roadways and foundations in soft ground.

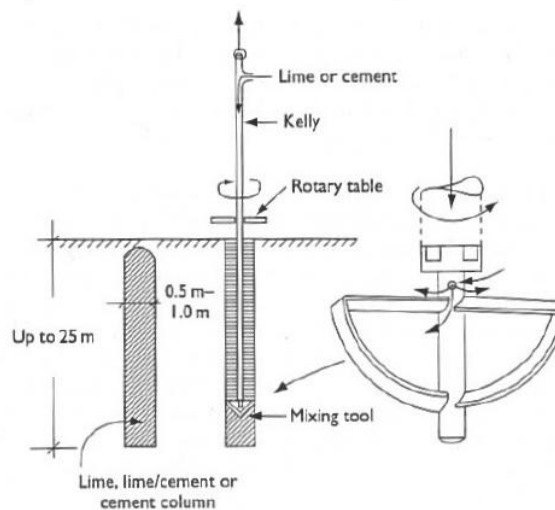


Figure 2.27 - Execution of dry mixing lime, lime-cement or cement pile (Moseley & Kirsch 2004)

Most commonly used at the present time in Japan and in Scandinavian countries, such as Sweden and Finland, KC Piles have turned out to be a competitive solution for soil improvement and stabilization. It actually became an alternative for ground improvement that, although may appear more costly due to use of finely ground quicklime, has a lower total cost as less lime than cement is required (Moseley & Kirsch 2004).

The main idea of soil improvement when using blocks of KC Piles is increasing bearing resistance and shear strength. This is mainly achieved by the chemical reactions between lime, cement and soil particles. What can be observed is that the quicklime reacts with fine particles of clay, occurring flocculation, whereas the cement reacts and agglomerates granular particles. So, lime-cement mixes are recommended to use in organic soils when the desired shear strength cannot be obtained with other mixes.

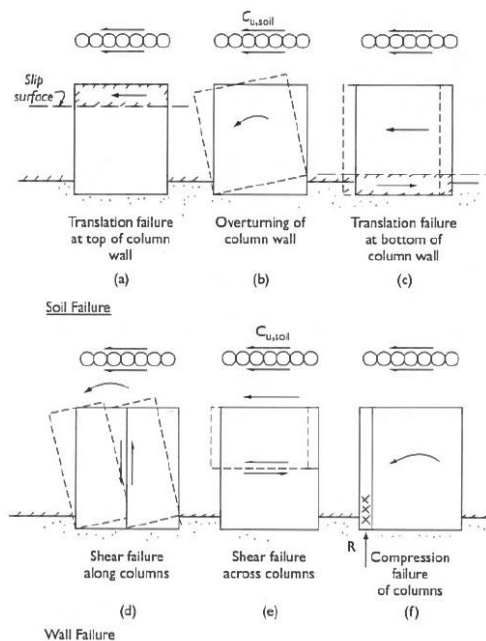


Figure 2.28 - Representation of the failure modes assumed in a block of piles (Moseley & Kirsch 2004)

By increasing the resistance and shear strength, the stabilized soil, which works as a block, will have failure modes different from the previous not stabilized soil. Such failure modes are represented in Figure 2.28. The design of these structures have to take into account the assumed failure modes, which depends on the penetration depth into a stiff layer below the wall and in the bearing capacity of the columns themselves.

In the situations where KC Piles are applied in the stability of deep excavations with sheet pile walls (Figure 2.29), such as the case of the Stockholm Port, these will have two functions, depending on where the columns are placed. If a block of piles is located behind the sheet pile wall, then they will reduce the active earth pressure, assuming they transfer the load to the bottom of the block without spreading. However, if located in front of the sheet pile wall, the columns will increase the passive earth pressure, reducing the risk of toe failure.

KC Piles are characteristic for its ductility and high permeability, compared to unstabilized soil. Actually, lime-cement piles have been reported to have failure strain values around 2% for ultimate strength of 130 kPa, revealing to be less brittle than cement piles (Moseley & Kirsch 2004). Also, their undrained shear strength can rise up to 200 kPa and to have a modulus of deformability  $E_{50}$  of  $200C_u$ .

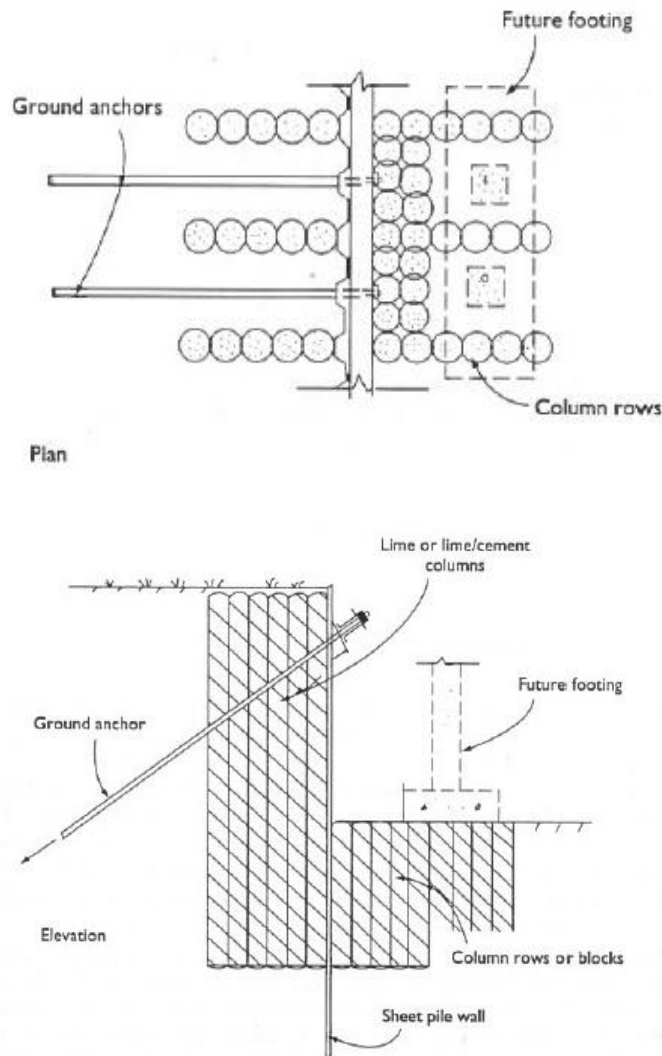


Figure 2.29 - Example sheet pile wall with lime-cement piles used as soil reinforcement (Moseley & Kirsch 2004)

Single columns located below an embankment might suffer lateral displacement caused by high lateral earth pressure due to the fill. Such situation may be possible to occur in the present case study. However, these displacements are usually small and large values may only be expected when the stability of the embankment is low and the global factor of safety is lower than 1.5 (Moseley & Kirsch 2004).

### 2.5.2. JET GROUTING PILES

Among the available solutions in the market, jet grouting is one of the most versatile forms of ground improvement. Although it is a technology with a high technical demand, with this technique it is possible to increase ground strength, prevent groundwater flow and provide structural stiffness with one single application.

Jet grouting technique started being developed in the 1950s mainly in Japan, where it was first used to improve effectiveness of water tightness. In this situation, the untreated soil was eroded and then ejected to the surface, being afterwards replaced by cement-based slurry to provide imperviousness. Later, jet grouting was used to create thin cut-off walls as well as to seal gaps between sheet piles. In the 1970s, rotating jet grouting emerged in Japan to satisfy new demands and was later introduced in Europe, becoming worldwide popular since then.

The principle idea of this technology is to physically erode the ground using a high-pressure water or grout, in order to improve the surrounding soil. Normally, the drill is first introduced to the required depth and only afterwards the pressured jet (water or grout) is applied while withdrawing the equipment, creating the desired jet grout column (see Figure 2.30).

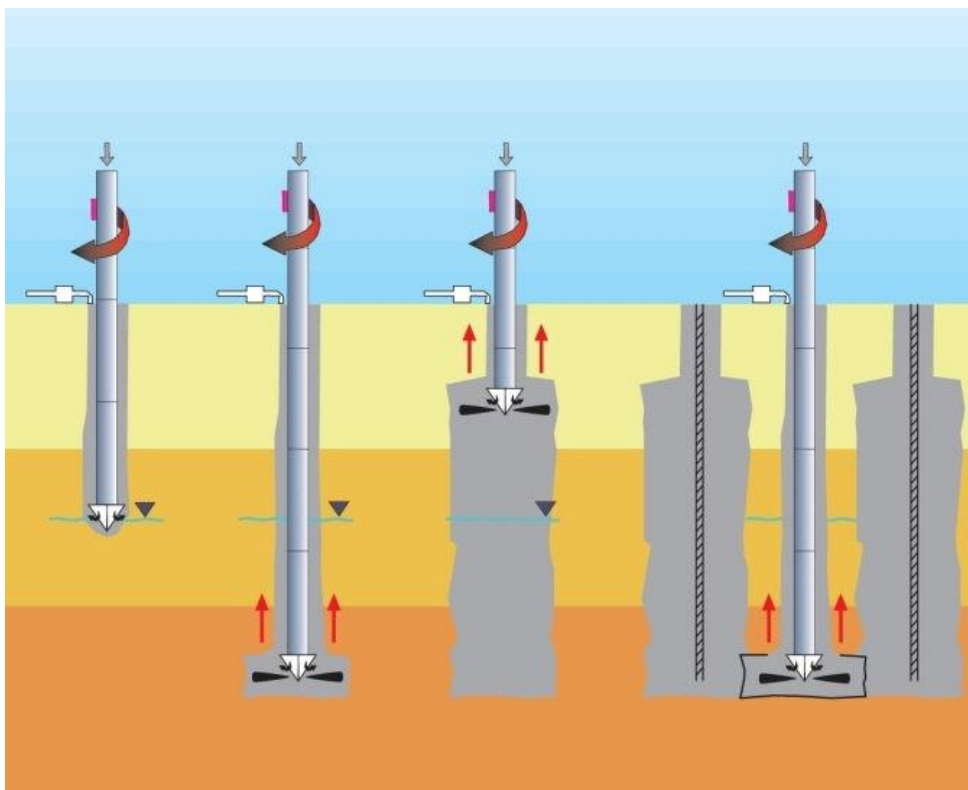


Figure 2.30 - Steps of application of jet grouting (ArchiExpo)

After the globalization of the jet grouting, three main variants emerged, as shown in Figure 2.31.

The single system is a simple form of jet grouting, with a single jet grout eroding and mixing the soil. It is not so much controlled process as below ground water level (where often jet grouting occurs) the eroding distance can be reduced due to the absence of surrounding air, increasing the necessary energy to cut the desired diameter.

The double system is similar to the single system with the addition of compressed air that shrouds the grout jet. This way, the eroding capacity is increased especially below the water table, due to the creation of an atmosphere around the grout. Still, this option is not so controlled and can produce more spoil than expected, this is, more residual grout than the eroded volume of soil.

The triple system uses grout, water jet and compressed air surrounding the water. This method consists of a single grout jet that is located approximately half a metre below a composite jet of water shrouded by compressed air. This way, it is a method that is better controlled and the quality of the final product can be defined according to the necessary.

In addition to these systems, later in the 1980s and 1990s the jet grouting technique evolved to a more complex system called "Crossjet grouting", allowing for a better control of eroding capability and therefore columns diameters. This basically consists in two non-horizontal jets that collide at a certain distance, limiting their eroding capacity. In some cases, it can be coupled with conventional deep mixing methods in order to enhance control of soil mixing.

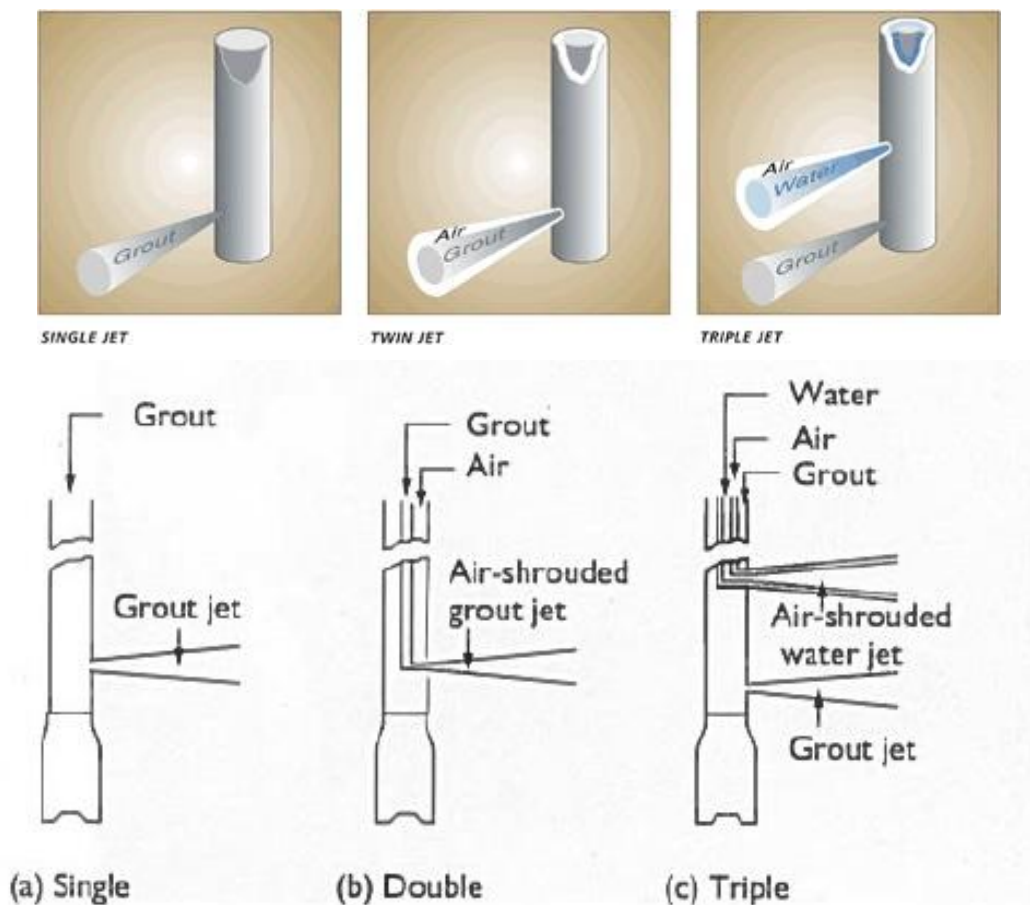


Figure 2.31 - Three techniques of jet grouting: single, double (or twin) and triple. Top (Solentanche Bachy) and bottom (Moseley & Kirsch 2004)

In the present case study there are several reasons for the use of jet grouting in the area of the corner instead of the lime-cement piles used in the rest of the reinforced zone along the wall.

Firstly, the ground in the corner zone presented boulders and rock fragments of large size mixed with the soft soil. Therefore, the equipment used in the execution of KC Piles, the rotating "egg beater", was not suitable for these ground conditions, as it could not fragment such large and strong particles to provide a good soil mix. As jet grouting only uses the water or grout jet pressure to erode the soil, the big boulders could be fragmented with high pressure jet if necessary.

Secondly, the structural stability could not be assured with certainty due to many unpredictable three dimensional effects and deformations, as explained before. So, in order to maintain a conservative and safe approach, the jet grouting was a reasonable solution. As already mentioned, it is expected that the jet grouting piles would work as a monolith with high compressive strength, up to 1 MPa, and absorb earth pressures from the fill, reducing instability factors.



# 3

## ANALYTICAL ANALYSIS

### 3.1. INTRODUCTION TO ANALYTICAL ANALYSIS

In the analysis of deep excavation problems with multi-tied retaining walls, independently of the type of analysis, the first requirement is obtaining a correct distribution of earth pressure. When designing an earth retaining structure, the main point is determining the correct lateral earth pressures and the resultant response of the retaining structure.

However, depending on the construction process, if it is an excavation or backfilling, the methods to calculate the earth pressure distribution along the wall may be different. This is related mainly to the deformation mode of the wall and mechanisms of load transfer through arch effects in each of the processes.

In this chapter are presented different approaches to design retaining structures in multi-tied excavations, such as Terzaghi & Peck diagrams, the Equivalent Tie Support Method and the Sub-grade Reaction Method. Besides, a simple analysis of the sheet pile wall in the case study presented in the previous chapter is provided, assuming three different cases of lateral earth pressure distribution. This serves as a reference for the three-dimensional analysis in chapter 4.

### 3.2. TERZAGHI & PECK DIAGRAMS

Terzaghi & Peck diagrams were developed by Terzaghi and Peck in 1967 as a result of observations of strutted excavations (Figure 3.1). They were suggested based on empirical information of braced excavations, where compression forces in each strut were measured and afterwards the apparent diagrams could be derived, i.e. the pressure distribution on the wall based on the strut force per area of influence. Terzaghi & Peck (T&P) diagrams were then formulated both for cohesionless and cohesive materials. Although for cohesionless soils they are directly applicable and no further concerns exist, for cohesive soils the diagrams should be used taking into account stability numbers, based on stability of the excavation base.

As T&P diagrams were developed from braced excavations, they are commonly accepted as a reliable method for calculating this type of retaining walls but may not be used for tie-back walls in some situations. However, they can be used to calculate initial pre-stresses in pre-stressed tie-back walls, as these may show as much stiffness as braced excavations.

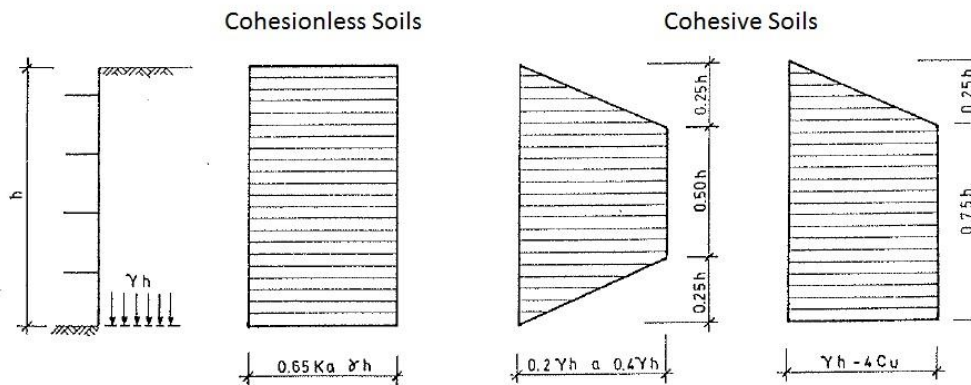


Figure 3.1 - Terzaghi and Peck Diagrams (Matos Fernandes 1990)

Nevertheless, it is important to introduce the understanding of such diagrams as an accepted method for calculation of design earth pressures in excavations.

### 3.3. EQUIVALENT TIE SUPPORT METHOD

The Equivalent Tie Support Method (ETM) is a tool that can be used to calculate multi-supported structures using simple equilibrium equations. In short, this method assumes an equivalent tie for each excavation stage, which represents the resultant force of the tie forces system. For using this method, it is necessary to resort to the classical design methods. Therefore, these have to be explained before fully understand this method.

#### 3.3.1. CLASSICAL DESIGN METHODS

The main two classical design methods are free and fixed earth support. They are based on the existence of limit equilibrium state (active and passive) in both sides of the wall, which is simply supported in the tie and in the tip and it is analysed as a beam subjected to lateral earth pressures. These methods differ from each other mainly in the type of support adopted in the tip of the wall (Vieira & Matos Fernandes 2000).

The free earth support method admits the soil on the embedded part of the wall cannot produce negative bending moment, therefore admitting a simple support on the tip of the wall. By means of moment equilibrium to discover the necessary embedded length and horizontal force equilibrium it is possible to obtain the anchor forces (Figure 3.2).

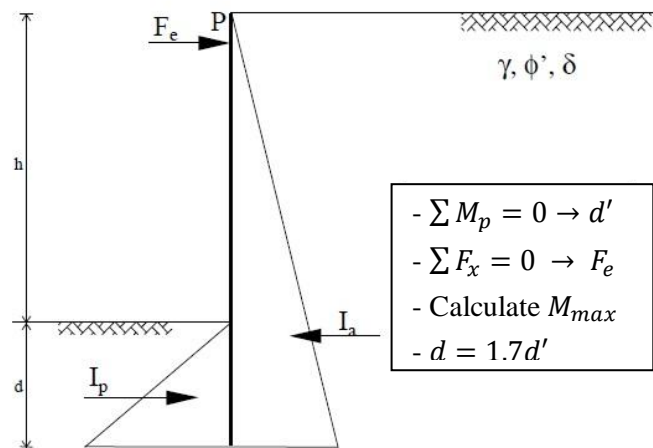


Figure 3.2 - Free earth support method (Vieira & Matos Fernandes 2000)

The fixed earth support method considers that the soil embedding the wall produces negative bending moment, thus admitting a fixed support on the tip of the wall. In this case, it is necessary to have a resistant force  $R_d$  that represents passive force in front of the wall. Considering an "equivalent beam" it is necessary to identify the location of null bending moment where a hinge will be placed, splitting the wall in two statically determined beams. Afterwards, using static equilibrium equations it is possible to determinate the anchor forces, passive reaction  $R_d$  and embedded length of the wall (Figure 3.3).

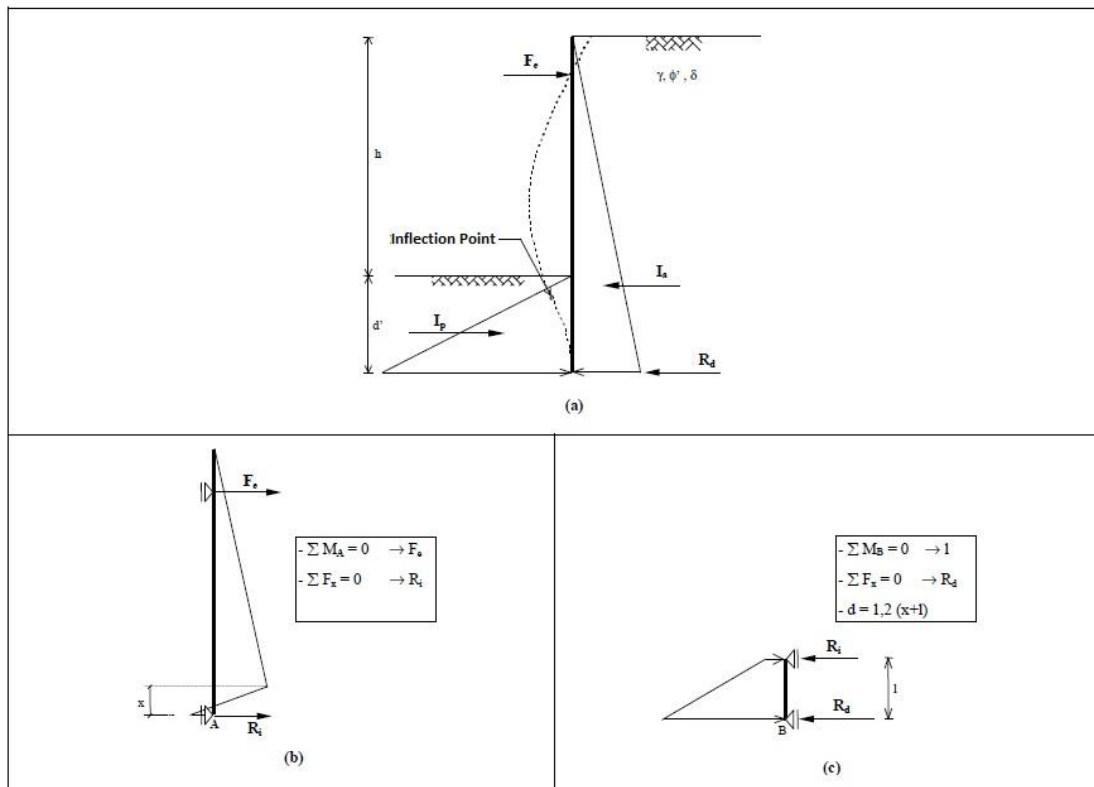


Figure 3.3 - Fixed earth support method (Vieira & Matos Fernandes 2000)

### 3.3.2. EQUIVALENT TIE SUPPORT METHOD PROCEDURES

In this method, unknowns of the problem are wall embedment and force at each anchor row. It assumes that soil pressure reaches active and passive states in every stage of excavation. Although the problem is statically indeterminate, it is possible, by assuming simplifications, to only use equilibrium equations to determinate the unknowns. Considering an equivalent tie at a certain position for each excavation stage, it becomes possible to solve this equivalent single wall using the classical design methods, such as free and fixed earth support.

Basically, using horizontal forces and bending moment equilibrium on the wall system at each stage of excavation one can determinate anchor forces. For a generic  $i$  step, the equation (3.1) can be applied, where  $x_i$  is the distance of the equivalent force  $R_i$  to the top of the wall and  $T_i$  and  $y_i$  are the force in anchor  $i$  and distance from the top of the wall to the anchor, respectively. These are described in the drawing of Figure 3.4.

$$x_i = \frac{T_1 y_1 + T_2 y_2 + \dots + T_i y_i + \{R_i - [T_1 + T_2 + \dots + T_i]\} y_{i+1}}{R_i} \quad (3.1)$$

As an example, the first excavation stage is explained. First, anchor force on the first row  $T_1$  can be calculated using the conventional methods described before. Afterwards, using an equivalent reaction force  $R_1$  to represent both  $T_1$  and  $T_2$  (not yet known), the structure is again a single anchored wall. However, the position of  $R_1$  ( $x_1$ ) comes dependent of the value of  $T_1$ . So, assuming a position of  $x_1$ , moment equilibrium and horizontal force equilibrium has to be achieved by an iterative process of changing the position values, until convergence is reached. This procedure has to be repeated in every excavation stage.

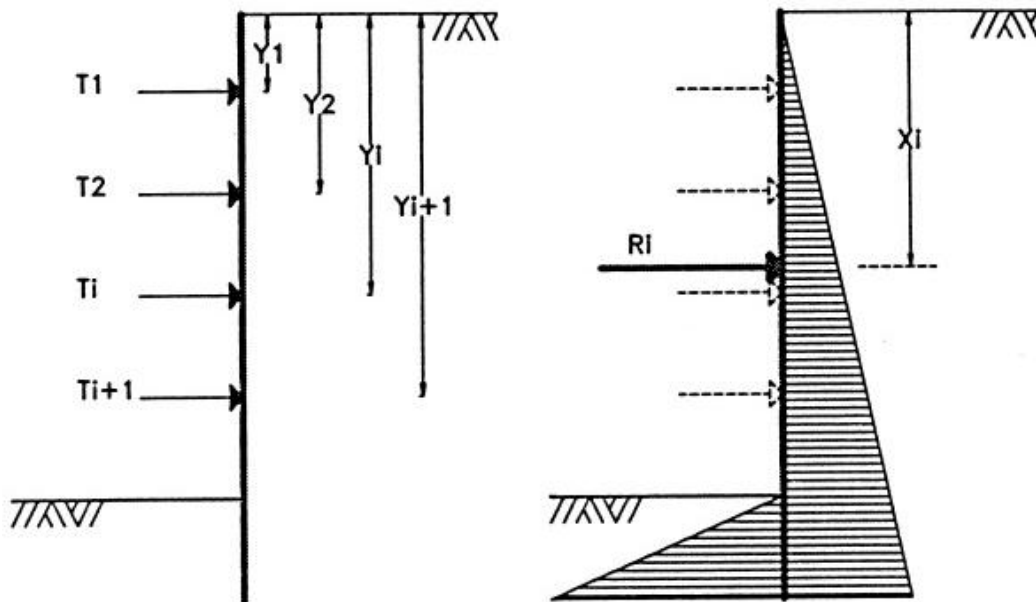


Figure 3.4 - Representation of ETM procedure (Carrubba & Colonna 2000)

This is a simple method that only requires limited information about soil parameters. Yet, it cannot predict wall displacements and variations of tie forces during excavations stages (Carrubba & Colonna 2000).

### 3.4. SUB-GRADE REACTION METHOD

The Sub-Grade Reaction Method (SRM) is an approach that reduces the soil-structure interaction from a two-dimensional to a one-dimensional problem. It assumes the wall as a continuous beam and the soil modelled by a series of single horizontal springs. Also, the anchors or struts are represented by springs with equivalent stiffness.

This process is based in the elastic beam and its integration equation (3.2), where  $E$  is the elastic modulus of the wall,  $J$  the moment of inertia,  $k_h$  the horizontal subgrade reaction modulus and  $w$  the horizontal wall displacement at depth  $z$ . By integrating the equation for each excavation stage it is possible to obtain a theoretical solution of forces in the wall, anchor forces and horizontal displacements in the wall. It is solved by iterations assuming the wall is constituted by beam elements connected by nodes placed where horizontal springs are applied.

$$EJ \frac{d^4 w(z)}{dz^4} = k_h w(z) \quad (3.2)$$

The soil is represented by node springs that have a bilinear stress-displacement relationship, allowing for representation of transition from at rest state to active or passive pressure conditions. Figure 3.5 shows the graph representative of this bilinear elastic-plastic behaviour, with a parameter  $K$  in the linear elastic phase.  $K$  represents the spring stiffness, which depends not only in wall-soil relative stiffness but also in the geometry of the problem.

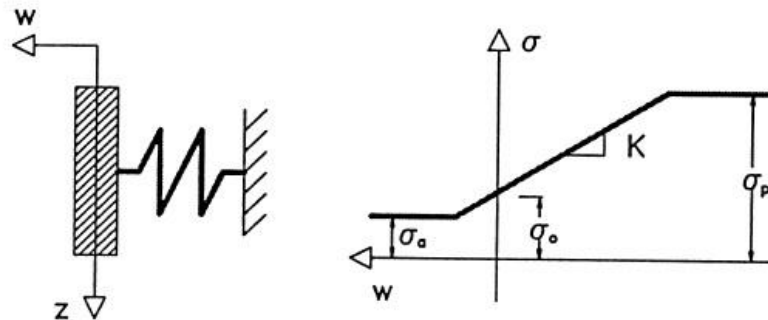


Figure 3.5 - Bilinear stress-displacement relationship (Carrubba & Colonna 2000)

Equation (3.3) was proposed by Becci & Nova (1987) to obtain the soil spring stiffness, where  $t$  is the space between two contiguous springs,  $a$  is a non-dimensional coefficient and  $L$  a dimension of the problem that accounts for the extent of the deformed active and passive soil zone.

$$K = a \frac{E}{L} t \quad (3.3)$$

### 3.5. STABILITY ANALYSIS OF SHEET PILE WALL

#### 3.5.1. LATERAL EARTH PRESSURES CALCULATION

This simple analytical analysis of the sheet pile wall will serve as introductory interpretation and understanding of the problem. The first step in analysing a retaining wall is obtaining the lateral earth pressures.

As the main difficulty in the situation of backfilling is to understand the lateral earth pressures distribution, the author decided to calculate these using three known approaches:

- Terzaghi & Peck Diagrams (T&P), which are commonly used in design of multi-tied excavations, as described before;
- Using at rest earth pressure coefficient  $K_0$ , assuming the structure is stiff enough and the deformations may not be sufficient to obtain active lateral pressures;
- Using active earth pressure coefficient  $K_a$ , assuming wall deformation is enough to activate such lateral active earth pressures.

The at rest earth pressure coefficient relates the effective vertical stresses with effective horizontal stresses on soil when there is no soil movement, i.e., when the soil is at rest and no strain occurs in all the soil mass. The expression in equation (3.4), where  $\varphi$  is the friction angle, was derived by Jaky (1944) from analysis of the stress field in a wedge prism of loose sand. Although it was developed through an elaborate and still discussed procedure, this empirical formula is widely accepted as a good representation for stress coefficient at rest for granular soils and normally consolidated clays (Michalowski 2005). Therefore, it is possible to use this coefficient to calculate lateral earth pressures on the wall considering that soil displacement is small enough and soil is deposited by horizontal layers<sup>1</sup>. This may occur in cases with very stiff retaining structures, for example in silos with granular materials.

$$K_0 = 1 - \text{sen}(\varphi) \quad (3.4)$$

The active ( $K_a$ ) and passive ( $K_p$ ) earth pressure coefficients are the limit values which vertical-horizontal stress ratio can reach. They depend on the value and direction of the deformation the soil suffered. Rankine developed equations (3.5) and (3.6) based on the idea of a rigid and absolutely smooth wall retaining a mass of purely frictional material, represented in a Mohr circle.

$$K_a = \frac{1 - \text{sen}(\varphi)}{1 + \text{sen}(\varphi)} \quad (3.5)$$

$$K_p = \frac{1 + \text{sen}(\varphi)}{1 - \text{sen}(\varphi)} \quad (3.6)$$

---

<sup>1</sup> It has been observed that stress ratio may vary from active to passive coefficient of earth pressure at the symmetry plane of a wedge sand prism, depending on history of deposition of material or deflection of the base (Michalowski 2005)

At first, the lateral earth pressures on the structure would be the at rest pressures, as referred before. However, as the structure moves away from the retained mass, tensions will be generated in the soil, reducing the horizontal stresses until plastic limit state is reached (active limit equilibrium state).

The same experiment can be done, but with contrary direction of movement, with the wall pushing the soil. In this case, the horizontal stresses will increase until the passive limit state is reached, when the soil is in plastic state.

For both limit equilibrium states described before, Rankine, based on Mohr-Coulomb failure criteria for a cohesionless soil, derived  $K_a$  and  $K_p$  expressions. The deformations required to achieve both of these limits are different and variation of these coefficients with deformation is not linear (Matos Fernandes 1990). Lambe & Whitman (1969) described this in an experiment on sand, where they verified that to reach the passive limit state it was necessary, approximately, four times more deformation values than to reach half it.

In reality, it is possible that the real lateral earth pressures may be related to a varying lateral earth pressure coefficient along the depth. It was observed in some construction sites with backfilling conditions that lateral pressure coefficient on the soil mass near the retaining wall may vary between  $K_a$  and  $K_0$ . This is related to the fact that it is required a minimum displacement to achieve active pressures, as shown in Figure 3.6.

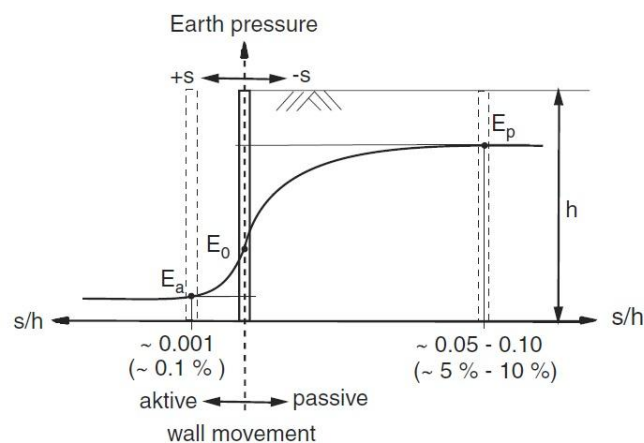


Figure 3.6 - Representation of wall deformations associated with active and passive limit states

For these situations, it was proposed an approach known as enhanced active earth pressure approach to calculate intermediate earth pressure values, which can be mainly used in propped excavation enclosure or in retaining walls with pre-stressed ground anchors. The magnitude of these earth pressures can be calculated using equation (3.7), where  $E_a$  is the active earth pressure,  $E_o$  at rest earth pressure and  $\mu$  a factor between 0 and 1, according to German norms (DIN 4085:2007):

$$E'a = \mu \times E_a + (1 - \mu) \times E_o \quad (3.7)$$

Later, Müller-Breslau set up more complex equations for determination of active and passive earth pressure coefficients that would include parameters not accounted in the previous formulas. These

now consider a wall friction angle  $\delta$ , a sloping of the ground surface  $\beta$  and an inclined wall  $\alpha$ . Still, such equations will not be used for this analysis, as there is no sloping ground surface or inclined wall, and is despised the existence of roughness between wall and soil, i.e., with friction angle of zero.

### 3.5.2. SOIL CHARACTERISTICS

Based on the example case study of the Värtahamnen port, the situation observed on site was chosen to be the basis of this analysis. Therefore, based on provided conceptual drawings and on the ground geotechnical profile presented in Figure 2.13 and Figure 2.15, a simple lateral profile of the soil and structure was prepared to carry the calculations.

The soil profile in Figure 3.7 describes the soil units assumed to be acting on the back of the wall. These take into account the already present geotechnical profiles in combination with the filling material that will be deployed. It represents the *in situ* conditions, which consist in six layers of soil:

- Fill above deck;
- "Compact" fill;
- "Uncompact" fill;
- Monolith, either of Jet Grouting or Lime-Cement (KC) piles;
- Glacial Till;
- Rock.

Layer	Elevation (m)
Top Fill	2,4
	1
Compact Fill	a.w.l. -0,4
	-0,36
	m.w.l. -0,9
Uncompact Fill	
	-11
Monolith	
	-18
Till	
	-25
Rock	

Figure 3.7 - Soil masses generating earth pressures on retaining wall

All three layers of fill are made of the same material, the *Sprängsten*, but in different conditions of application. The top fill above deck, as the layer in direct contact with applying loads and infrastructure, is a more compacted granular material, thus with higher unit weight. However, the layer below named "compact" fill is actually not as compacted and only differs from the "uncompact" fill due to the fact that this last is submerged and not compacted, hence with reduced strength properties.

Such nominations ("uncompacted" and "compacted") are just used to be in accordance with the names used in the soil profiles provided by COWI.

The monolith is a dense and compact layer representative of a block of jet grouting or KC Piles, depending on the location. As referred in the previous chapter, a ground improvement to the soft clay had to be done behind the retaining wall in order to reduce or even completely absorb the lateral earth pressures generated by the untreated soil. This results in a complete replacement of the clay layer (see Figure 2.13) by a monolith that will be assumed to apply no pressure to the sheet pile wall. In the case of jet grouting no spoil thickness was considered.

The glacial till will not have influence on this analysis. It is only taken into consideration that this layer provides enough tip resistance, but will not be able to embed the bottom of the sheet pile wall, allowing rotation of the tip.

The required soil parameters for this analysis related to the materials described above are detailed in Table 3.1. These were provided by COWI as characteristic values to be used in any calculations. The earth pressure coefficients were then calculated using equation (3.4) and (3.5).

Table 3.1 - Soil parameters used for lateral earth pressure calculation

Soil Layer	Unit Weight (kN/m <sup>3</sup> )	Friction Angle (°)	At rest earth pressure coefficient, K <sub>0</sub>	Active earth pressure coefficient, K <sub>a</sub>
Top Fill (above deck)	22	45	0,29	0,17
Compact Fill	21	45	0,29	0,17
Uncompact Fill	21	38	0,38	0,24

As described before, the top fill presents a higher unit weight value due to higher level of compaction, while "compact fill" and "uncompact" fill show the same unit weight. However, the friction angle is considerably lower in "uncompact" fill. The reason for this is that the material is simply deposited under the water by layers, using a dredge to complete such task. As a result, the void ratio will be close to the maximum. Since it is only subjected to compression forces applied by overlying layers, the friction angle will not increase as much as it increases on top layers where compaction techniques have been used.

Beside the earth pressures due to soil weight, surcharges and water pressure has to be accounted. Movement of trucks and handling of equipment during construction phase generate surcharges of 25 kPa, which is a rather conservative value.

Due to changes in sea level related to high and low tide, water levels may be different in both sides of the wall. The sheet pile wall and the layer of glacial till below behave as a barrier with very low permeability that is capable of retaining water. When there is a variation in water height because of change from high tide to low tide, water from the back of the wall will tend to flow to the front of the wall. However, as permeability is so low, the level reduction rate is almost zero. Consequently, the resultant water difference will generate a uniform lateral pressure along all the wall depth. According to the provided information, this pressure will be 4.91 kPa, corresponding to an average water level of -0.4 m and a minimum water level of -0.9 m.

### 3.5.3. SHEET PILE WALL SYSTEM

As it can be observed in the sketch in Figure 3.8, the structure analysed is a single 24.4 m height retaining wall supported by two levels of anchors and embedded on the soil in the bottom tip. However it is assumed that there will be rotational movement around the tip, without any restraint. Therefore, the structural model adopted is a vertical beam, simply supported on the bottom and with two elastic supports representing the anchors. The properties of the structural elements are similar to the ones used on site, described in Table 3.2.

The stiffness of the elastic supports (i.e. springs) was calculated using the real parameters and based on Hooke's law in equation (3.8), where  $k$  is anchor axial stiffness,  $E$  its elastic modulus,  $A$  the cross section area and  $L$  the length of the anchor rod.

$$k = \frac{E \cdot A}{L} \quad (3.8)$$

The two levels of anchors have different lengths and spacing. According to the provided plans, the upper rods are spaced 2.80 m have 50 m length, while lower rods are spaced 1.40 m and have 25 m length. Therefore, it is expected that anchors have different stiffness.

An important aspect to notice is that soft clay present *in situ* does not provide enough reliable strength. This means that for conservative reasons the layer of clay in front of the sheet pile wall was not taken into account when calculating earth pressures. Thus, it is assumed it will not generate any passive earth pressure resistant to the rotation of the wall.

Table 3.2 - Properties of structural elements

Element	Description	Material	Inertia $y$ (m <sup>4</sup> /m)	Stiffness, $k$ (kN/m)	Young Modulus, $E$ (kN/m <sup>2</sup> )
Sheet Pile	AZ 46-700 <sup>2</sup>	Steel S430	1,154x10 <sup>-3</sup>	N/A	200x10 <sup>6</sup>
Upper Anchor Rods	SAS 670/800 <sup>3</sup> (φ63,5)	Steel 670/800	N/A	12668	200x10 <sup>6</sup>
Lower Anchor Rods	SAS 670/800 (φ75)	Steel 670/800	N/A	35344	200x10 <sup>6</sup>

<sup>2</sup> AZ 46-700 are Z-section sheet piles of the AZ series marketed by Arcelor Profil Luxembourg. It is a Z-section with 4400 cm<sup>2</sup>/m section modulus and 700mm driving step. They are different of similar section piles from other companies. Therefore, specifications are retrieved from the commercial product detail, which can be found in Appendix.

<sup>3</sup> SAS 670/800 are anchor rod systems marketed by Stahlwerk Annahütte. They are threaded bars with yielding stress (0,2% strain) and maximum stress of 670 and 800 N/mm<sup>2</sup> respectively. Specifications are retrieved from the commercial product detail, which can be found in Appendix

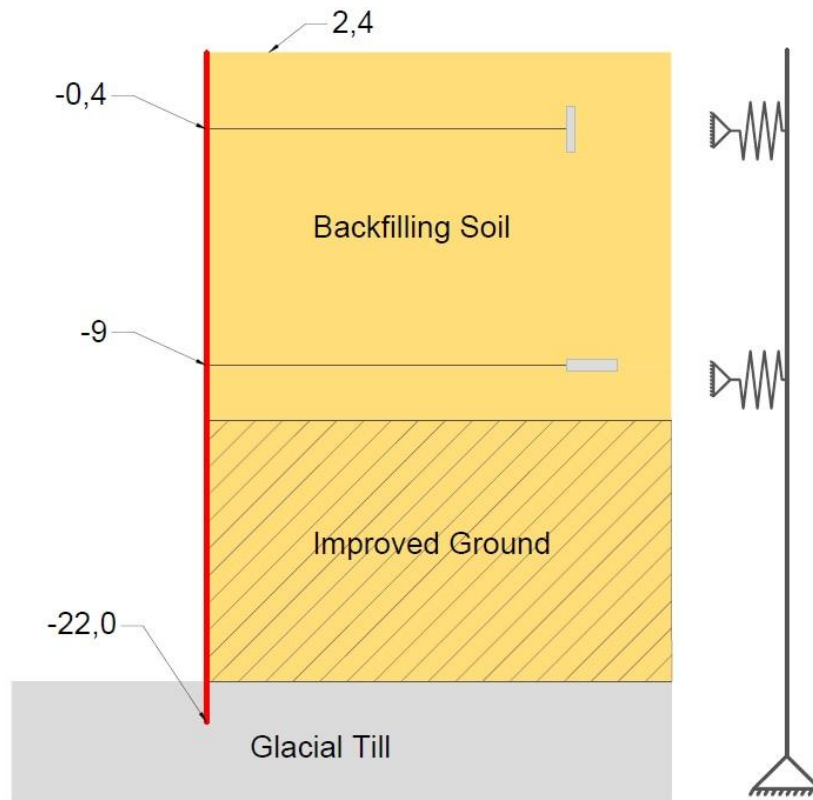


Figure 3.8 - Sketch of the retaining wall system (left) and adopted representative structural model (right)

### 3.5.3. ANALYSIS OF THE RESULTS

The analytical analysis performed to the sheet pile wall is based on a simple adoption of the structural model presented before with lateral earth pressures applied on the wall, calculated using the three different approaches already discussed.

The total lateral earth pressures applied on the wall for each of the approaches are shown in the graph on Figure 3.9 (calculations in Appendix). It is possible to observe that on top the wall the earth pressures are higher for the T&P, while below -3 and -9 m earth pressures are higher for  $K_0$  and  $K_a$ , respectively.

In the layer where the monolith is located, only lateral pressure due to water differential is acting on the wall. As it was assumed in the beginning of this analysis, the monolith is supposed to absorb earth pressures from soil layers above and untreated soil behind the block. Hence, it explains the inexistence of lateral pressures besides the differential water pressure below -11 m.

These diagrams shape were already expected, as lateral pressures calculated by earth pressure coefficients are increased with depth due to overburden. Furthermore, lateral earth pressures present higher values for the situation where at rest coefficient was used, which is valid since  $K_a$  is logically smaller than  $K_0$ .

As the two cases that use earth coefficients to calculate lateral earth pressures have higher values on the bottom of the sheet pile wall compared to the case using T&P diagrams, it can be expected higher forces in the lower anchor level for such situations.

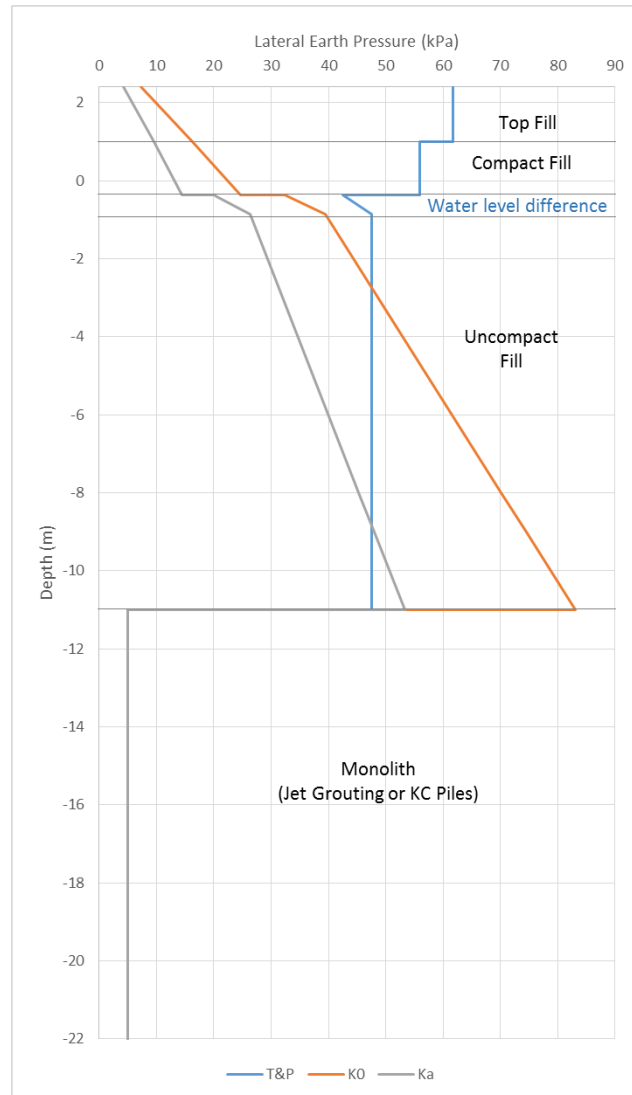


Figure 3.9 - Lateral earth pressures on the wall produced by the three scenarios

For the structural analysis, the retaining wall is studied as a beam subjected to lateral earth pressures. It was then input in structural calculation software with the loads correspondent to the three study approaches.

After running the structural analysis using calculation software (Robot Structural Analysis, by AutoDesk), the obtained bending moments, shear forces and reaction in the supports are shown below in Figure 3.10, Figure 3.11 and Table 3.3, respectively.

By observing Figure 3.10 it is possible to conclude that using Terzaghi & Peck diagrams there is a higher distribution of bending moment along the structure. This is acceptable as T&P diagrams were empirically obtained after observation of strutted excavations, where arching effect and consequent bending moment redistribution are highly present. In the  $K_0$  case maximum values of bending moment are higher than the T&P. It can be noticed as well that bending moments are higher than the  $K_a$  scenario, which is obvious since earth pressures calculated using coefficient  $K_a$  are smaller than in  $K_0$ . In all three cases, extreme bending moments occur in the lower anchors level and in the area between both anchor levels, approximately at same depth.

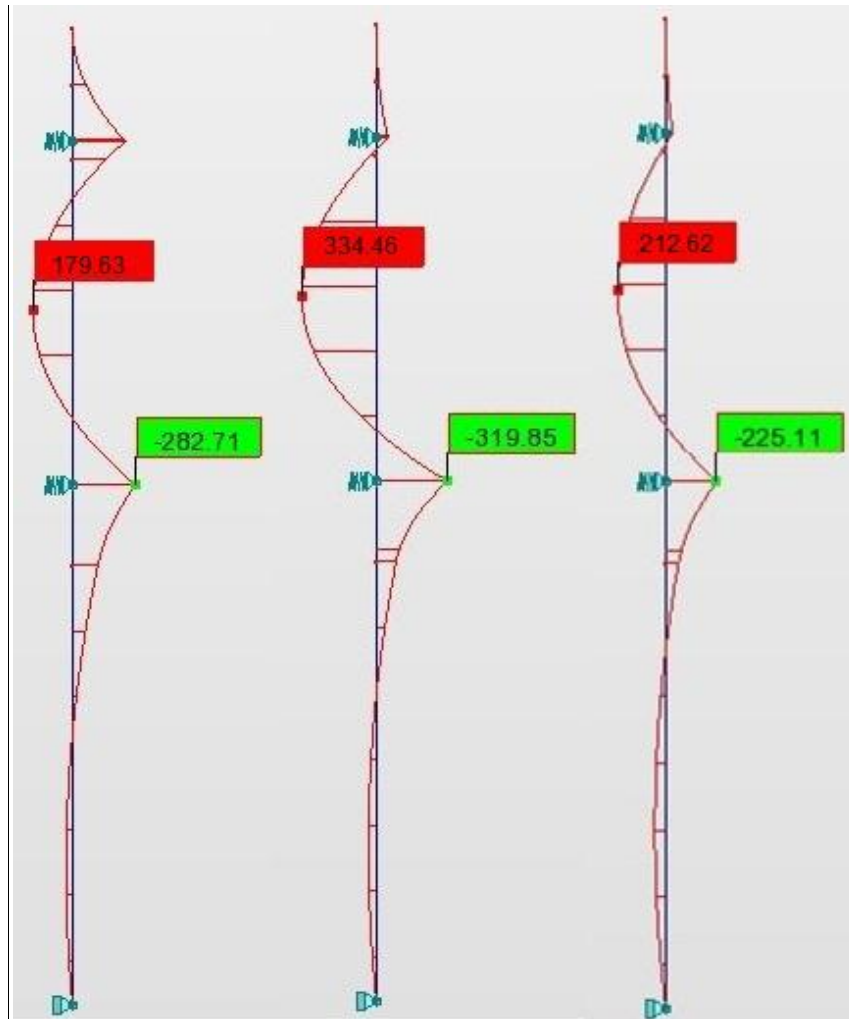


Figure 3.10 - Bending moments (kN.m/m) on the wall for the three case scenarios: T&P,  $K_0$  and  $K_a$  (from left to right)

By examining both Figure 3.11 and Table 3.3 it is possible to verify that again maximum shear force value is higher for  $K_0$  case. Also, reaction forces are approximately the same for both levels of anchorage in T&P case, while for the other situations they are approximately two times higher in lower anchors in comparison to upper anchors. This is expected and can actually be closer to the real forces distribution for situations of backfilling, where arching effects and consequently load distribution to anchors are not as influencing as in excavations.

Another interesting aspect is the total lateral force applied in each case. T&P diagrams have a higher resultant than  $K_a$  and similar to  $K_0$ . Actually, the resultant using T&P diagram is 45% higher than the resultant force from the active lateral earth pressures. This percentage is close to what is stated in Matos Fernandes (1990) that in cohesionless soils, T&P diagrams result in lateral force at least 30% higher than the resultant force due to active earth pressures.

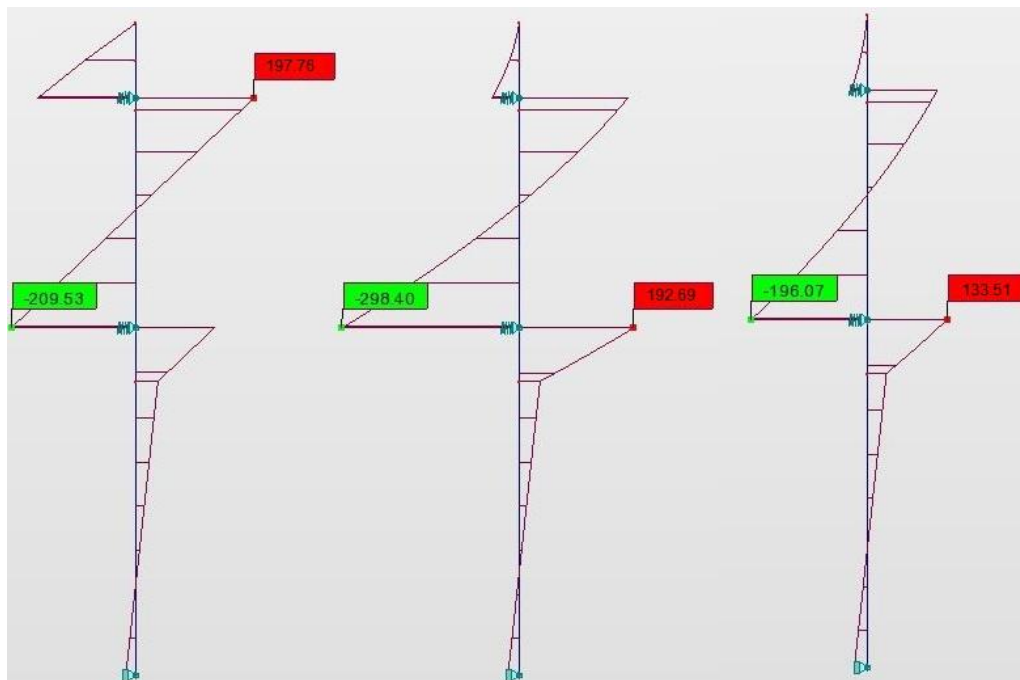


Figure 3.11 - Shear forces (kN/m) on the wall for the three case scenarios: T&P,  $K_0$  and  $K_a$  (from left to right)

Table 3.3 - Reaction forces for the three case scenarios

Reactions (kN/m)	T&P	$K_0$	$K_a$
Upper Anchor	362,00	227,91	143,87
Lower Anchor	341,79	491,09	329,59
Tip	16,72	18,90	21,77
<b>Total</b>	<b>720,51</b>	<b>737,90</b>	<b>495,23</b>

To calculate anchor forces in upper and lower level it is only necessary to multiply the obtained values with by rod spacing. Taking into account the characteristic yielding capacity of the rods specified in the commercial products (see note <sup>3</sup>) and using the basic relation of stress, force and area, one can do simple ultimate capacity verification. The maximum yielding force (with no partial coefficients) of the upper and lower rods is 1845 kN and 2960 kN, respectively. In fact, observing the maximum reaction values of the three cases for both for upper and lower anchors and multiplying by rod spacing, one obtains 1014 kN and 687 kN, respectively. This is an indicator that the stresses are in a safe load field, yet it should be considered that no partial safety coefficients were used.

The obtained wall deformation for three scenarios is represented in Figure 3.12. In all cases the main deformation mode is rotation along the bottom tip of the sheet pile. However, in T&P scenario the top of the wall has the higher deformation value because T&P diagrams consider a constant earth pressure distribution. So as the top is not restrained horizontally and has a higher load compared to the rest of the wall, it is expected that it will have higher lateral movement. On the contrary, for the cases  $K_0$  and

$K_a$  the top has lower deformation, while maximum values of lateral movement occur in the zone of positive bending of the sheet pile.

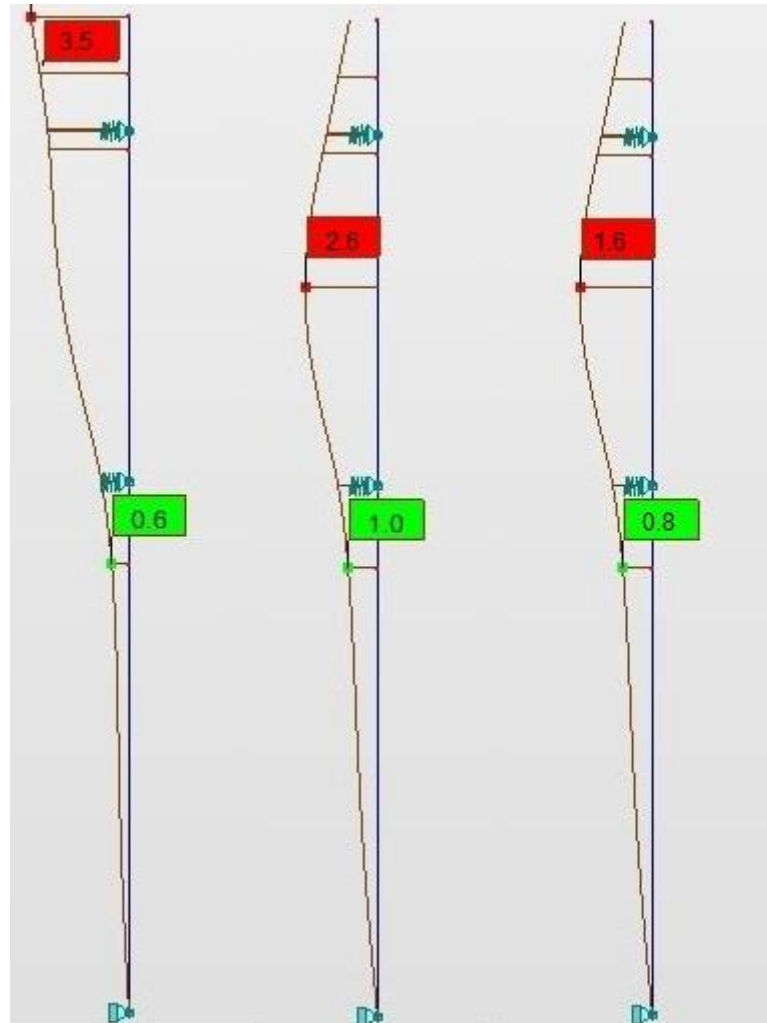


Figure 3.12 - Wall deformation (mm) for the three case scenarios: T&P,  $K_0$  and  $K_a$  (from left to right)

Another important aspect to note is the low deformation in the area right below the lower anchor. This reflects the inexistence of lateral earth pressures representing the absorbing behaviour of the monolith. Actually, in case the anchors' stiffness is higher than expected, it is possible that in this lower zone back bending (wall deforms backwards) may occur, which in extreme values could generate unexpected pressures on the back of the wall due to leaning of sheet pile wall against the monolith.

Having the analytical study of the sheet pile wall, it is possible now to proceed to the three dimensional analysis with a base reference.



## 4

## THREE-DIMENSIONAL MODELLING IN PLAXIS 3D

### 4.1. NUMERICAL ANALYSIS

#### 4.1.1. 3D ANALYSIS

The complex case of a mutually supported corner under backfilling conditions is not a common situation and, as it has already been referred, research around these problems is reduced and practically non-existent in the literature. Retaining structures have been studied mainly in the cases of enclosed excavations. However, the backfilling process is much different and retaining structures under such conditions require separate studies.

The existence of the corner itself intuitively leads to the necessity of a 3D analysis. In these situations the distribution of earth pressures is relevant in all three Cartesian directions, in opposition to the supposed in a 2D plane strain analysis, that the third Cartesian stress perpendicular to the plan (i.e. direction of the infinite length - Figure 4.1) is constant and not used in calculations. Furthermore, the behaviour of the two mutually supported walls is dependent on the interaction between both. So, using two dimensional analysis, the corner (i.e. the two connected walls) mode of deformation is not predictable.

Another relevant aspect that may require a third dimensional analysis is the significant 3D effects that may arise from lateral arching of retained soil and lateral flexure of the wall-waling system, as suggested by Lee et al. (1998). Actually, the simple 2D plane strain analysis does not replicate such lateral action. Therefore, deformations and stresses in the structure may differ from the results of the analytical analysis.

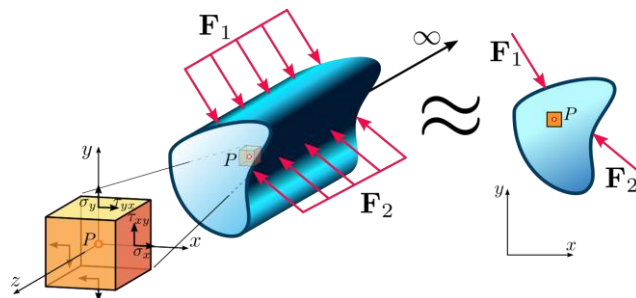


Figure 4.1 - Plane Strain conditions

As summary, 3D analysis is relevant as different levels of deformations, structural forces and earth pressures are expected along the sheet pile wall system.

#### 4.1.2. FINITE ELEMENT METHOD

Due to the already explained complexity of the presented case study a three-dimensional analysis is required, which is the central idea of this thesis. A finite element analysis in a third dimension environment is a complex method to analyse geotechnical problems that consume much time and resources. Therefore, it is normally used in cases where analysis using plain strain or axisymmetric conditions cannot represent accurately the real conditions and boundaries of the problem.

The finite element method is a numerical method of analysis commonly used to solve highly undetermined and complex problems. In Geotechnics it is a usual situation to face this sort of problems that are not accurately solved with simple models. In fact, for the case of multi-propped walls, some authors concluded that simplified methods of analysis where an appropriate calibration of the geotechnical data is made could provide comparable values of bending moment and anchor forces with those of finite element analysis (Carrubba & Colonna 2000). However, simplified methods, such as the Equivalent Tie Support Method (ETM) or the Sub-grade Reaction Method (SRM), do not take into account interactions between soil, wall and anchors, as they assume only the final limit equilibrium condition. Therefore, these do not provide complete information about the variations of soil displacement through all the phases and certainties about global stability, that is worsened for a three dimensional situation.

Although the finite element analysis gives results close to the reality, it is a very sensible method that encloses a correct modelling of boundaries and geometry, an efficient and good quality mesh, the adequate choice on the constitutive models of the soil as well as of the soil parameters.

#### 4.1.3. PLAXIS 3D

The software chosen to perform the required computations was PLAXIS 3D. It is a common and very popular finite element analysis program, specialized in geotechnical applications and with three dimensional capacities. The fact that it provides wide information regarding displacements, stresses and strain in soil and structural elements with a considerable level of accuracy makes PLAXIS 3D an acceptable and desired program in the geotechnical field.

Three types of calculations are possible to perform, namely Plastic, Consolidation and Safety Analysis. For the presented case, plastic calculations are necessary as it is required information regarding movements of soil and stress-strain conditions.

PLAXIS 3D is based in the finite element method with basic equations of static equilibrium and kinematic relations. By associating constitutive relations representative of the soils, it provides a realistic representation of soil behaviour.

The soil is discretised into 10-node tetrahedral element (Figure 4.2). However, structural elements have different types of element. As shown in Figure 4.3, plates have 6-node triangles, while interfaces have 16-node element with pair nodes (two nodes in the same coordinates); beams and node-to-node anchors have 3-node line elements. These differences in element types have to be considered when analysing outputs, because shape functions are different and therefore interpolated results may have different meanings.

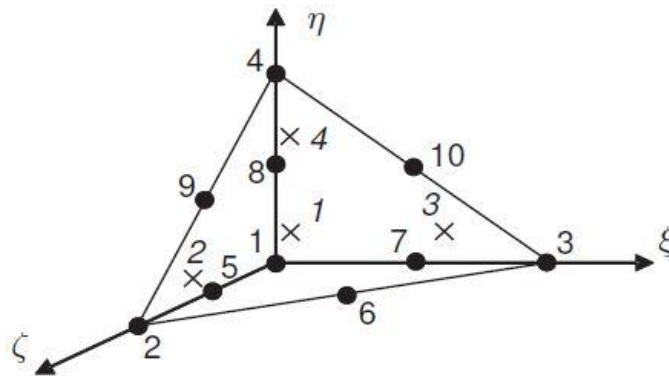


Figure 4.2 - 10-node tetrahedral element used in PLAXIS 3D for soil discretisation (adapted from PLAXIS 2013a)

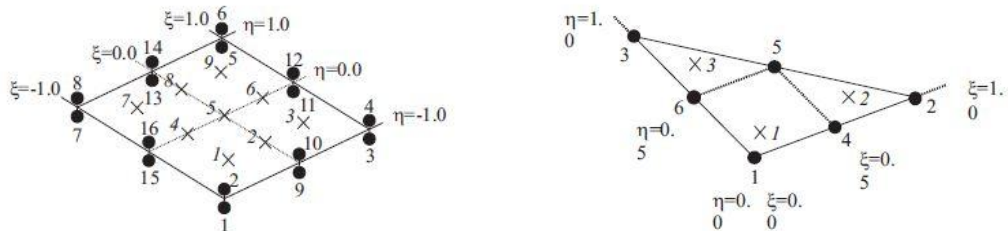


Figure 4.3 - 16-node element used for interfaces (left) and 6-node triangles used for plate elements (right) (adapted from PLAXIS 2013a)

## 4.2. INPUT INFORMATION

### 4.2.1. SOIL LAYERS

The soil volume is composed by three soil layers, shown in Figure 4.4, which are input in the model via representative boreholes, represented in Figure 4.5. The soil profiles used in the boreholes were based on Figure 2.15, after simplifications of layers' thickness. To avoid unnecessary density of images, all boreholes can be found in the Appendix.

The lower layer represents glacial till and develops from the bottom of the model at -25 metres, which represents bedrock, up to a depth varying between -20.5 and -16 metres, depending on the location.

The medium layer is the soft clay, from the top of glacial till up to -11 metres. The material of this layer may change to a material simulating KC Piles or Jet Grouting, depending on the study scenarios that are presented afterwards.

The top layer consists of the fill material, which is deposited in layers and is only existent in the back of the retaining wall. Actually, on site this top layer is constituted by the same material (*Sprängsten*) in three different conditions and therefore these are soil layers with different properties. These layers were detailed in the previous chapter for the analytical analysis, where they were all considered. However, as the named compact fill is only 0.40 metres thick and has the same unit weight as the "uncompact" fill, the layer from surface to depth of -11.0 metres was assumed for the modelling as "uncompact" fill. The material placed on the top deck, over 0.0 metres is replaced by a surface load.

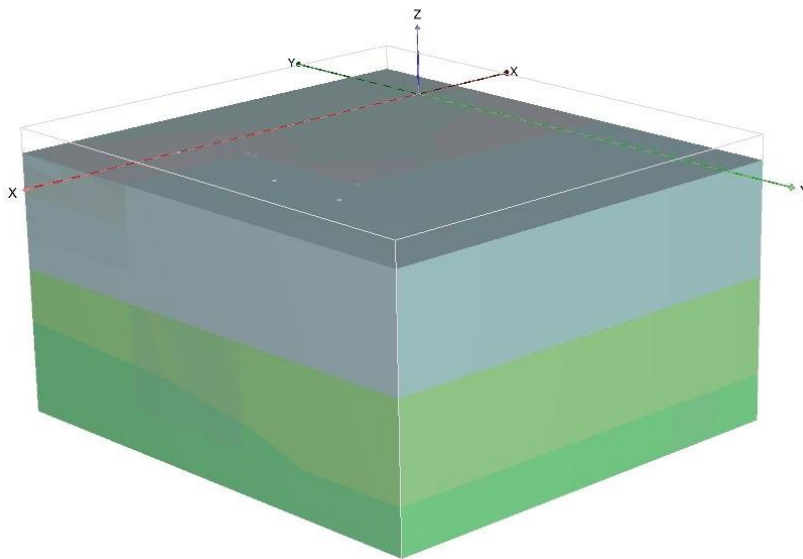


Figure 4.4 - Soil layers in three dimensional display using PLAXIS 3D

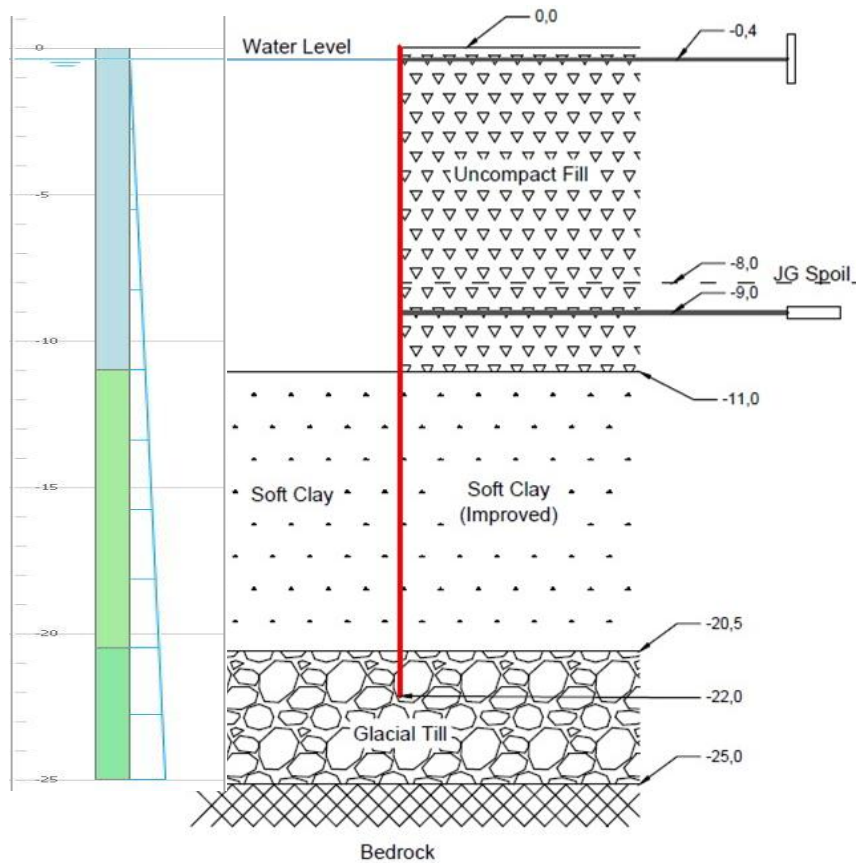


Figure 4.5 - Borehole used to input soil layers in PLAXIS 3D (left) and soil-structure profile (right)

#### 4.2.2. GEOMETRY

The structure used in the present thesis has a geometry that is not symmetric and is very specific. It was based on plans of the Stockholm Port, with approximate dimensions. As described before, the structure is constituted by two walls. Wall 1 has 31 m of length in the model, but is in reality more than four times the length of the smaller wall 2, with 15 m. This limitation in the wall 1 length is due to the boundaries' dimensions chosen to be used in the model

The main wall 1 develops from the surface at  $z=0$  to the glacial till at depth of 22 m, while wall 2 has a decreasing length from the corner to the end of the wall, having the tip at -18 m. This adaptation intends to approximate the model with the real case, where sheet pile walls could not reach the desired depth and have reduced length because glacial till appears at a higher depth (see Figure 4.6)

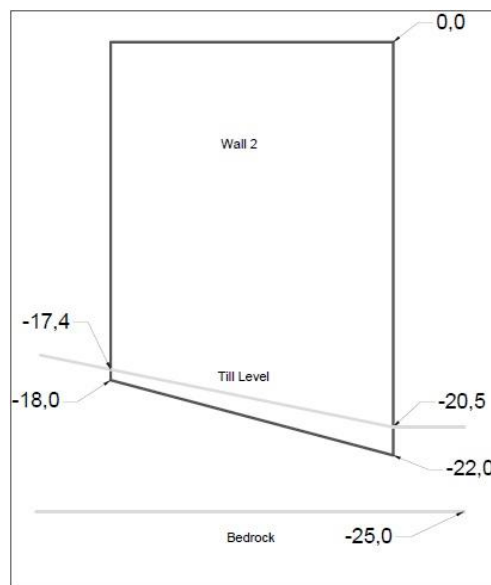


Figure 4.6 - Detailed drawing of wall 2, showing variation of till level.

In Figure 4.7 shows a plan of the retaining walls, as well as anchors distribution in upper and lower levels at depths -0.4 m and 9 m, respectively (see Figure 4.5). The main wall 1 is supported by two levels of anchorages, deadman type. The anchorages in the upper level are spaced by 2.80 m and the rods have lengths up to 50 m, while the rods in lower level are spaced by 1.40 m and have lengths of 25 m.

The retaining walls 1 and 2 are connected perpendicularly by interlocks and mutually supported by 10 tie rods in both upper and lower levels. The interlocks are assumed to be rigid, so the  $90^\circ$  angle should keep the same throughout the loading phase. The gravity wall in Figure 4.7 represents the gravity L walls used in the construction site in specific locations, as described in Figure 2.3. It is mainly responsible for retaining the filling material and although its behaviour may have some influence in the results, as there is a large mass of soil retained, it is modelled as a boundary condition to avoid a complex interaction of effects (see section 4.2.4).

Figure 4.8 shows the modelling of the structural elements using PLAXIS 3D. With this 3D representation it is possible to notice the extra  $30^\circ$  sloping anchor in the top end of wall 2, which provides stability against rotation of the wall system.

The capping beam and the lower waling beam run along perpendicularly to the sheet pile wall, whereas the top waling beam (at -0,4 m) is not applied where mutually supported walls occur, as observed in a visit to the construction site done by the author.

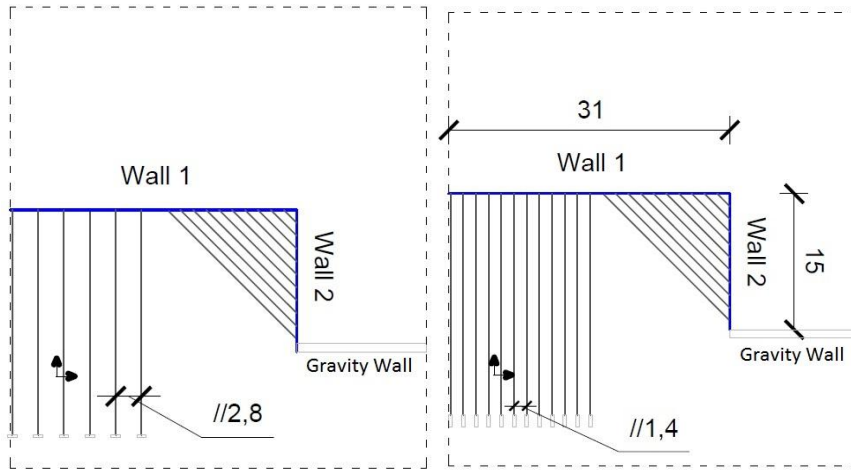


Figure 4.7 - Plan of sheet pile wall and anchors distribution: upper level at -0.4m (left) and lower level at -9m (right)

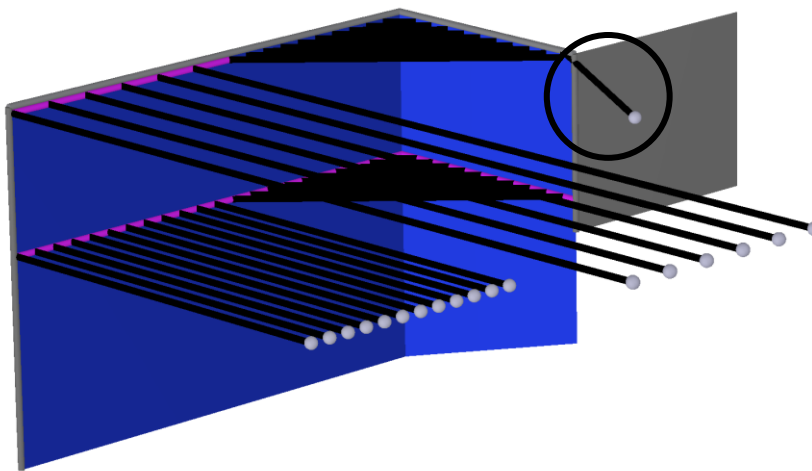


Figure 4.8 - Structural elements modelled in PLAXIS 3D: Sheet pile wall (blue), Gravity wall (grey), Waling (pink) and anchors (black), with highlighting of anchor on wall 2.

#### 4.2.3. STUDY SCENARIOS

To create a better understanding of the behaviour of the structure under scope, three study scenarios were thought and defined:

- No soil reinforcement (NR);
- Soil reinforcement with lime-cement piles (KC);
- Soil reinforcement with lime-cement piles and jet grouting (KC&JG).

These cases differ only on the ground improvement conditions, as all structure properties and geometry stay the same. By taking in consideration the soil profiles and the top views, the explanation of the three study scenarios becomes simpler.

In Figure 4.9 is shown the first case where no reinforcement is applied to the soil (scenario NR). It is used to understand the three dimensional effects caused by the existence of a corner. By studying how the soil-structure interaction works in such conditions, it is possible to understand and figure out which mechanisms of load transfer may be present in the soil and in the structure itself.

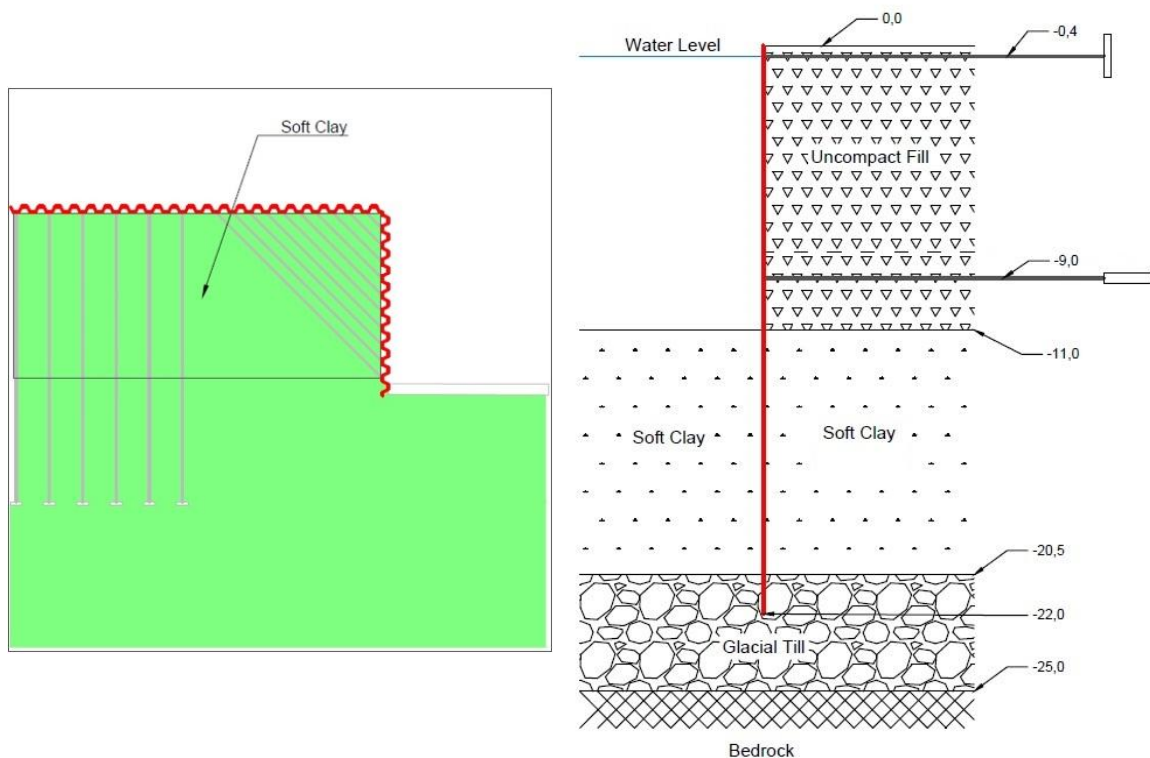


Figure 4.9 - Scenario with no reinforcement: left - top view at depth -14m and right - general cross section

In the second situation, represented in Figure 4.10 and in Figure 4.11, the soil is reinforced only with lime-cement piles along the area next to the wall (scenario KC). Basically, all the seabed soft clay is mixed with lime-cement applied with deep mixing technique and consequently gets different geotechnical properties. This way, one can comprehend how improved ground may affect the soil-structure interaction and the stresses distribution in the structural elements. Comparing with the scenario without soil reinforcement, it is possible to obtain improvement ratios and stresses reduction coefficients, which may lead to different design approaches.

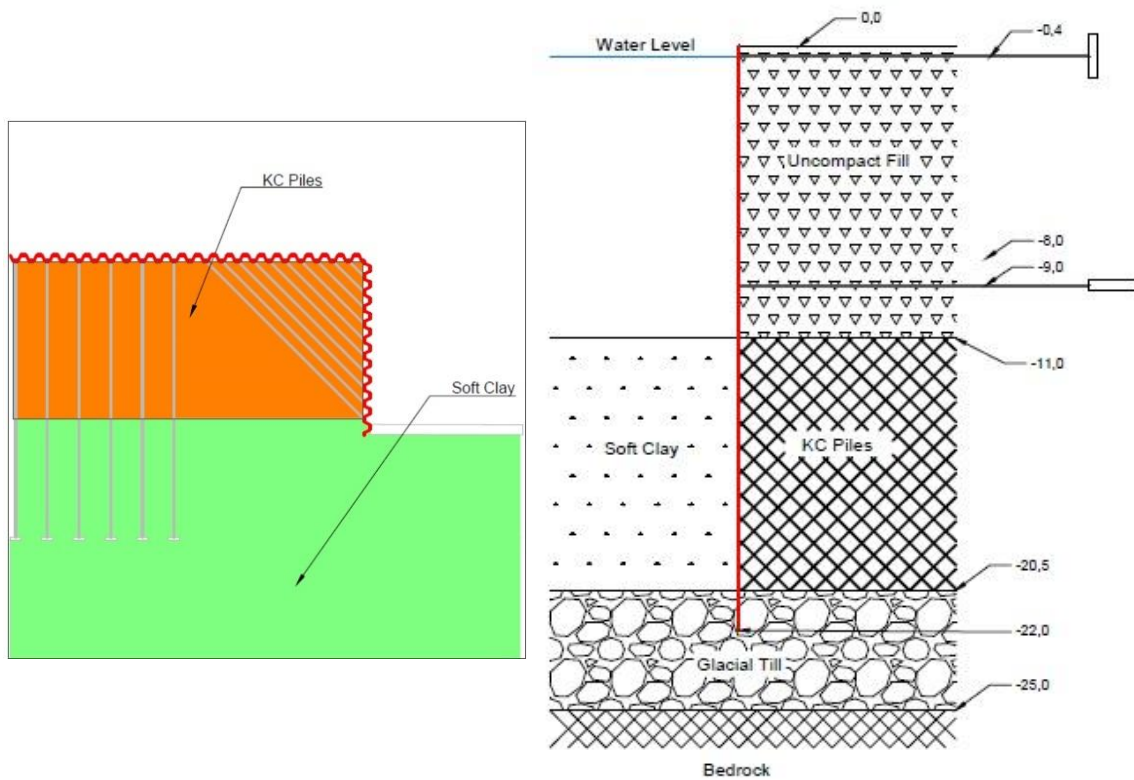


Figure 4.10 - Scenario with KC Piles: left - top view at depth -14m and right - general cross section

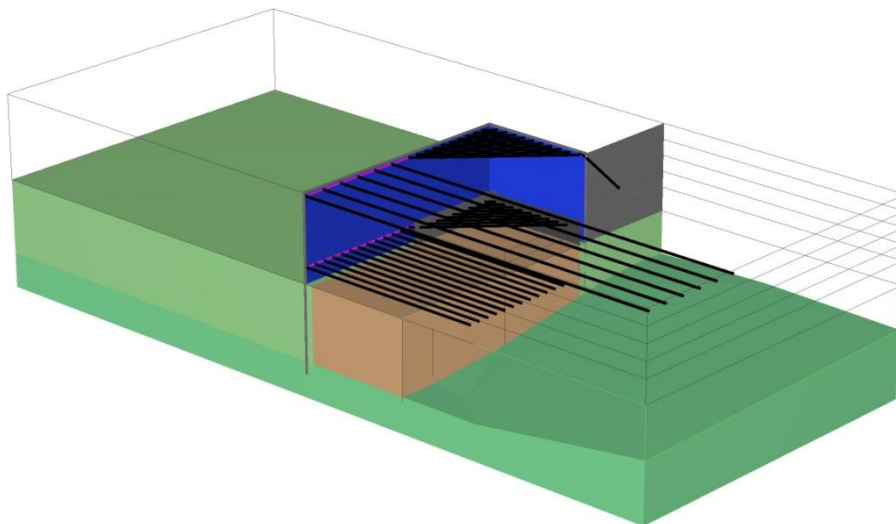


Figure 4.11 - 3D representation of KC scenario, showing the KC Piles (brown)

In the last study scenario, represented in Figure 4.12 and Figure 4.13, the real *in situ* conditions are modelled, reflecting the example case (Värtahamnen Port). KC piles are applied along the wall, but in the corner, where tie rods are located, jet grouting is implemented (scenario KC&JG). Comparing with the previous scenario, it can be observed if the application of jet grouting provides considerable benefits to the wall stability or if it is too conservative. It is important to note that in the KC&JG study

scenario, the spoil created by the jet grouting ascends up to -8 metres, reducing the thickness of the fill layer.

The two scenarios KC and KC&JG face difficulties when being modelled in PLAXIS 3D. In reality the reinforced soil is composed by a group of piles close to each other. Therefore, the treated mass will behave as a composition of KC or jet grouting piles and untreated soil in between. However, it has been observed in some reports that to simplify this problem equivalent properties of the composite ground can be used in the analysis while still providing satisfactorily results compared with observed values (Ou et al., 2008). Consequently, in these situations the author opted to model the reinforced soil as a soil mass with equivalent improved properties,

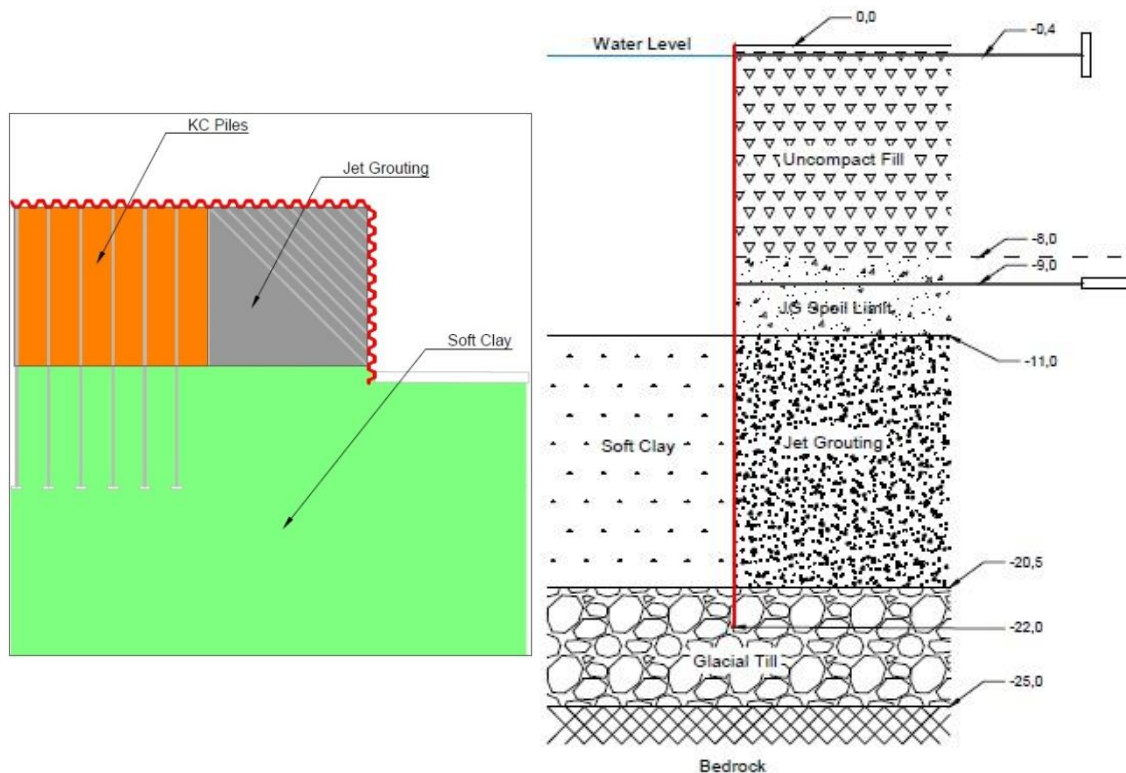


Figure 4.12 - Top view of the scenario with KC Piles with Jet Grouting reinforcement (KC&JG) at depth -14m and general cross section

Another aspect to take into account is the construction procedures of such ground improvements. For example, the piles should be placed far from the wall, to avoid any deformation due to too wide grouting. In reality, it was observed on site that while applying the jet grouting piles, the sheet pile wall showed deformations up to 40 cm, which is a rather relevant value. Yet, during the modelling it was assumed no initial deformation of wall due to grouting.

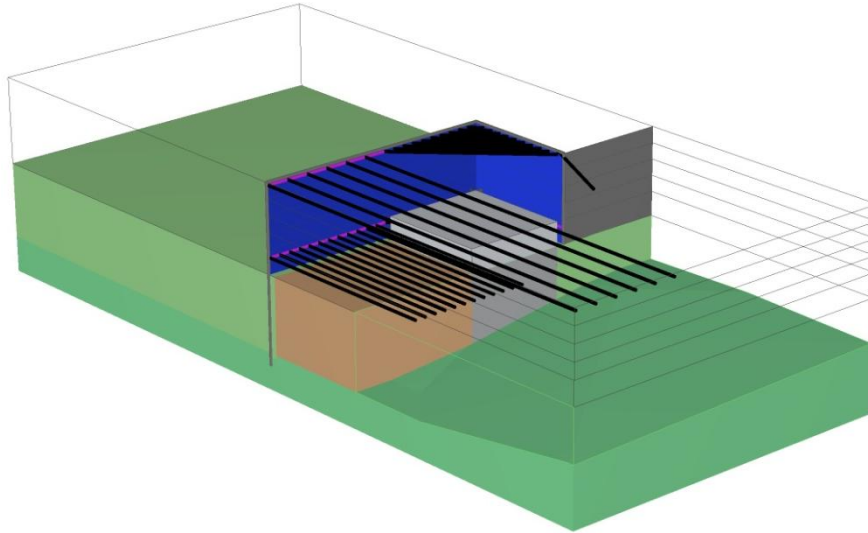


Figure 4.13 - 3D representation of KC&JG scenario, showing the KC Piles (brown), jet grouting (dark grey) and spoil (light grey)

#### 4.2.4. BOUNDARY CONDITIONS

The boundary conditions in the limits of the model are set by default to the following configuration:

- Vertical boundary planes are fixed in the perpendicular direction, but free in plane vertical and horizontal directions, i.e. boundaries with their normal in X-direction have  $u_x = 0$  and boundaries with their normal in Y-direction have  $u_y = 0$ ;
- Bottom boundary plane is fixed in all direction ( $u_x = u_y = u_z = 0$ );
- Ground surface is free in all directions.

The limits of the model were defined to  $x_{\min} = -5$ ;  $x_{\max} = 40$ ;  $y_{\min} = -30$  and  $y_{\max} = 70$ , as schemed in Figure 4.14. Such values were obtained after trials so that a plane strain deformation state at all vertical model boundaries was achieved and boundaries conditions would have low influence on the results.

The boundaries perpendicular to Y-direction and the boundary at  $x = -5$  should be carefully chosen and understood. First, the boundaries at  $y_{\min} = -30$  and  $y_{\max} = 70$  were chosen so that there would exist enough space to model the anchors as well as to provide place for the occurrence of a passive failure slip in the till. The necessary distance  $D$  for these failure curves to happen can be approximately determined *a priori* using the equation (4.1), where  $H$  is the high of soil layer with failure and  $\varphi$  is the friction angle.

$$D = H * \tan\left(45 + \frac{\varphi}{2}\right) \quad (4.1)$$

The boundary at  $x = -5$  is crucial as this must represent plane strain deformation conditions. Otherwise, the results will come highly influenced by the movement restriction provided by the default boundary settings. However, it should be reduced to a minimum amount of structural elements, in order to decrease computation time. The necessary conditions are achieved at the plane strain deformation cross section (PSD), which is demonstrated in Chapter 5.

An important aspect not yet described is the connection between the sheet pile wall and the existent gravity wall. Actually, wall 2 is assumed as being simply supported by the gravity wall and its movement in the backend prevented in X-direction. However, as it is not of interest studying the gravity wall and taking into account that its movements will not affect largely the structure's behaviour, L walls were modelled as surfaces with both movements in X- and Y-direction fixed. Only settlement in Z-direction is allowed (see Figure 4.15).

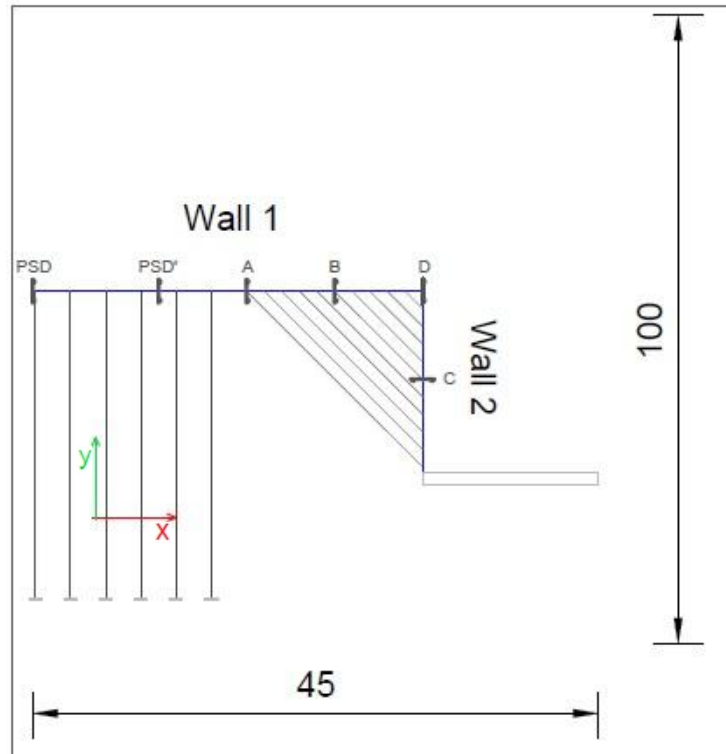


Figure 4.14 - Horizontal plan describing the lengths of the model's borders

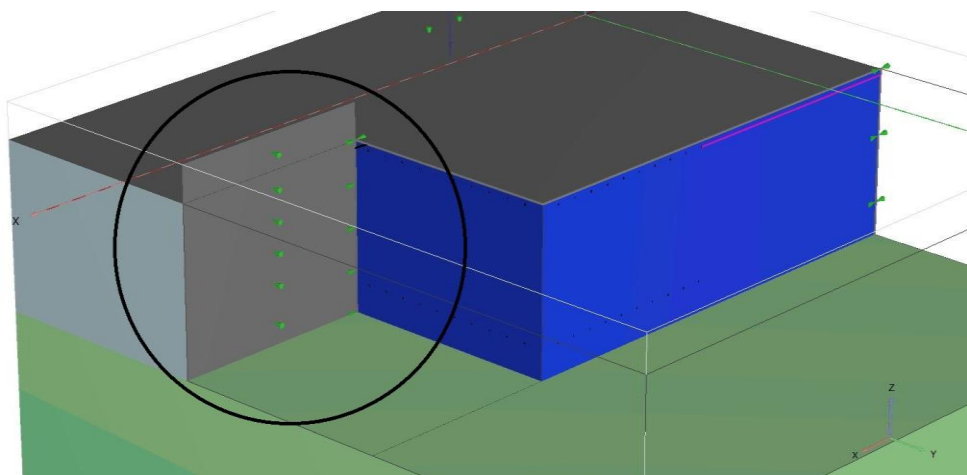


Figure 4.15 - Detail of the surface with fixed displacements in X- and Y-directions, simulating L gravity wall

#### 4.2.5. SOIL MODELS AND PARAMETERS

In order to obtain an acceptable output from any computation it is necessary to have selected adequate constitutive laws that represent accurately the soils' behaviour in the model.

Among the available soil models, the simple elastic-plastic model with Mohr-Coulomb (MC) failure criteria was chosen for all types of soil. This model is a constitutive soil model that provides a simple representation with need for few and easily obtained parameters, such as friction angle ( $\varphi$ ), dilation angle ( $\psi$ ), cohesion ( $c$ ), *poisson* coefficient ( $\nu$ ) and elastic modulus ( $E$ ). Due to its simplicity based on perfectly elastic-plastic behaviour, it is normally used to perform faster initial approximate calculations before opting for more complex soil models (see Figure 4.16). However, it may not provide accurate and so realistic behaviour in some kinds of soil such as in normal consolidated clays, where some hardening may occur. In this case, other models such Soil Hardening or Soft Soil Creep could be used to obtain a closer behaviour to reality, yet in detriment of computation speed (PLAXIS 2013b). Besides, such models require advanced parameters that need to be determined with more soil tests and afterwards calibrated to the model.

Despite the fact that these models should be used for representing the clay layer, the author still opted to use Mohr-Coulomb because it was intended an initial approach to the problem.

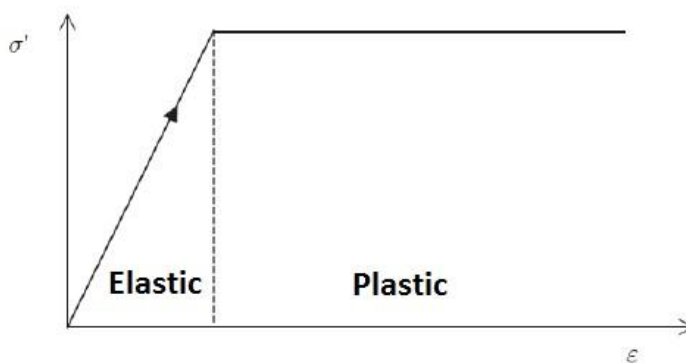


Figure 4.16 - Diagram representative of perfectly elastic-plastic model (PLAXIS 2013b)

For the soil mass representing soil improvement with lime-cement piles (KC Piles) was also used MC model. However, for modelling jet grouting and the grout spoil a linear elastic model was chosen. This choice was based on the assumption that the monolith will not plastify and there will be no internal rupture. In reality this assumption is not correct, but as the yielding of the grouting occurs much later than the soil and the objective is to study soil behaviour, it is an acceptable option.

In Table 4.1 are described all soil parameters that were used in the input of PLAXIS 3D. Most of the values were based on provided information by COWI, regarding soil *in situ*. However, *Poisson* ratio values were obtained from average observed values in the literature. As no information regarding the coefficient of earth pressure  $K_0$  was provided, it was set to *Auto* in PLAXIS 3D, which means that the program automatically computes this value based on Jaky's formula, in equation (3.3).

Fill and glacial till are described as having a drained behaviour, whereas clay and improved clay (KC Piles) appear to show undrained conditions, due to low permeability. Therefore, in these materials undrained properties should be used, as described in Table 4.2, instead of the initially presented drained parameters in Table 4.1.

Table 4.1 - Input soil parameters used initially in the model

Soil	Unit Weight, $\gamma$ (kN/m <sup>3</sup> )	Poisson ratio, $\nu$	Friction Angle, $\varphi$ (°)	Cohesion, $c$ (kPa)	Oedometric modulus, $E_{oed}$ (MPa)
Clay	12,82	0,4	27,6	0,85	310
Fill	21	0,2	38	0,001	10
Glacial Till	21	0,3	40	0,001	100
Jet Grouting	24	0,1	N/A	N/A	$3,17 \times 10^7$
JG Spoil	22	0,1	N/A	N/A	$2,56 \times 10^7$
KC Piles	14	0,15	36,8	46	16500

The friction angle and cohesion, resultant of interpretation of geotechnical tests, are used without application of specific partial factors and thus are characteristic values. For purely frictional soils cohesion value is 0,001 because PLAXIS shows numerical issues if the cohesion is null.

Table 4.2 - Input undrained soil parameters

Soil	Undrained shear strength, $c_u$ (kPa)
Clay	8,68
KC Piles	104,1

Another parameter that needs to be introduced in the material information for granular materials is the dilation angle  $\psi$  (Figure 4.17). This characteristic is particularly important in plastic analysis using Mohr-Coulomb model as it is associated with volume deformations in plastic domain. The dilation angle indicates how the soil volume changes with shearing, which means that positive dilation angle will result in volume increase in a pure shearing condition.

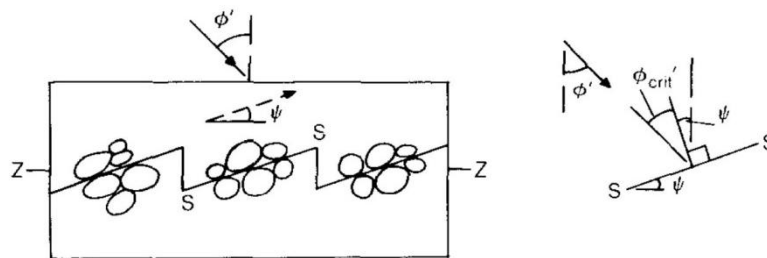


Figure 4.17 - Concept of dilation angle

The granular fill is simply deposited (i.e. no compaction) thus initial void ratio is smaller than the critical, typically close to the unity. After loading resultant from the weight of soil layers placed above, void ratio will reduce until it reaches (if it really does) critical state (see Figure 4.18). Therefore, the dilation parameter, which in Figure 4.18 is represented by  $\Psi$  ( $e - e_{crit}$ ), is positive, so the

soil is contractive. Consequently dilation angle will be negative, which means reduction of volume. So, dilation is assumed to be zero in the granular materials as the settlement is not relevant for the studies in the present thesis.

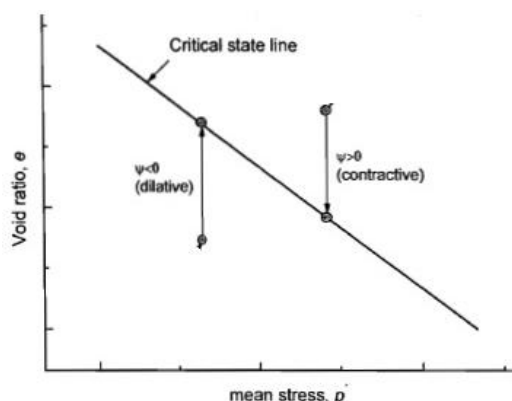


Figure 4.18 - Critical State line

Regarding the *Poisson* ratio, it is relevant to refer that clayey soil show a higher value than granular soil. As glacial till can be assumed as a mixture of both types of soil and based on commonly used values, an average ratio was chosen. Concerning more rigid structures like the jet grouting and the KC Piles, typical values of concrete were input.

It is important to denote that Oedometric (or Constrained) Modulus,  $E_{\text{oed}}$ , is obtained after *in situ* geotechnical tests. The Young Modulus,  $E$ , is then derived from the equation (4.2).

$$E_{\text{oed}} = \frac{(1-\nu) \cdot E}{(1-2\nu) \cdot (1+\nu)} \quad (4.2)$$

#### 4.2.6. STRUCTURES AND INTERFACES

The elements in PLAXIS 3D used to represent the retaining wall and the anchors were plate elements and node-to-node anchors, respectively. To simulate no-displacement deadman anchors, fixed displacement nodes were used, as anchors displacement are not under study. For the capping and waling beams, beam elements were chosen.

In Table 4.3 are presented the real element description. The sizes and type of the elements were based on information about the construction site used as example, which was provided in an internal document of COWI. It was decided to use similar sheet pile walls, beams and anchors profiles so the analysis could provide an acceptable representation of the real structure, in order to the results to be useful.

Plates and beams were modelled using purely elastic models. However, anchors were modelled with elastic-plastic models, with yielding tensile strength of 1877 kN and 1312 kN for lower and upper anchors, respectively. To simulate failure to buckling, yielding compressive strength was set to 1 kN, because PLAXIS does not accept 0 kN.

Table 4.3 - Description of structural elements used *in situ*

Element	Description	Material
Waling	2x UNP 400	Steel S355
Sheet Pile	AZ 46-700	Steel S430
Upper Anchor Rods	SAS 670/800 ( $\phi 63,5$ )	Steel 670/800
Lower Anchor Rods	SAS 670/800 ( $\phi 75$ )	Steel 670/800
Capping	Beam (1,00x1,00)	Concrete

The input parameters for the structural elements are shown in Table 4.4. The required parameters are unit weight, *Poisson* ratio, elastic modulus, area and inertia  $x$  and  $y$ ,  $I_2$  and  $I_3$  in PLAXIS, respectively.

Table 4.4 - Input structural element parameters used in the model

Element	Unit Weight, $\gamma$ (kN/m <sup>3</sup> )	Poisson ratio, $\nu$	Elastic Modulus, $E$ (kPa)	Area, $A$ (m <sup>2</sup> )	Inertia $y$ , $I_2$ (m <sup>4</sup> )	Inertia $x$ , $I_3$ (m <sup>4</sup> )
Waling	77	0,3	$2,10 \times 10^8$	$1,82 \times 10^{-2}$	$3,00 \times 10^{-5}$	$4,07 \times 10^{-4}$
Sheet Pile	3,15	0,3	$2,00 \times 10^8$	$2,87 \times 10^{-2}$	N/A	N/A
Upper Anchor	78	0,3	$2,00 \times 10^8$	$3,17 \times 10^{-3}$	$7,98 \times 10^{-7}$	$7,98 \times 10^{-7}$
Lower Anchor	78	0,3	$2,00 \times 10^8$	$4,42 \times 10^{-3}$	$2,00 \times 10^{-6}$	$2,00 \times 10^{-6}$
Capping	25	0,1	$3,00 \times 10^7$	1,0	$8,33 \times 10^{-2}$	$8,33 \times 10^{-2}$

When doing the input of the structure parameters, some adaptations had to be made, such as in the plate elements representing the sheet pile wall. In Table 4.5 are described specific input parameters of plates.

Table 4.5 - Adapted input parameters for sheet pile

Element	$E_1$ (kN/m <sup>2</sup> )	$E_2$ (kN/m <sup>2</sup> )	$G_{12}$ (kN/m <sup>2</sup> )	$G_{13}$ (kN/m <sup>2</sup> )	$G_{23}$ (kN/m <sup>2</sup> )	$E'A$ (kN)
Sheet Pile	$2,20 \times 10^7$	$1,10 \times 10^6$	$1,10 \times 10^6$	$1,47 \times 10^6$	$4,41 \times 10^5$	N/A

To obtain the equivalent properties of the sheet pile AZ 46-700, the true values of the sheet pile were input in a transformation spreadsheet provided by the developer of PLAXIS. The calculations occurring in this transformation are based in the equations (4.3) to (4.7), where  $E_{steel}$  is the elastic modulus of steel,  $E_1$ ,  $E_2$ ,  $G_{12}$ ,  $G_{13}$  and  $G_{23}$  are calculation parameters,  $I_1$  is inertia and  $d$  the section height, equivalent to  $h$  in Figure 4.19.

$$E_1 = \frac{12 \times E_{steel} I_1}{d^3} \quad (4.3)$$

$$E_2 = \frac{12 \times E_{steel} I_2}{d^3} \quad (4.4)$$

$$G_{12} = \frac{6 \times E_{steel} I_{12}}{(1 + \nu_{steel}) d^3} \approx \frac{6 \times E_{steel} \times I_1}{10 \times d^3} \quad (4.5)$$

$$G_{13} = \frac{E_{steel} A_{13}}{2 \times (1 + \nu_{steel}) d} \approx \frac{E_{steel} \times A}{6 \times d} \quad (4.6)$$

$$G_{23} = \frac{E_{steel} A_{23}}{2 \times (1 + \nu_{steel}) d} \approx \frac{E_{steel} \times A}{20 \times d} \quad (4.7)$$



Figure 4.19 - Horizontal cross section of idealized sheet pile

The correct interaction between soil and sheet pile wall has to be modelled using an interface. This interface, characterized for having pair nodes in the area elements, will provide a better simulation of the thin layer between the sheet pile wall and the soil. Interfaces use similar soil models to reproduce its real behaviour. For the case of Mohr-Coulomb model, the interface friction angle input represents in reality the skin friction of the sheet pile wall, i.e. the roughness of steel.

For this model, the model and parameters of interfaces are set to be the same as the adjacent soil. However, the skin friction angle representing roughness between the sheet pile wall and soil mass will be  $2/3$  of the soil friction angle, which is set when describing interface strength properties for each soil. In equation (4.8),  $R_{inter}$  symbolizes the variation factor of the strength parameters represented by the friction angle,  $\varphi$ . Therefore, using the suggested value will result in the reduction of resistance in the interface elements. This value was initially chosen based on reviewed literature (PLAXIS 2013a) and experience of the author. Although it is a high value, as roughness between sand and steel plate may vary from 0 to 0.5, it was suggested as a first approach taking into account corrosion of steel plate and Z shape of the sheet pile wall. However, the roughness value should be subject of a parametric study, to understand its influence in the behaviour of the wall and load distribution.

$$\tan(\delta) = \tan(\varphi) \times R_{inter} \quad (4.8)$$

For the situation of rigid structures such as the Jet Grouting monolith and the KC Piles,  $R_{inter}$  is the unitary value because it is assumed that both types of material do not have reduced strength in interfaces.

#### 4.2.7. LOADING AND STAGES OF CONSTRUCTION

As the structure behaviour is highly dependent on the construction process, it was necessary to apply different loading phases to simulate initial conditions, implementation of anchors and sheet piles, jet

grouting, application of KC Piles and backfilling by layers. So, seven stages of construction were configured in the model for the three study scenarios. In Table 4.6 is a description of the different phases of loading and in Figure 4.20 a 3D representation.

It is important to note that lime-cement columns are applied before driving the sheet pile walls in place and jet grouting is done afterwards, as described on site. The backfilling material is deposited on layers of two metres, although first layer is three metres thick. Also, the capping beam is only activated before filling the last two metres. In reality, the capping beam uses the last layer of filling material as base for the concrete deployment, so it should simulated similarly.

Table 4.6 - Description of phases of construction for each study scenario

Phase	NR	KC	KC&JG
Initial Phase	Initial Stress State	Initial Stress State	Initial Stress State
P1	Sheet Pile Wall, Waling Beam and Corner Ties	KC Piles	KC Piles
P2	Anchors	Sheet Pile Wall, Waling Beam and Anchors/Ties	Sheet Pile Wall, Waling Beam, Jet Grouting (w/ spoil) and Anchors/Ties
P3	Fill 3 m (to -8m)	Fill 3 m (to -8m)	Fill 3 m (to -8m)
P4	Fill 5 m (to -6m)	Fill 5 m (to -6m)	Fill 5 m (to -6m)
P5	Fill 7 m (to -4m)	Fill 7 m (to -4m)	Fill 7 m (to -4m)
P6	Fill 9 m (to -2m)	Fill 9 m (to -2m)	Fill 9 m (to -2m)
P7	Fill 11 m (to 0m) and capping beam	Fill 11 m (to 0m) and capping beam	Fill 11 m (to 0m) and capping beam
P8	Surface loading 90kPa	Surface loading 90kPa	Surface loading 90kPa

Over the top layer is applied a surface loading which represents the application of the 2,4 m layer of fill material above deck in combination with an equivalent load representative of differential water load and traffic loads. In total, the final surface loading applied is 90 kPa, providing a conservative load case scenario.

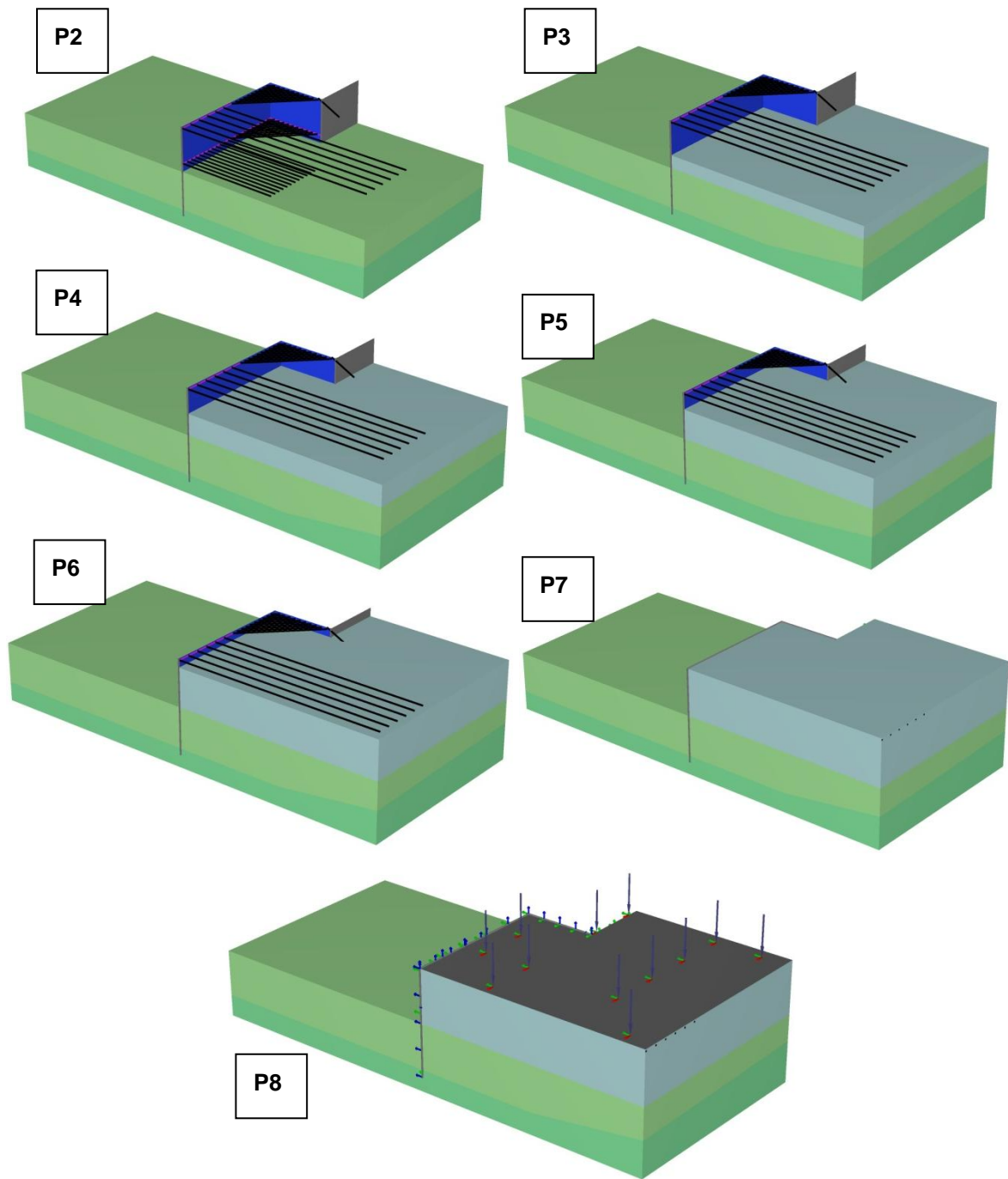


Figure 4.20 - Loading phases 3 to 8 for the no reinforcement case (NR)

## 5

## ANALYSIS OF RESULTS

## 5.1. METHODOLOGY

To fully understand and comprehend the case study, it is necessary to choose the relevant information to extract from the output of computations provided by PLAXIS 3D. These must provide a clear and simple view of the wall behaviour and soil-structure interaction. Therefore, an important aspect to examine is the deformation mode of wall system (i.e. wall 1 and wall 2). The wall movements can then be related to the distribution of stresses in the structural system, which is significant information to this study.

Also, information of high relevance is the reduction of lateral earth pressures that is expected to occur on the sheet pile wall. One of the first assumptions made before studying this case was the transfer of loads from the soil mass above and behind the monolith to the bearing stratum (glacial till and bedrock), for the situation KC and KC&JG. This load transfer mechanism should be verified by studying the stress distribution inside the block.

Table 5.1 shows a summary of the cases explained in Chapter 4, which are throughout this chapter analysed and compared. Firstly, the base situation with no soil reinforcement (NR) is deeply scrutinized, followed by a less detailed study of the cases with soil reinforcement, KC and KC&JG.

Table 5.1 - Three cases (NR, KC and KC&JG) analysed with PLAXIS 3D

Case	Abbreviation	Description
No soil Reinforcement	NR	Model with no soil reinforcement
KC Piles Reinforcement	KC	Model with lime-cement piles (KC Piles) reinforcement
KC Piles and Jet Grouting Reinforcement	KC&JG	Model with lime-cement piles reinforcement and jet grouting near the corner

## 5.1.1. CROSS SECTIONS

In order to obtain a clear visualization of the results and progress along the wall development, several key cross sections were selected. These cross sections, with the location as in Figure 5.1, are distributed along the wall and are expected to represent all the relevant aspects introduced before.

The cross section PSD, with coordinates (-5;20), works as the reference section with plane strain deformation conditions. This section is accepted as so based on initial larger models that showed that at  $x=-5$  m deformation in Y-direction was practically uniform, hence in plane strain. Consequently, section PSD is assumed to represent a state of plane strain. Cross sections A (12;20), B (19;20) and D (26;20) are equally spaced along Wall 1, in the region where the walls are mutually supported. With these three sections it is possible to observe any changes related to distance from the corner. An extra section PSD' (5;20) may be used in situations where the transition from anchored wall to mutually supported wall should be considered.

To observe the deformation mode of the sheet pile corner it is enough to study cross section C (26;12.5), which will be representative of wall 2.

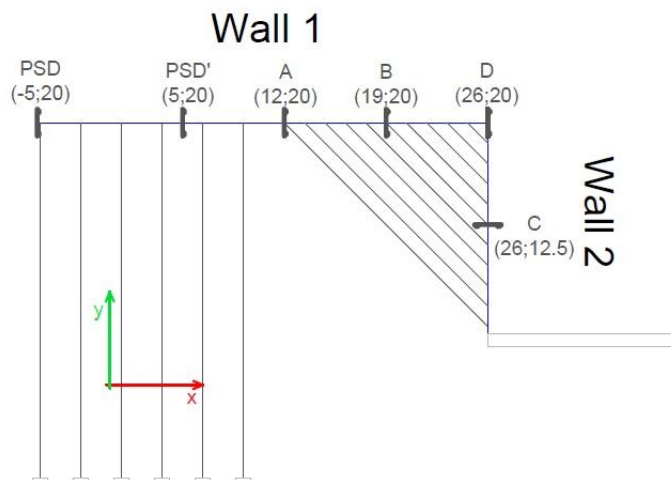


Figure 5.1 - Location of selected cross sections

### 5.1.2. EXTRACTION OF EARTH PRESSURES

Initially, lateral earth pressures were extracted using the interface that was applied between the sheet pile wall and the soil. The advantage with this method is that the interface element in PLAXIS 3D allows extraction of normal stresses acting on the element, which are coincident with the lateral earth pressures acting on the sheet pile wall. However, these often show many numerical peaks, resulting from interpolations of stresses between nodes. In such situations, the results are impractical as they show many fluctuations. They may even be useless without any mathematical data processing.

To go around the explained problem, it was thought to obtain the lateral earth pressures from two vertical cross sections at different distances from the sheet pile wall, 0.5 m and 0.05 m. These two distances are compared to see if there are any relevant changes in earth pressure values and if there are numerical advantages.

The comparison between the three extraction methods is shown in Figure 5.2. As observed, values obtained in the interface show high fluctuations and it is not practical to use them. Additionally, it should be noted that the earth pressure diagram from the interface shown is not the raw diagram extracted from PLAXIS 3D. In fact, for the results to be readable they had to be mathematically processed to remove repeating values and zero stress points.

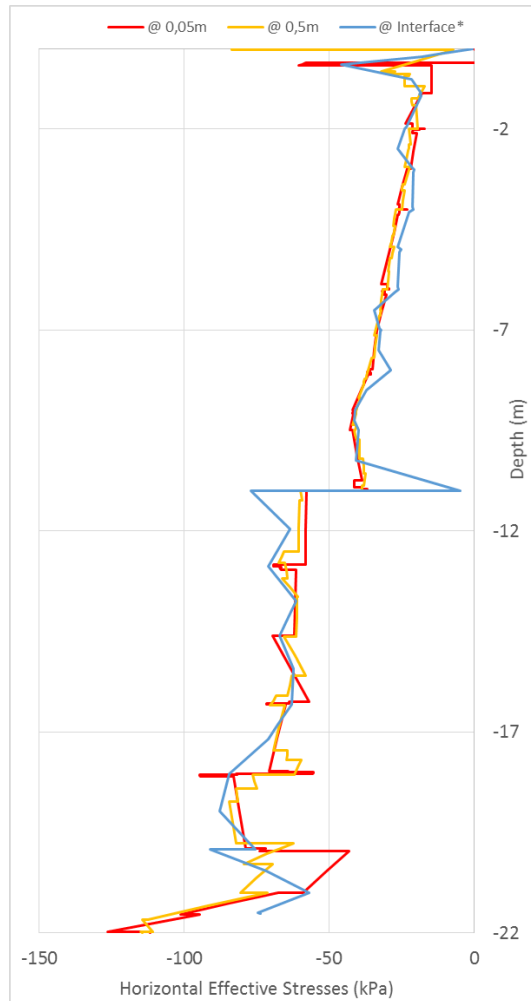


Figure 5.2 - Horizontal effective earth pressures extracted in three different locations: at the interface, at 0.05 m and at 0.5 m from the wall

With no further data processing, the earth pressure diagrams at 5 cm and 50 cm from the wall still show some numerical interference. However, it is important to understand that, initially, a qualitative study is more relevant than a quantitative study, as this is a specific and particular situation representing an existing project. Therefore, it is intended to obtain tendencies and approximate values for comparison. So, among the two methods of extraction of earth pressures, the author opted to search at a distance of 0.5 m from the wall because it shows less numerical variation, though the differences in comparison with the extracted profile at 0.05 m are not as relevant.

## 5.2. VERIFICATION OF THREE DIMENSIONAL EFFECTS

As it was stated before in the introductory chapters of this work, it is expected effects resulting from three dimensional phenomenon, such as arching effect and structure stiffening due to horizontal structural elements. Therefore, it was necessary to verify the existence of these effects and compare them with the expected, based on the reviewed literature. Only by verifying and observing such occurrences in the simple scenario with no soil reinforcement (NR) it is possible to understand the 3D interaction of the soil-structure.

Firstly, the deformations of the sheet pile wall were analysed. The PSD section was compared with section A (12;20), B (19;20) and D (26;20). Results are presented in Figure 5.3 in terms of wall deformation normalized to wall height, in percentage.

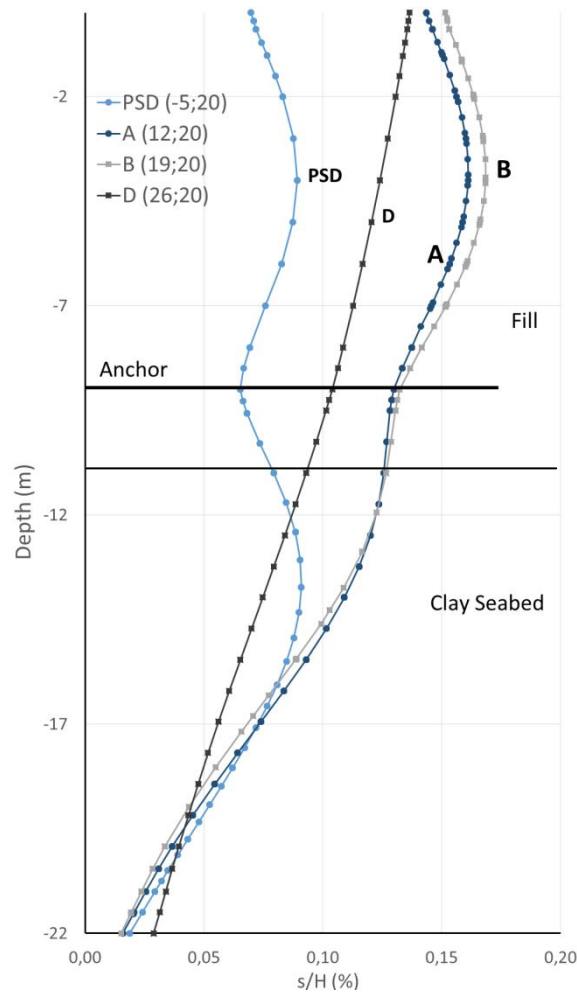


Figure 5.3 - Wall deformation normalized to wall height, for NR ( $s/H$ )

By examining Figure 5.3 it is possible to observe that closer to the corner (therefore, farther from the plane strain section) movements in sheet pile wall increase to more than the double of the PSD values on the top of the wall. Although this observation does not go accordingly to what is stated in reviewed literature, where the cases were mainly enclosed excavations, it is important to understand that in this situation wall 2 has relatively small length and is only supported by a top anchor. It is not enclosed and represents the extreme end of a wall system. Therefore, it is possible to admit that deformation is worsened by a global rotation of wall 2, as visible in section D.

Also, the deformation shape is similar along the wall, with less movement in anchor zones and higher bending in intermediate areas. However, in the section that corresponds exactly to the corner (connection between wall 1 and wall 2), the deformation shape is close to a straight line. This represents the stiffness provided by wall 2 on the interlock connecting both sheet pile walls.

In Figure 5.4 is displayed the transverse displacement of the capping beam. It is possible to distinguish the different movements in the area influenced by the corner with the mutually supported wall and in

the anchored length of the wall (closer to the PSD section). This is in accordance with the Figure 5.3 shown before, where deformation on the top of the wall varies in the various cross sections.

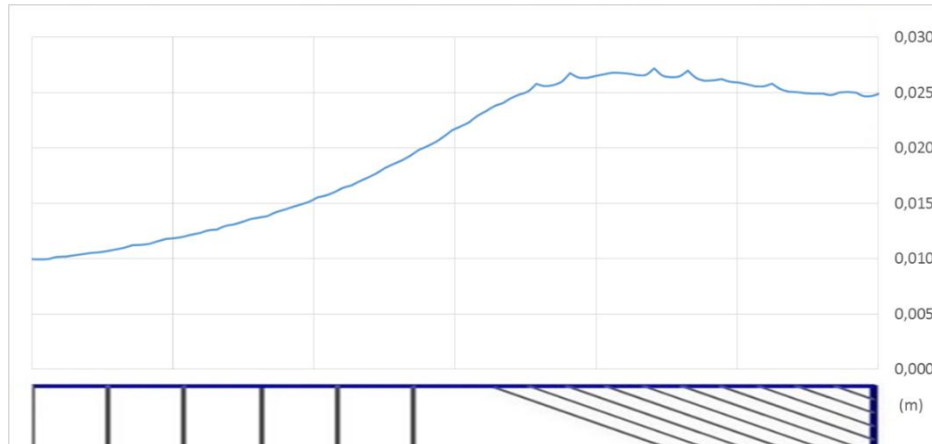


Figure 5.4 - Transverse displacement of capping beam (m)

So, as there is a wall behaviour that is most probably influenced by three dimensional effects and is not always similar to the results obtained from a plane strain situation, as shows the deformed wall represented in Figure 5.5. It becomes now clear how relevant and recommended is an analysis in a third dimension environment.

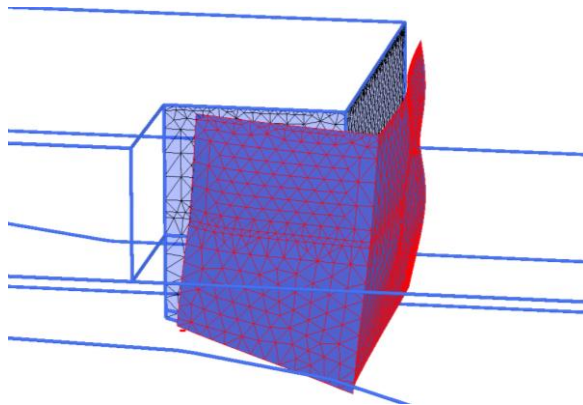


Figure 5.5 - Deformation of sheet pile wall in a 3D environment

### 5.3. NO SOIL REINFORCEMENT (NR)

#### 5.3.1. EARTH PRESSURES

Horizontal and vertical effective earth pressures were retrieved directly from the output of PLAXIS 3D at vertical cross sections 50 cm from the wall, as explained in section 5.1.2. In Figure 5.6 are presented the earth pressure diagrams for cross section B (CSB) and plane strain deformation section (PSD). Also, it is presented the "at rest" earth pressures. Following is provided an analysis of these diagrams.

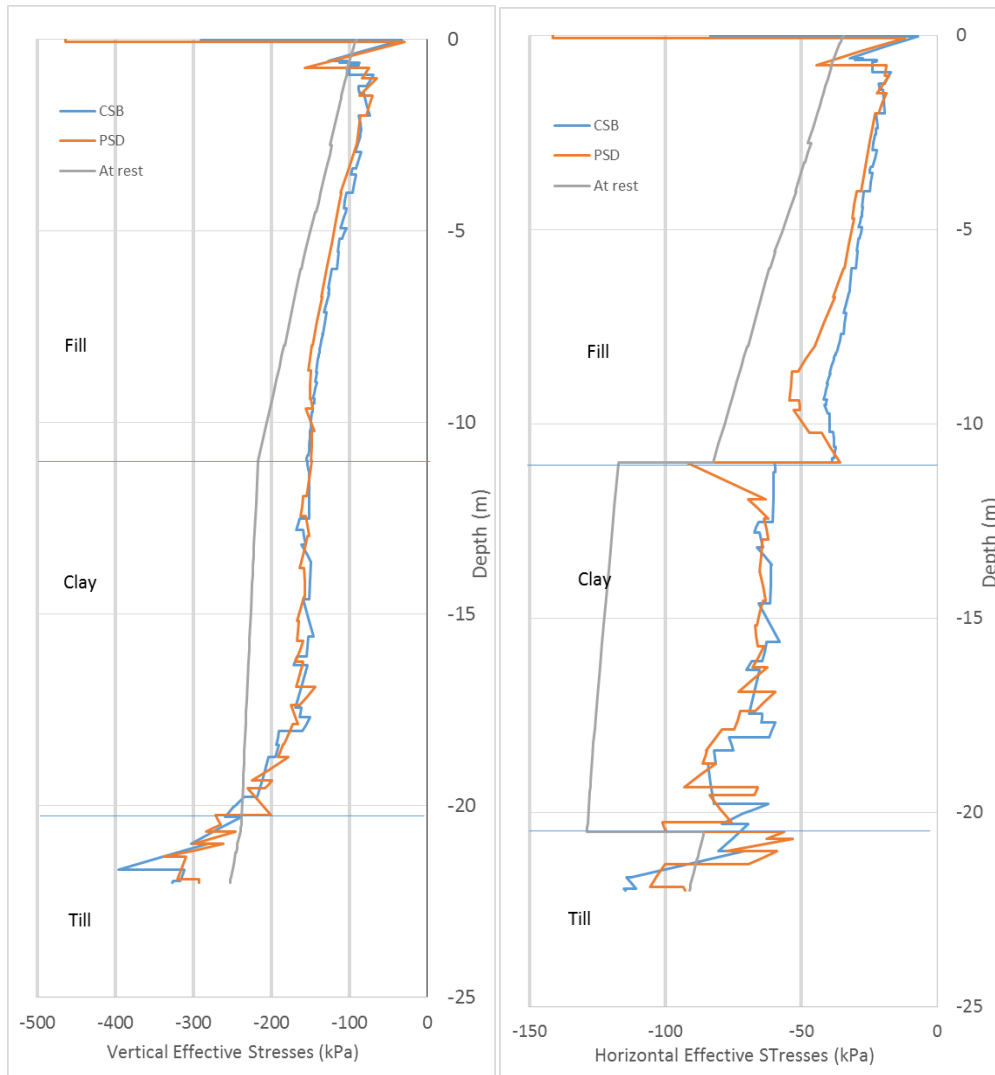


Figure 5.6 - Effective vertical (left) and horizontal (right) earth pressures at CSB, PSD and "at rest" section, for NR

To understand the development of vertical and horizontal stresses it is recommended to use a ratio of earth pressures. The ratio between effective horizontal and vertical stresses is a good indicator to understand how it changes along the depth of the wall and is useful to compare different cross sections. Therefore, in Figure 5.7 is shown a comparison graph of earth pressure ratio in cross sections B (CSB) and PSD, as well as the theoretical earth pressure coefficients (active and at rest) for each of the soil layers calculated in Chapter 3.

It is possible to observe that in both cross sections the earth pressure coefficients are between  $K_a$  and  $K_0$  in all soil layers. This might indicate that those soil masses did not reach the active limit state, but have suffered enough deformation to leave at rest conditions. Another interesting observation is that at PSD the earth pressure ratio globally appears to have values closer to  $K_0$  than at CSB. Such tendency may be associated with possible less deformation of the wall in the PSD section and therefore a stiffer wall in this area.

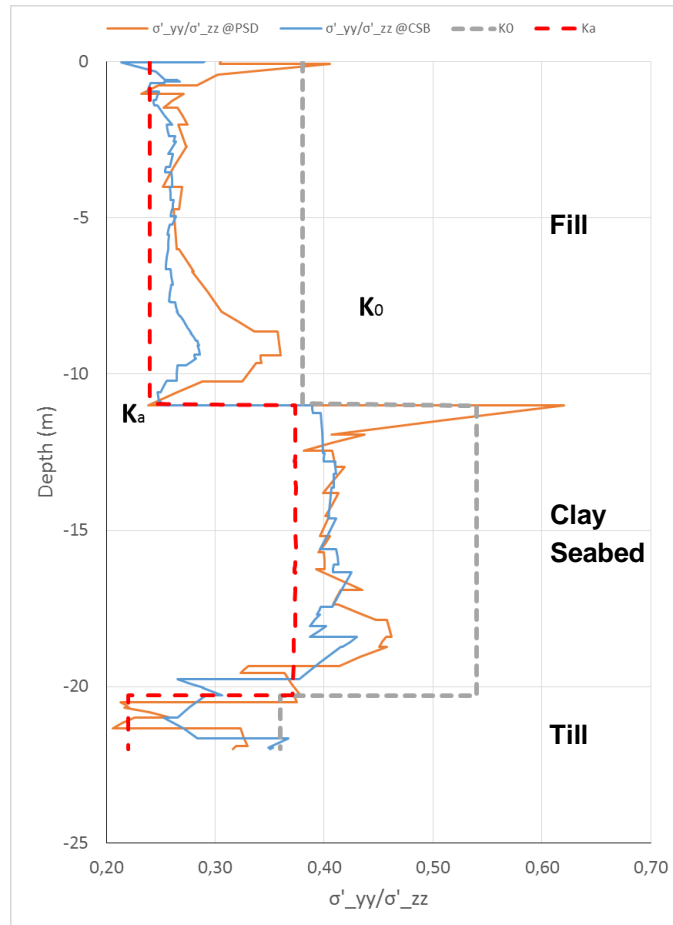


Figure 5.7 - Ratio of effective horizontal and vertical stresses at CSB and PSD

A relevant effect that is predominant in the behaviour of the retaining system is the earth pressure redistribution due to arching effect of the ground. The arching effect is responsible for the transfer of earth pressures from flexible to rigid zones, affecting distribution of earth pressures and consequently changing bending moments and anchor forces.

Figure 5.8 shows horizontal earth pressures at depth -9 m. The horizontal earth pressures acting on the wall are higher in PSD section and reduce closer to the corner, where a minimum is reached. It is possible that some of these differences may be resultant of arching effect from the areas where wall has more deformation to zones with less. So, this should be verified after analysing wall deformation.

Moreover, in Figure 5.7, there are values higher than  $K_0$  which do not make sense if the wall is not pushing against the soil. In fact, as it can be seen in Figure 5.6, for the same depth of -9 m, there is an increase of lateral earth pressures at PSD in comparison with CSB, while vertical earth pressures remain practically the same. These increases may be related to arching effects.

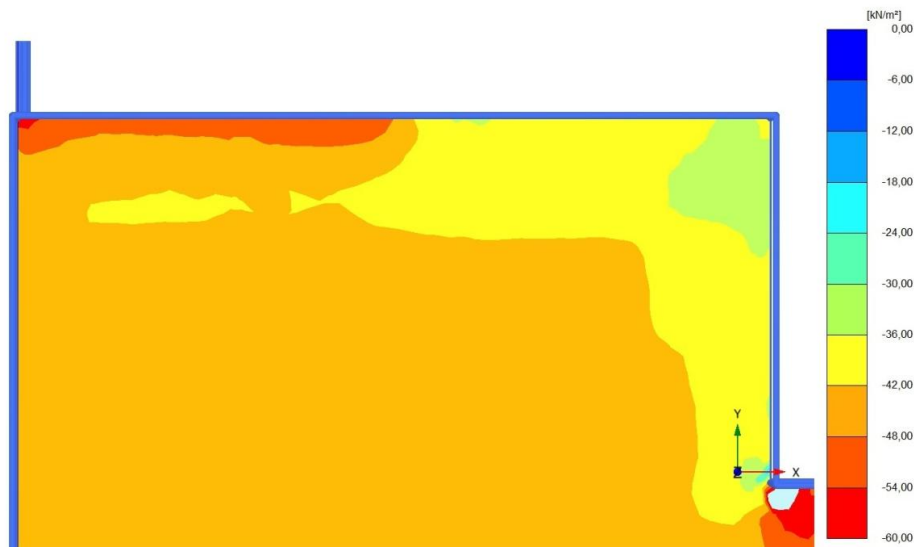


Figure 5.8 - Horizontal (Y-direction) earth pressures at -9 m

As introduced in the Chapter 2, another consequence of corner effects may be the reduction of vertical stresses, similarly to what happens in a silo. This is probable to occur in areas closer to the connection between both walls.

Figure 5.9 shows the effective vertical stresses at depth -10 m, located in the fill layer. It is clear the reduction of vertical earth pressures closer to the wall. However, such reduction is more remarkable near the corner, in the proximity of the walls connection.

In Figure 5.10 are represented the effective vertical stresses in two line vertical sections, L1 and L2. Vertical line section L1 (25.5;19.5) is located close to the corner and is compared with line section L2 (25.5;-5) in a region far from the wall's influence and in plane strain state. What can be observed is that there is a significant reduction in the effective vertical stresses, reaching 50% at some depths. This means that part of the vertical stresses may have been transferred to the sheet pile wall, where consequently an increase of axial forces is expected.

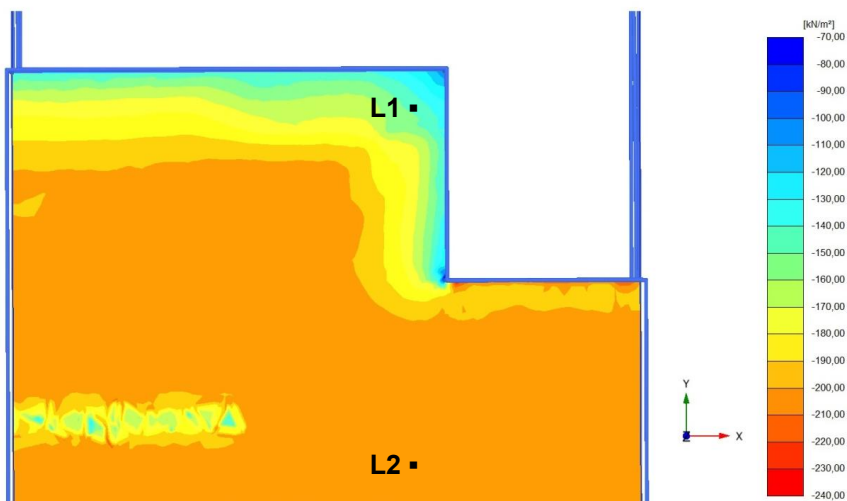


Figure 5.9 - Vertical effective stresses at depth -10m, revealing corner effect

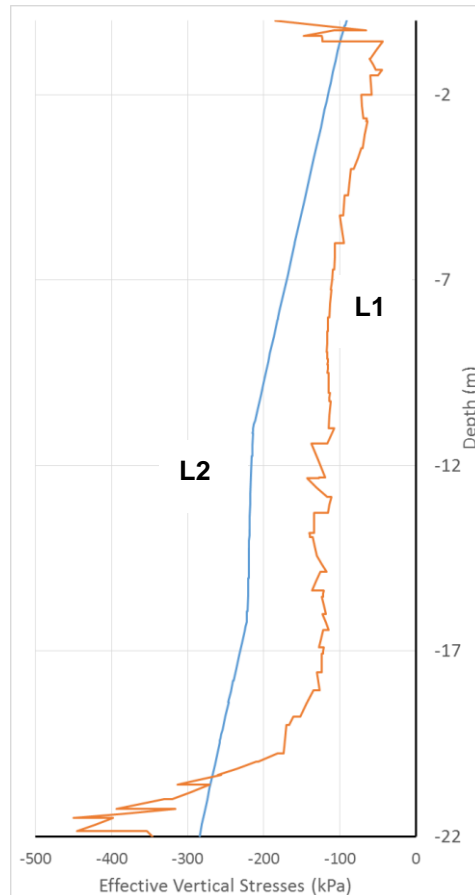


Figure 5.10 - Effective Vertical Stresses at vertical sections L1 (25.5;19.5) and L2 (25.5;-5)

### 5.3.2. WALL DEFORMATION MODE

The following aspect to analyse is the deformation mode of the wall along the loading phases. This is the first indicator of how the wall responds to the lateral earth pressures generated by the soil mass. Figure 5.11 shows the wall deformation at cross section B (CSB) in the zone of mutually supported wall, represented by normalized deformation to wall height.

It is possible to observe that during the initial loading stages the wall rotates along the top, which according to Terzaghi (1941) is theoretically typical of excavated multi-strutted walls, accompanied by small translation and bending. However, the wall immediately shows rotation around the wall tip in the following phases.

The described change of behaviour may be related to the fact that during the initial filling level (up to -6m), the resultant of earth pressures is located at a lower part of the wall, in comparison with the last loading stages. This aspect combined with high corner ties stiffness and reduced tip wall embedment results in a higher movement of the wall in the tip than in the top. Yet, this shape changes as the filling takes place and the location of total soil impulse ascends on the wall. As the last loading phase is reached, it is clear the rotation around the tip with higher deformation in the upper tie in comparison with the lower tie, similar to deformation of non pre-stressed multi-tied walls in excavations (Matos Fernandes 1990).

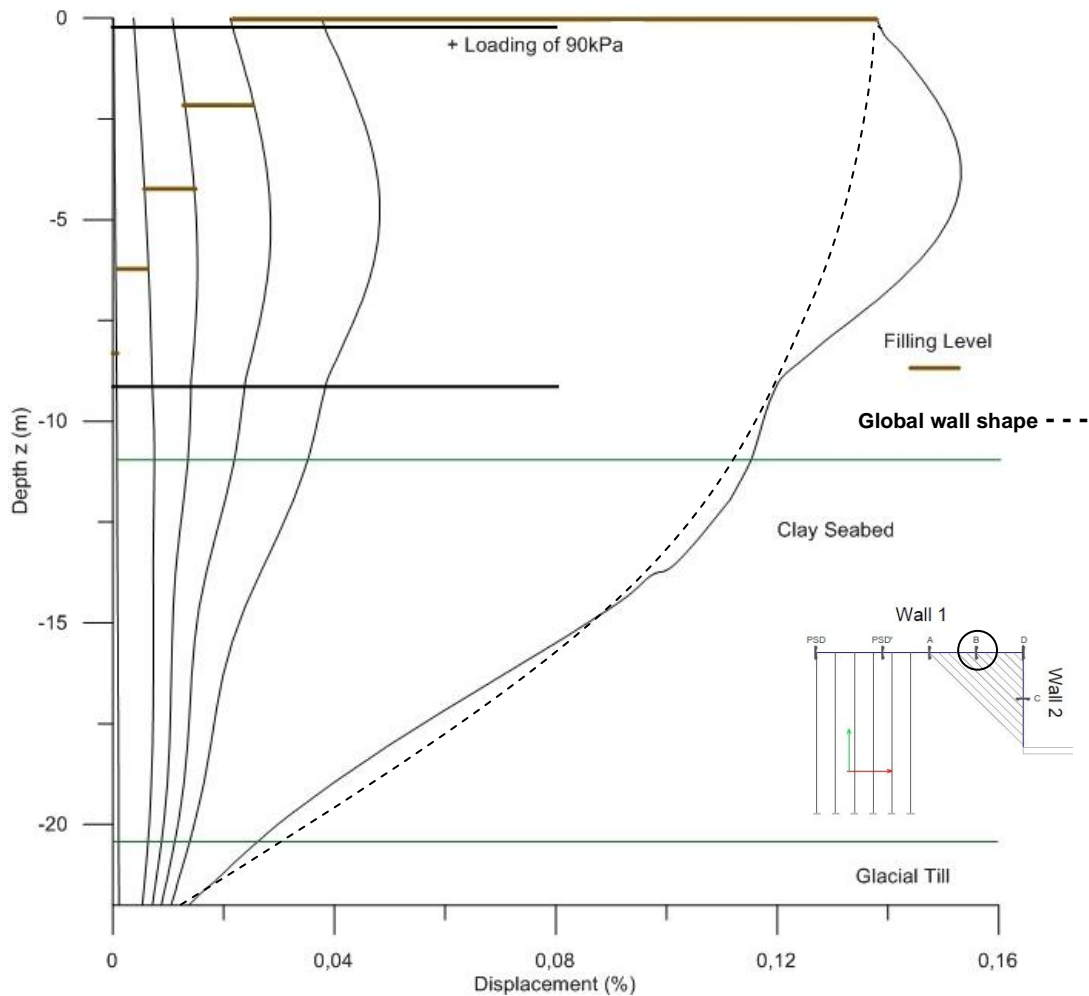


Figure 5.11 - Normalized wall deformation ( $s/H$ ) at CSB along loading phases, in percentage of wall height

In respect to the displacement values, the maximum observed value was 0.15% of total wall height, corresponding to absolute displacement of 3.3 cm and occurs in the bending zone of the wall, between the two levels of ties, due to flexibility of the sheet pile. On the top half of the wall, the normalized deformation is higher than 0.1% which can be, according to data collected by Matos Fernandes (1990), enough to mobilize active pressures (see Figure 3.8). Thus, in Figure 5.7 it was verified that earth pressure ratio was close to active coefficient, so it is possible that the soil is reaching the active limit state.

In Figure 5.12 it is shown the wall displacement in PSD section, which represents multi-anchored section. It is notable a significant difference in the deformed shape of the wall from the mutually tied section. In fact, the tendency for a rotation around the top of the wall during initial loadings maintains, but the final shape is different. There is still a rotation around the tip of the wall, but deformation in top and lower anchors is approximately the same, revealing a higher curvature in the lower part of the wall. This distinction can be explained by the fact that in the mutually supported corner the wall behaves as a rigid structure, due to both higher ties' stiffness and to the perpendicular connection with wall 2, leading to a deformed shape with less arching.

Deformation values in the PSD sections do not exceed 0.08% of wall height, revealing that the region where the wall is anchored is stiffer (i.e. less deformation) than mutually supported walls, which

corroborates what was suggested by Figure 5.7 . As briefly explained in section 5.2, this may result from the fact that the small wall 2 is simply anchored on top and does not provide the same stiffness to wall 1 as an enclosed retaining system or a continuous anchored wall would.

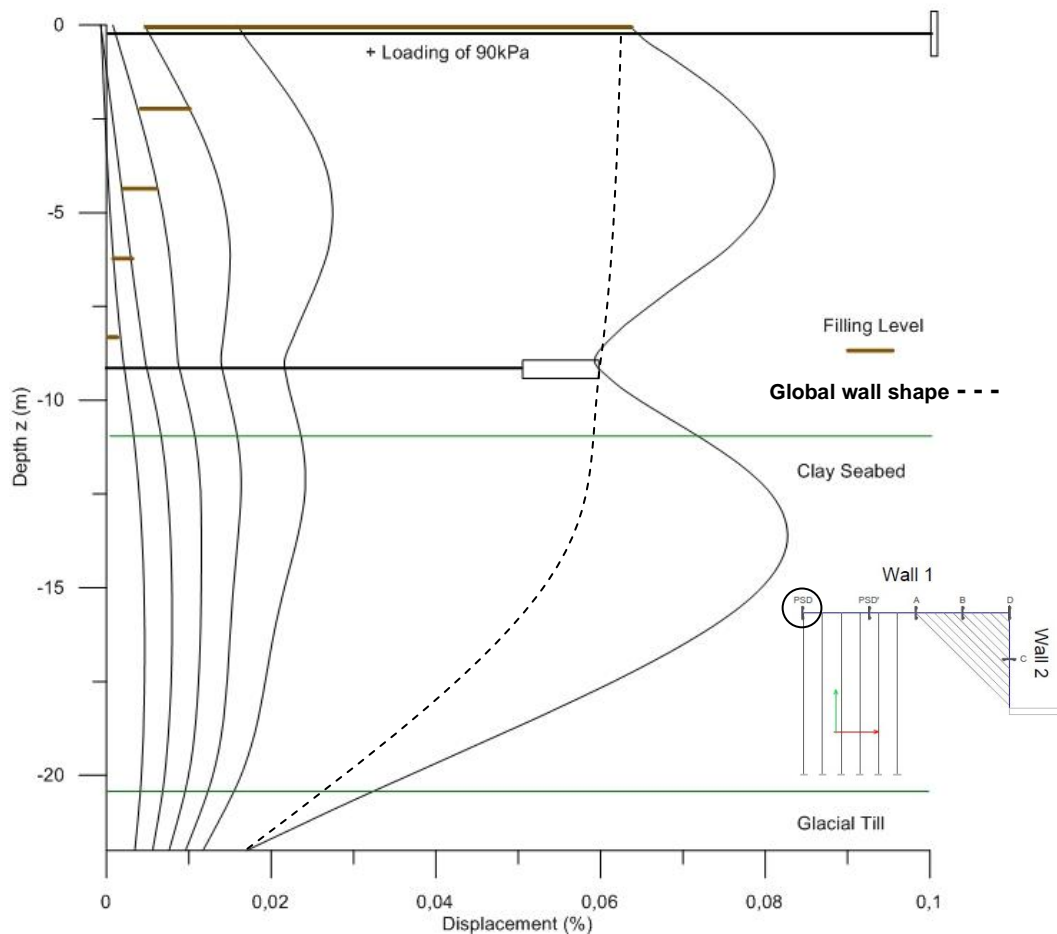


Figure 5.12 - Normalized wall deformation (s/H) at PSD along loading phases, in percentage of wall height

Another relevant elucidation that can be taken from observation of Figure 5.11 and Figure 5.12 is that the surcharge application of 90kPa is responsible for almost 70% of wall deformation at the top. Actually, the value of surcharge is equivalent to a loading of approximately 8 m of filling material, which corresponds to almost 40% of total filling (i.e. filling in the back of the wall and equivalent "surcharge" filling). So, it is possible to conclude that the surcharge is an important factor that should be carefully considered.

Still regarding the wall movement, Figure 5.13 shows the displacement of the wall in Y-direction at depth of -0.4 m and -9 m, where the waling beams and anchors (or ties) are placed. Once again, it can be verified that the displacement on top is higher than displacement in the middle, which describes a rotation of the wall around the bottom. However, this figure shows a better perspective of the relative displacements in the various cross sections. In fact, it can be observed that the wall stiffness in the mutually supported area is not constant, appearing to be more rigid in the connection of both walls (at cross section D) and more flexible in the first ties (near cross section A). This may be related to the fact that the first ties have considerable more length than the ties closer to the walls' connection, thus less rigid.

Similarly to what was introduced in section 5.2, the retaining wall displacement is opposite of the expected and stated in reviewed literature (section 2.1.3.1). The fact that this situation deals with a not enclosed retaining structure, as wall 2 is simply supported by a top anchor, it is reasonable that the corner has a global reduced stiffness compared with the mutually supported zone.

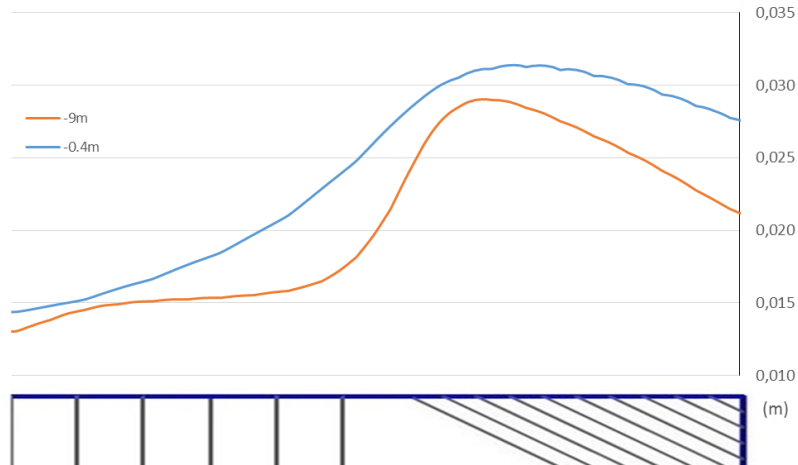


Figure 5.13 - Lateral displacement of wall in Y-direction at depths -0.4 m and -9 m

Also, Figure 5.13 reveals that earth pressure redistribution verified in Figure 5.8 can occur due to arching effects. Observing both figures side by side it is possible to conclude that the zones with less deformation have higher earth pressures, in opposition to zones with larger deformations.

Another interesting detail that can still be observed in Figure 5.13 is the deformation in the transition zone, from anchored to mutually supported wall. It can be seen that at the upper level (-0.4 m) there is a smooth variation of the displacement, whereas this variation is more abrupt at the lower level (-9 m). Such variations can be explained by the reduced anchor spacing and higher stiffness at lower level, which will not allow for a smooth bending of the wall.

### 5.3.3. DEFORMATION OF CORNER

To analyse the deformation of the mutually supported corner it is necessary to observe the cross section C (CSC), located in the middle section of wall 2. In combination with information in cross section B (CSB) and D (CSD), it is expected to provide a satisfactory view of the internal deformation of the corner regarding rotation around wall 1, as well as pulling of wall 2 and opening of the wall system. The pulling of wall 2 is an effect characterized by the outwards movement of wall 1 and inwards movement of wall 2. The opening of corner is a consequence of movement of walls 1 and 2 outwards, revealing the shape similar to the one of an opening book (see Figure 5.14).

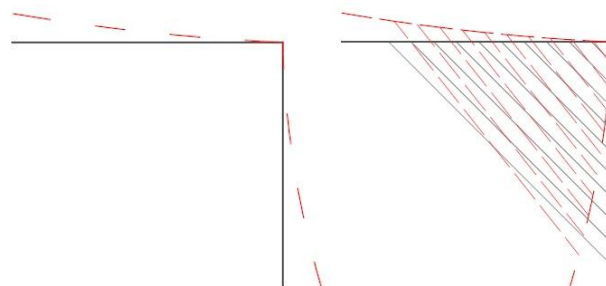


Figure 5.14 - Scheme of corner opening (left) and pulling of wall 2 (right)

The outwards rotation that is expected for the wall system, as described in Chapter 2, is visible by observation of wall displacements in Y- and Z- direction, i.e. in horizontal and vertical directions, schemed in Figure 5.15 and Figure 5.16. The movements are represented by a colour scale and simplified by the arrows indicating intensity and direction at different depths. The rotation around the tip of the wall results from the combination of settlement in vertical direction higher in the proximity of walls' connection and larger horizontal displacements on the top of the wall.

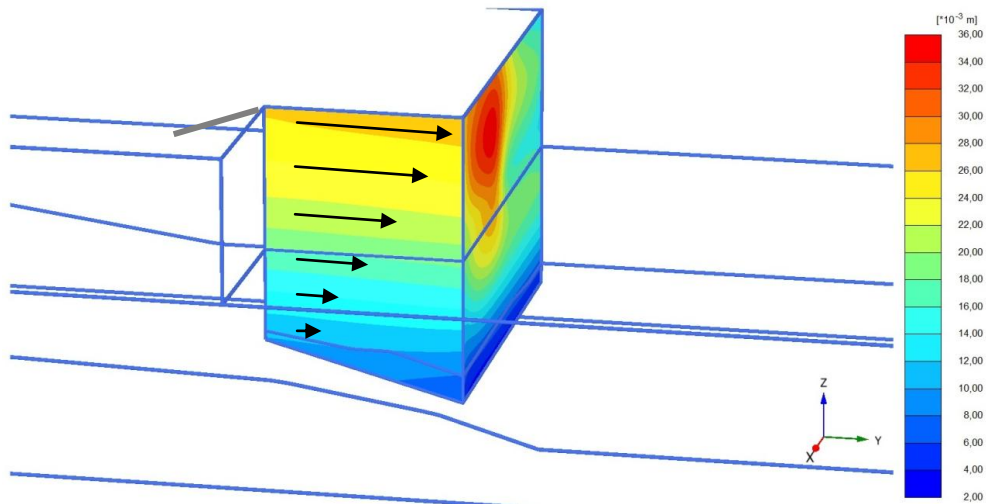


Figure 5.15 - Wall displacement in Y-direction (Horizontal displacement)

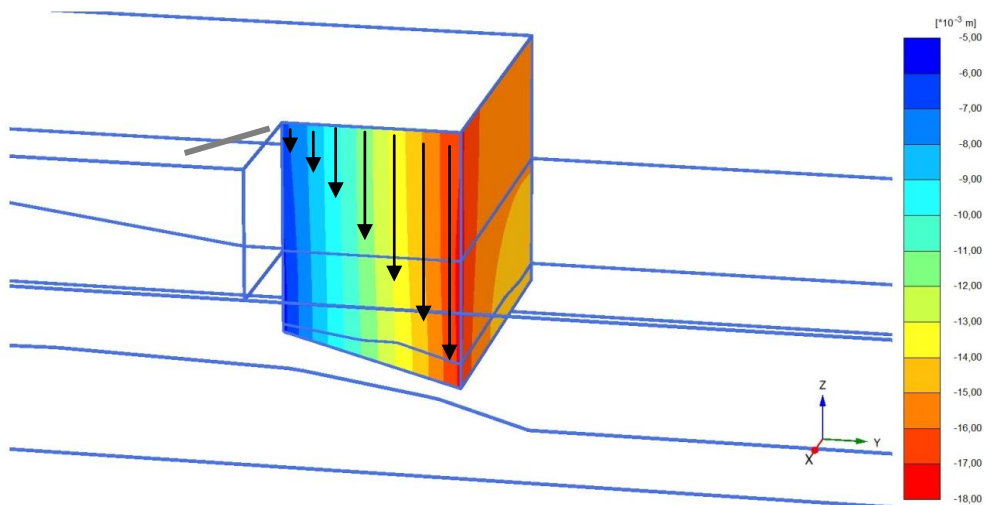


Figure 5.16 - Wall displacement in Z-direction (Vertical displacement)

The observed rotation movement is a result of two main characteristics of the wall. Firstly, wall 2 is only supported by an anchor on top, which is responsible for preventing rotation and providing stabilization, as referred before. Secondly, the existent ground slope does not provide sufficient embedment of wall 2 and contributes for a sliding (i.e. translation with settlement) of the wall in Y-direction.

After observation of displacements at CSC throughout loading phases displayed in Figure 5.17 it becomes clear that the rotation of the wall is practically the same in all depths, i.e. no lateral bending

occurs. Also, as the deformation is similar to CSD, disregarding minimal elastic deformation of the material, it can be concluded that the main movement in the corner is rotation along the tip combined with translation. However, it is interesting to notice that in the initial loading phases the rotation movement is in the opposite direction. This is possibly due to the anchor placed on top of wall 2 and lower location of earth pressure global force.

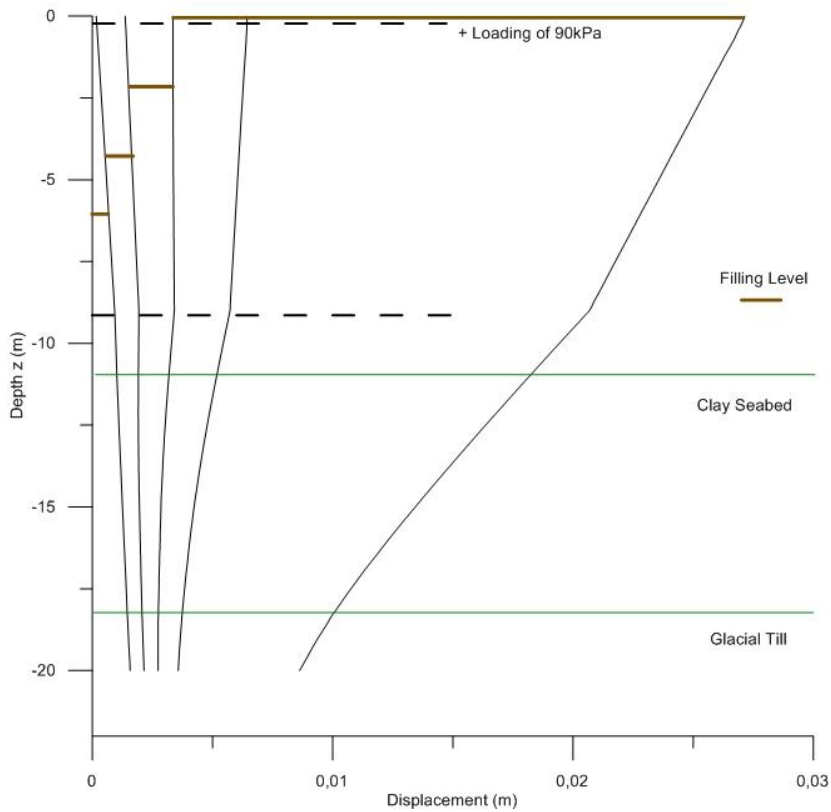


Figure 5.17 - Displacement in Y-direction at CSC, showing outwards wall rotation

The effect of opening of the wall system can be analysed by observation Figure 5.18. It shows the horizontal displacement of sheet pile wall at the two levels of anchorage (or tie). What can be concluded is that it is not a relevant effect at the top of the wall but becomes clearer in the lower level. At depth -9 m there is a lateral wall bending outwards, which reveals a situation of small opening of the corner.

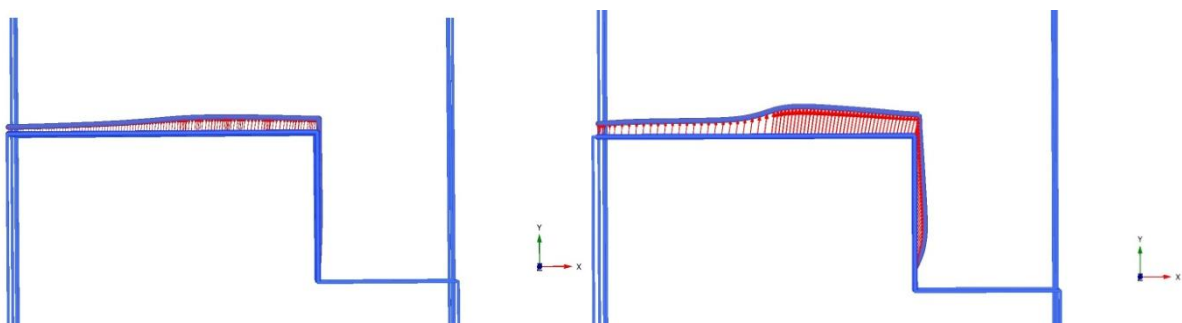


Figure 5.18 - Horizontal wall displacement at depth -0.4 m (left) and -9 m (right)

In Figure 5.19 is presented the wall displacement at CSC for different loading phases. It is possible to verify a large influence of the ties in restricting movement. In the initial filling phases, the top of the wall shows negative deformation which means the wall is moving inwards. Analysing Figure 5.19 side by side with in Figure 5.11, for the same initial loading stages it is possible to verify positive deformation (in Y-direction) in wall 1, leading to the idea that initially wall 1 is pulling the top of wall 2 inwards (X-direction), by activation of the corner ties. This reveals the pulling effect that was described Figure 5.14. However, in the following loading stages this effect is inexistent, probably because earth pressure is high enough to sufficiently stretch the corner ties.

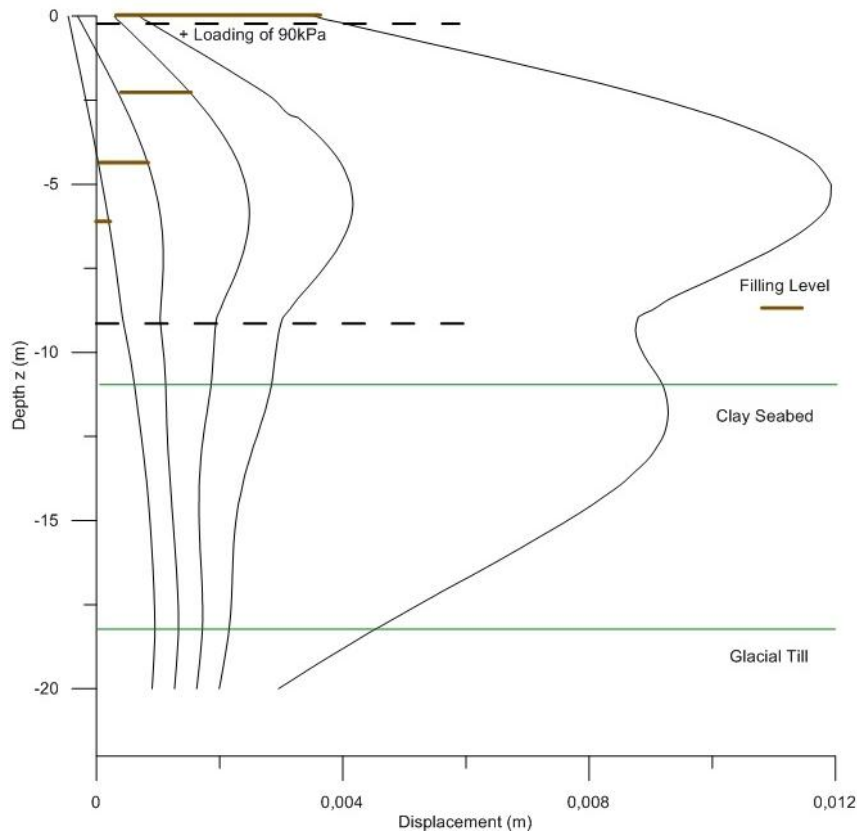


Figure 5.19 - Wall deformation at CSC, along loading phases

### 5.3.4. STRUCTURAL FORCES

#### 5.3.4.1 Anchors and Ties

The variation axial forces in the anchors and ties are an important factor to observe and understand. This is associated with different wall deformation and rods stiffness.

In Figure 5.20 are displayed the forces in anchors and corner ties for both upper and lower levels, at -0.4 m and -9 m respectively.

At first, it is possible to verify that globally, axial forces are higher in lower level than in upper level, with a maximum of 750 kN and 300 kN respectively. In the PSD section are observed the lower forces values that increase along the rods in the anchored wall, reaching the maximum in the transition zone to the mutually supported wall, which is normal taking into account this is the area with more displacement.

In the corner ties, the development of the forces reveals a different shape. It is observable a minimum at the longest and shortest tie, and the maximum values in the middle ties. This is associated with the various levels of displacement at this part of the wall (Figure 5.12), as well as with the varying stiffness of the ties.

An interesting aspect is the high drop of the forces from the anchors to the ties. This may signify that a higher amount of forces due to earth pressures is supported by the anchored wall than by the mutually supported wall. There might be some relations with lateral arching effects, which are a consequence of different stiffness along the wall.

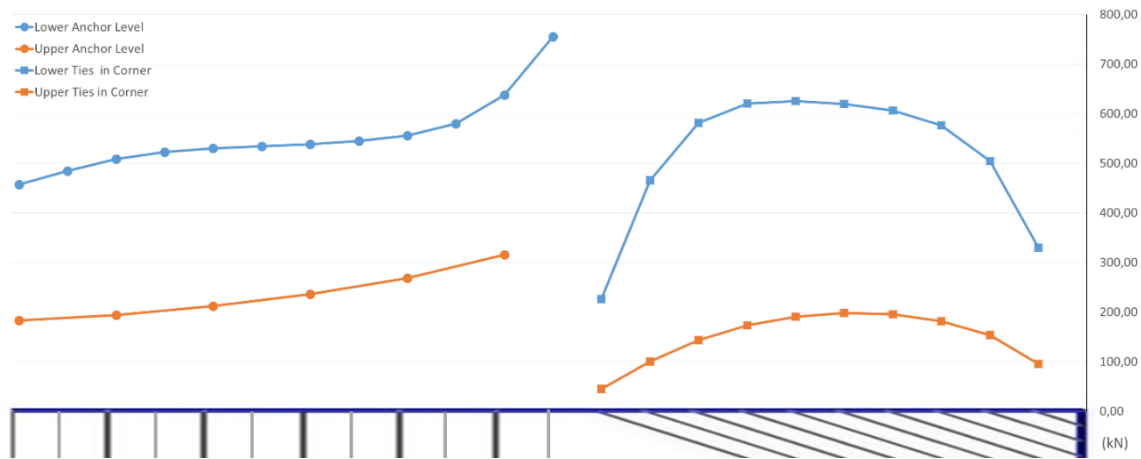


Figure 5.20 - Axial forces (kN) in anchors and ties at upper (0.4 m) and lower (-9 m) levels

The anti-rotation anchor on top of wall 2 reaches yielding, at 1312 kN. This is the critical structural element, responsible for maintaining stability of the corner and of the wall system. Therefore, any soil reinforcement is expected to change the force in this element.

#### 5.3.4.2 Waling and Capping Beam

The waling and capping beams are responsible for providing higher lateral stiffness to the wall and prevent relative settlement of the sheet piles.

Figure 5.21 shows the axial force in the waling located at -9 m. The axial force is 550 kN at PSD section and increases to 1000 kN, when starts the mutually supported wall. At the mutually supported zone, the axial force reduces until it reaches the corner, after which rises up again to 200 kN. The reduction of axial force in the beam as it gets closer to the corner is result of the distribution of forces to the corner ties and to the sheet pile wall.

Similar behaviour is observed for the capping beam, in Figure 5.22. Though, in capping beam maximum values reach 2500 kN in wall 1 and 1000 kN in wall 2.

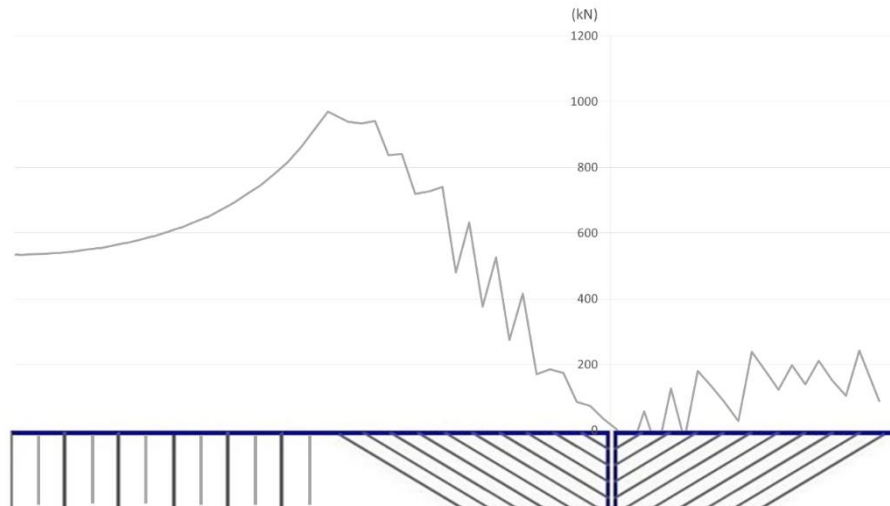


Figure 5.21 - Axial force in waling at -9 m (kN)

The existence of peaks in the axial force distribution for the waling beam, in opposition to the capping beam, is because of the interaction with the ties. In fact, it is expected a practically constant diagram of axial force between the ties support, with point drops at the ties connection. However, numerical calculations suffer much interference in such sensible areas. Consequently, peaks similar to what is observed in Figure 5.21 are probable to occur.

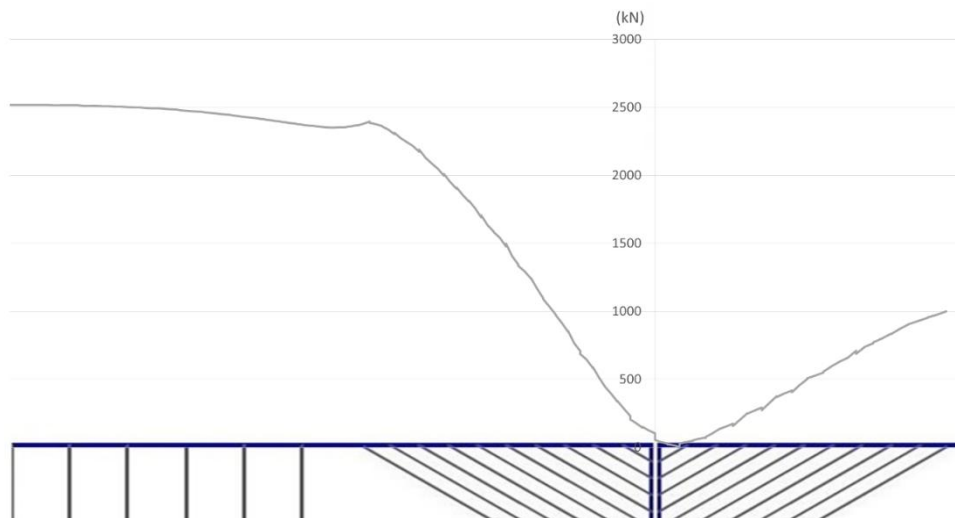


Figure 5.22 - Axial force in capping beam (kN)

Figure 5.23 and Figure 5.24 show the diagram of bending moments at waling beam and capping beam, respectively. The maximum positive and negative bending moments in the capping beam are 372.8 kN.m and -481.1 kN.m, respectively. These are much higher compared to the values in the waling beam, 147.6 kN.m and -119.8 kN.m for positive and negative bending moments, respectively. This is mainly explained by the fact that the introduction of anchors and ties reduces the maximum curvature of the beam, even introducing in extreme situations an opposite curvature. Consequently, bending moment is also reduced as to linear proportion with curvature.

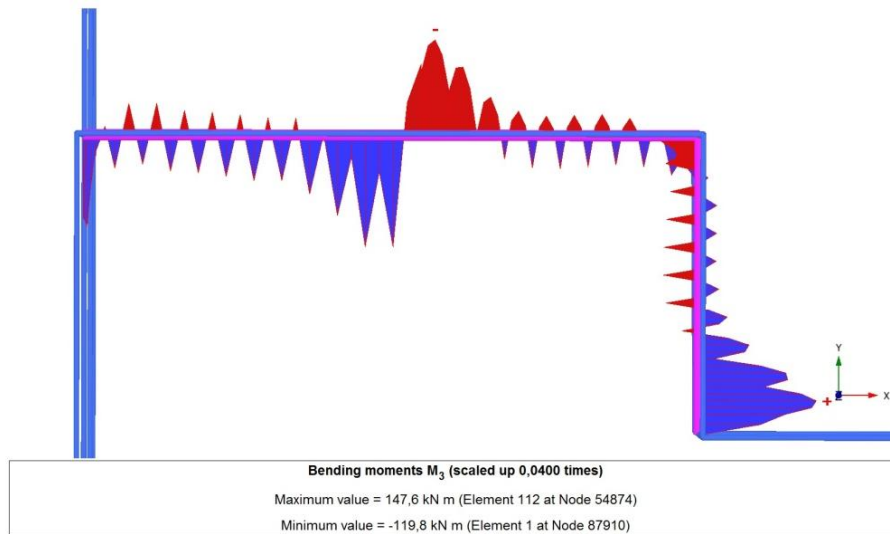


Figure 5.23 - Bending moments in waling beam at -9m (kN.m)

The fact that the capping beam is not connected to the anchors and ties explains the different shape of bending moment diagram, in Figure 5.24.

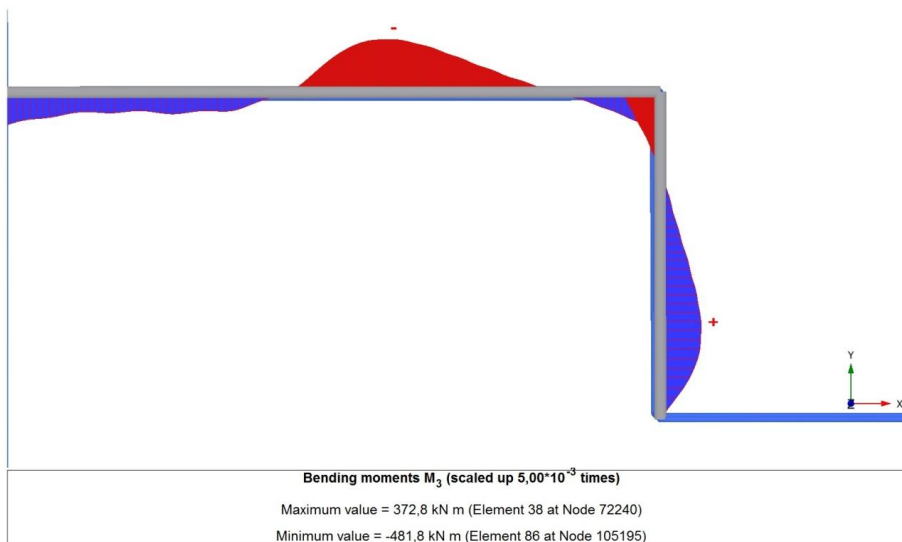


Figure 5.24 - Bending moments in capping beam (kN.m)

### 5.3.4.3 Sheet Pile Wall

In the analysis of the sheet pile wall, it is interesting to evaluate bending moments and vertical axial forces. The first are important for the design and selection of the sheet pile profile to use. Therefore, the bending moment is critical information sensible to earth pressure distribution and arching effects.

Figure 5.25 shows bending moment diagrams at cross sections PSD, CSB and CSC. The maximum values of -377 kN.m and 162 kN.m are observed at PSD section. However, at CSB and CSC maximum bending moments are up to -200 kN.m and 165 kN.m. These differences can be explained by the fact that PSD section shows higher lateral earth pressures closer to the anchor level at -9 m and in the lower clay layer. Besides, more pronounced variations generate higher curvatures and consequently higher bending moment.

Moreover, in the bottom of the wall exist positive bending moments, higher in CSB than in PSD. This is possibly associated with increasing of earth pressures in the front of the wall, at lower depths. Taking in consideration that at CSB, wall deformations in the clay layer are globally higher than at PSD, it is plausible that higher passive earth pressures are generated at CSB as it is closer to the passive limit (Figure 3.8).

In Figure 5.26 is represented the vertical axial force in the sheet pile wall. It is clear the increase of axial forces associated with the reduction of vertical earth pressures verified in Figure 5.9. It is possible to observe that axial compressive force reach 400 kN/m at wall 1 closer to the corner. However, in the upper part of the connection between wall 1 and 2, the sheet pile experiences tensile axial forces. This is associated with the high wall settlement in this area, visible in Figure 5.16. As the sheet pile probably settles more than the soil in that zone, the roughness is mobilized in the opposite direction, i.e. the dead-load from the pile is transferred to the soil, leading to tensional stresses in the sheet pile. However, there are some concerns regarding the modelling of the interface in this area, which should be further studied and calibrated. Possibly, a more deformable mechanism would be more appropriate.

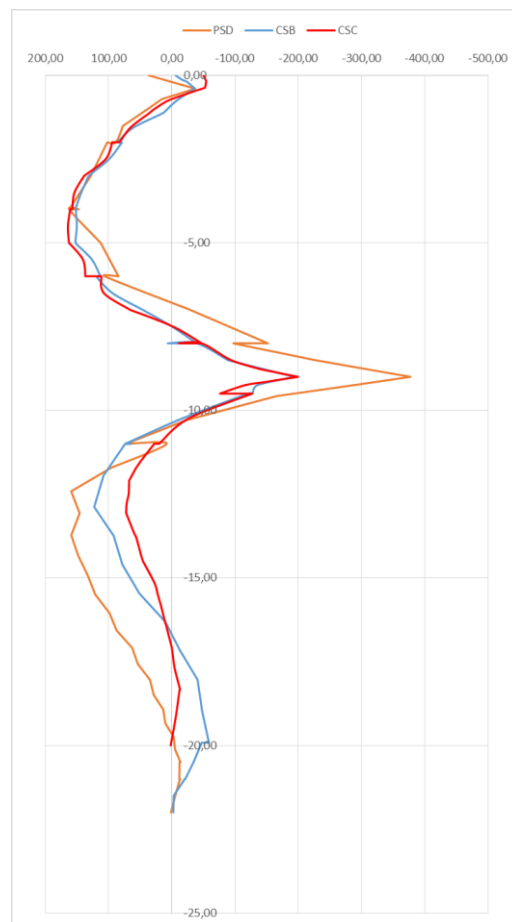


Figure 5.25 - Bending moment diagram at PSD, CSB and CSC (kN.m)

Figure 5.27 shows vertical axial force in the wall at section CSB. Again, it is possible to observe an approximately linear increase of axial forces until it reaches the maximum of -380 kN/m at half of the clay layer, at depth -15 m. Below this depth, axial forces reduce until the wall reaches the till layer,

where almost all the remaining axial forces are laterally absorbed, leaving a possible tip load of -25 kN/m.

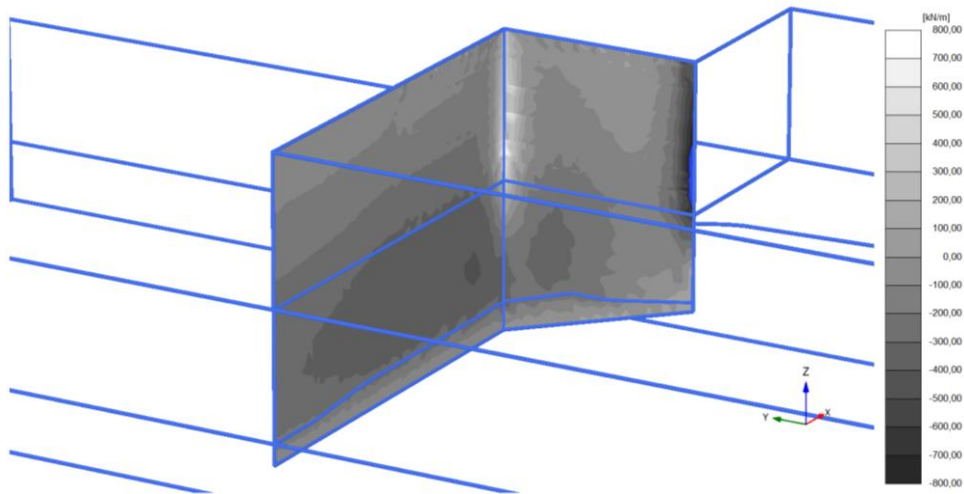


Figure 5.26 - Vertical axial force in sheet pile wall (kN/m)

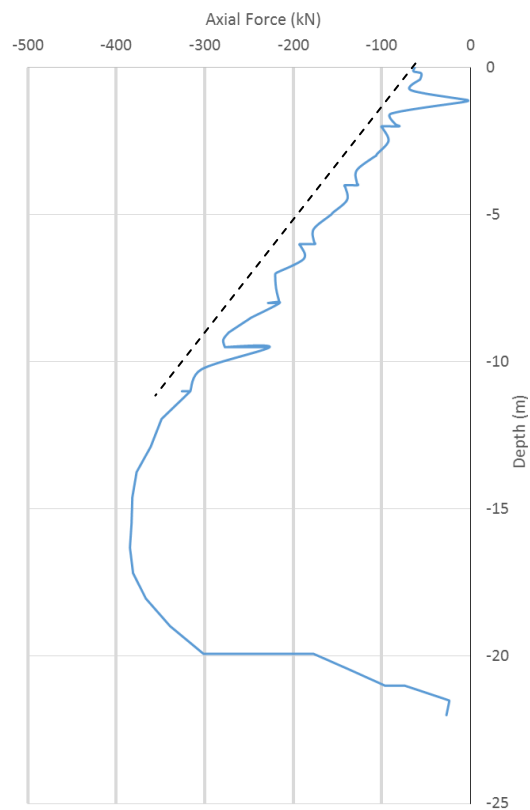


Figure 5.27 - Vertical axial force in sheet pile wall at CSB (kN)

## 5.4. KC PILES (KC)

### 5.4.1. EARTH PRESSURE

For the KC Piles scenario, the earth pressures were extracted similarly to the NR scenario, at a vertical cross section 50 cm from the wall. However, in this situation it is important to point out that the mentioned section is located in a 1m thick layer of soil, named spacing layer, between the sheet pile and the KC Piles monolith (Figure 5.28). As referred in Chapter 4, this layer not only intends to simulate the real space between the monolith and the wall, but also allows a correct extraction of earth pressures, not possible without such layer.

In Figure 5.29 are shown the horizontal and vertical effective stresses at sections CSB and PSD. As a first observation, it is possible to verify a considerable numerical oscillation. This may be associated with the fact that the mesh in the 1 m spacing layer shows reduced quality, probably due to difficult meshing in such conditioned space.

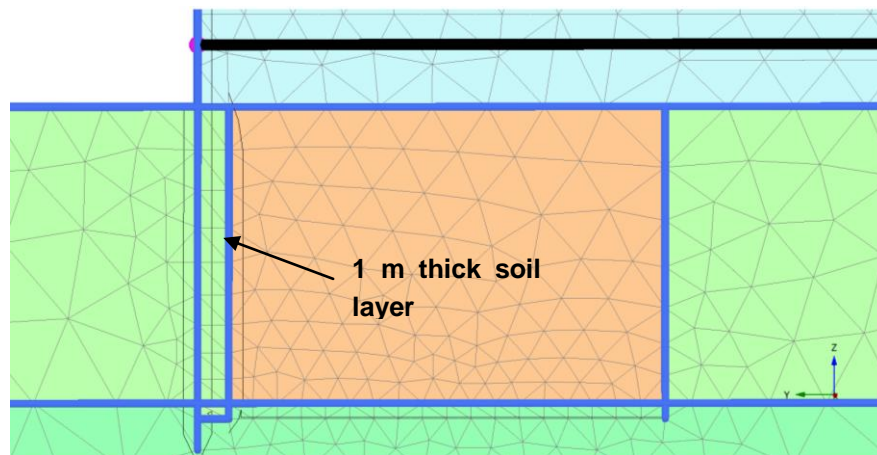


Figure 5.28 - Detail of the soil layer 1m thick, between sheet pile and monolith

Vertical and horizontal earth pressures are similar for both cross sections above the KC Piles depth (-11 m). However, at the initial depth of the KC Piles, both vertical and horizontal earth pressures seem to be slightly higher at PSD than at CSB. Yet, this tendency inverts for both stresses at approximately depth of -16 m.

#### 5.4.1.1 Coefficient of Earth Pressure

The first results expected from the application of KC Piles are the reduction of lateral earth pressures, consequence of the supposed transmission of earth loads by the monolith to the bearing stratum. In Figure 5.30 is displayed the coefficient of earth pressures along the depth at cross sections CSB and PSD. This coefficient is the ratio between the lateral earth pressures in KC scenario and lateral earth pressures in NR scenario, varying between 0 and 2. So, Figure 5.30 is based on Figure 5.29 and Figure 5.6.

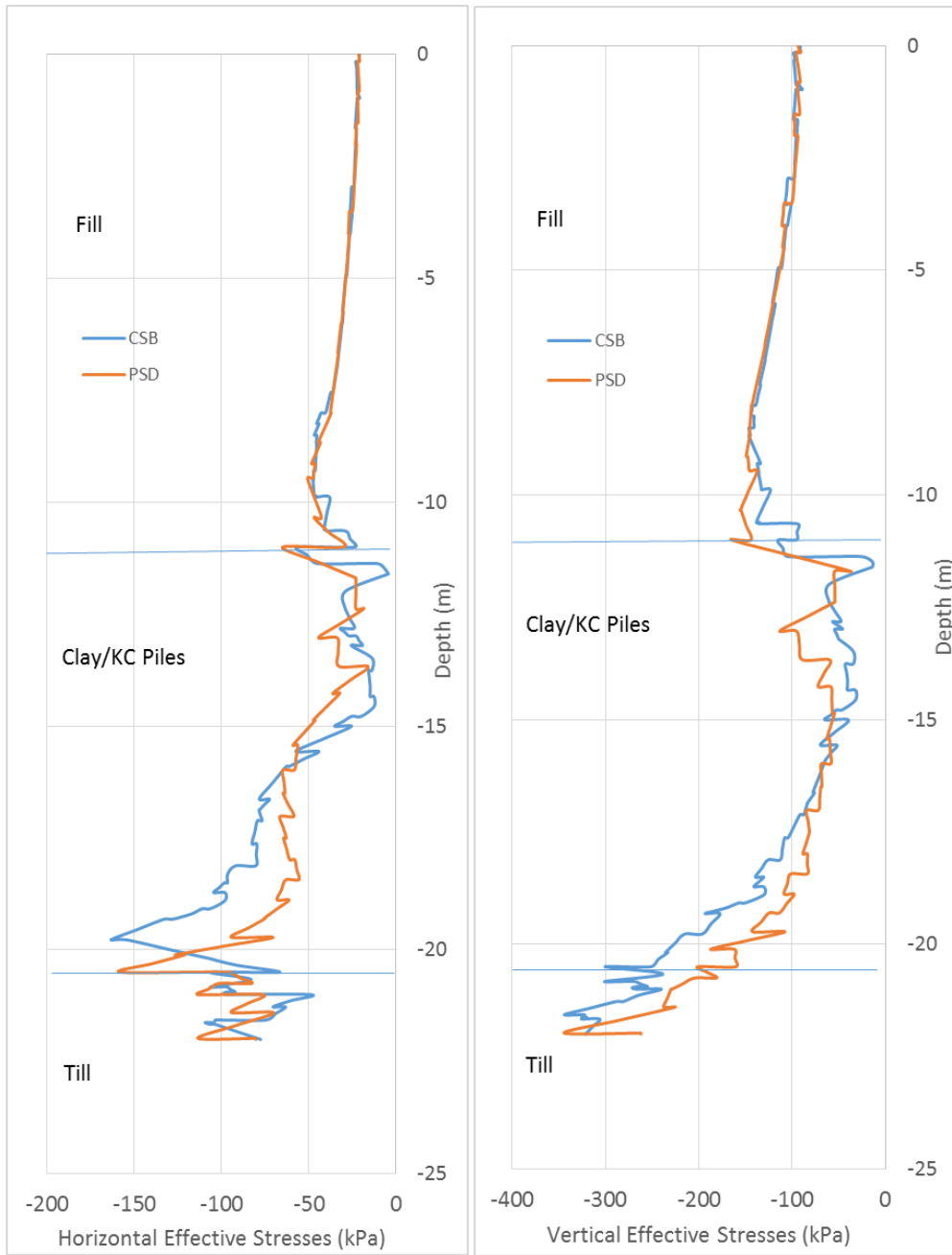


Figure 5.29 - Effective horizontal (left) and vertical (right) stresses at CSB and PSD

At first, it is interesting to note that at depths above the monolith (i.e. above -11 m) already some variations of earth pressures are observed, especially at PSD section. It is questioning that some gain of earth pressures exist at CSB section, which is not understandable and may be associated with mesh errors or stress redistribution.

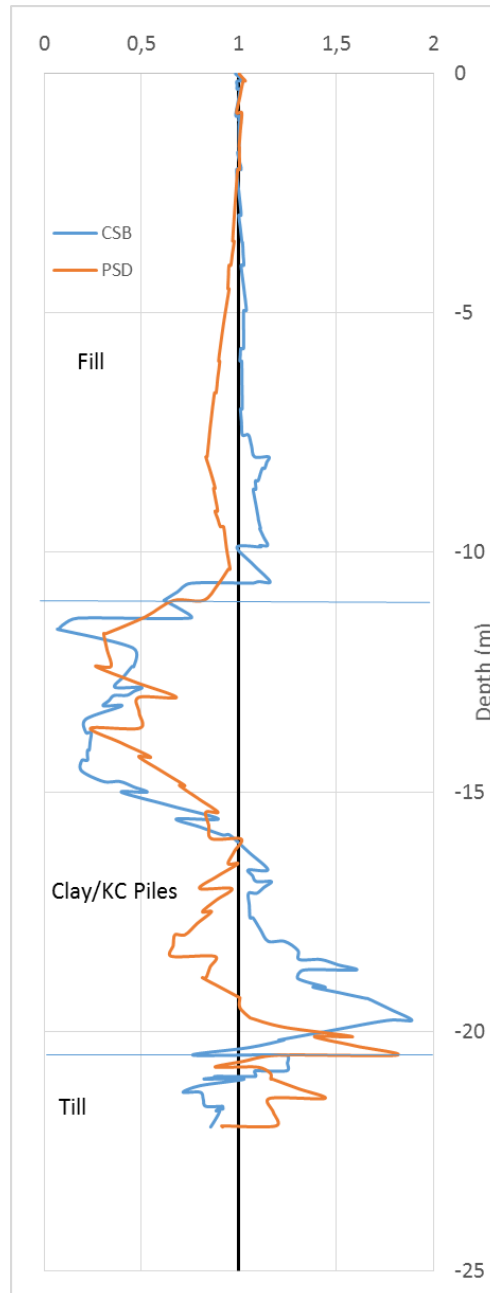


Figure 5.30 - Coefficient of Reduction of lateral earth pressures

Below -11 m, where the monolith is located, it is clear the reduction of pressures due to absorption in the monolith, reaching 50% of values in non reinforced scenario. However, at a certain depth there is a "gain" of earth pressures. This can be due to two effects:

- Leaning of the sheet pile wall against the spacing layer, activating passive earth pressures;
- Concentration of stresses due to change of soil layers (different stiffness).

In fact, it is seen that at PSD such gain occurs when at the top of the till layer. At CSB similar situation happens, taking into account that the ground slope is the cause for the till layer to show at a higher level (approx -19.5 m). Therefore, it is possible that it is this soil change that is responsible for the increase of horizontal stresses and not the leaning of the wall. Still, such hypothesis has to be verified.

Another interesting effect is the reduction of vertical stresses in the soil layer between the monolith and the sheet pile wall due to the so called *silo effect*. This is observable in Figure 5.31. The vertical stresses can be drastically reduced up to levels close to 0 kPa. However, in general reductions are up to 50% of at rest pressures, as it can be derived from Figure 5.32.

Relevant consequences of this effect are the increase of vertical forces in the sheet pile wall and increase of stresses in the monolith, which can be noticed by the increase of vertical stresses in the borders of the monolith in comparison with the values in the middle section.

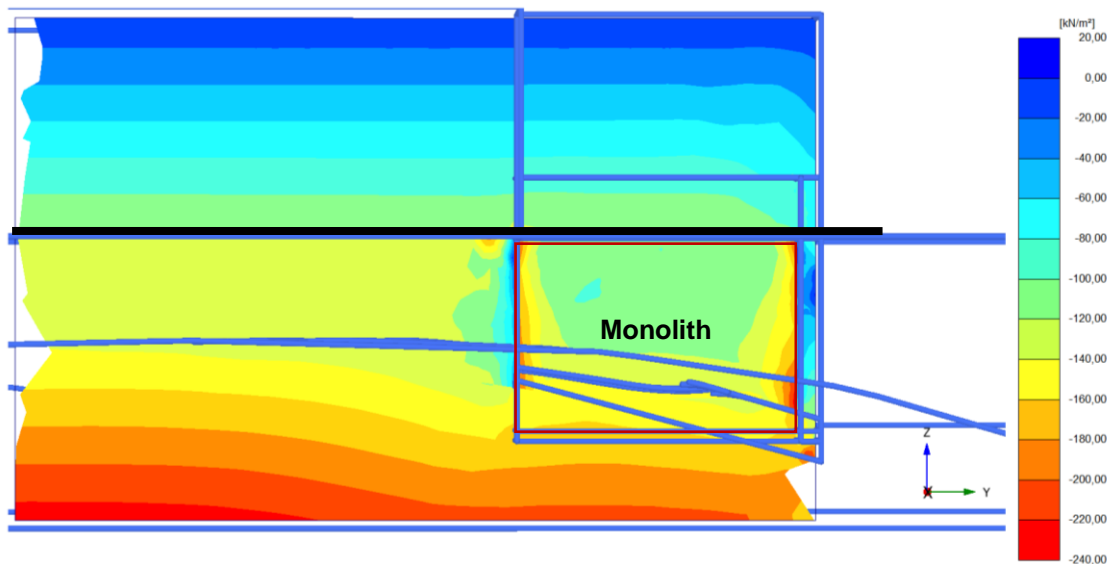


Figure 5.31 - Effective vertical stresses in cross section at x=19



Figure 5.32 - Effective vertical stresses at depth -11m, in a cross section at x=19

#### 5.4.1.2 Transfer of Loads through the Monolith

To verify the assumption that the earth pressures are absorbed by the monolith, it is necessary to observe the development and change of principal directions throughout the block of KC Piles.

Figure 5.33 shows the distribution of principal directions in a vertical plane cross section at x=19. In the back side of the monolith, horizontal earth pressures are taken by the monolith and transferred to the till layer. This is concluded by observing the paths illustrated by the directions of the principal stresses.

However, in the front side of the monolith, the vertical stresses that were relieved from the spacing layer are not transferred to the bottom layer. In fact, these are transmitted back to the soil layer at a lower depth, which can also contribute for the increase of lateral earth pressures observed in Figure 5.30 for CSB section around depth -19 m.

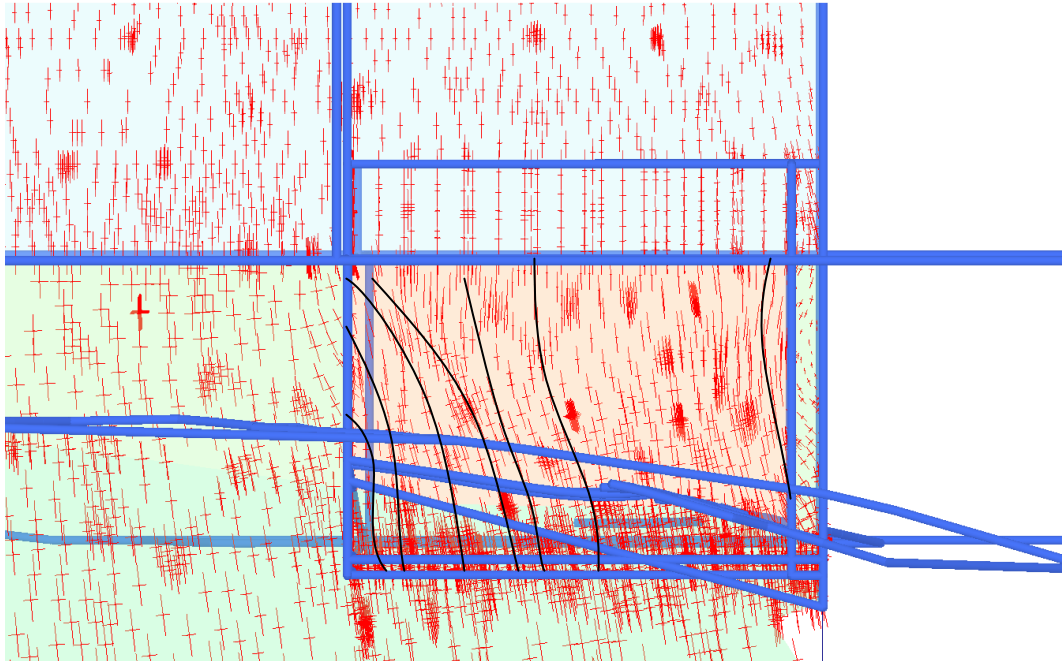


Figure 5.33 - Principal directions in a cross section at  $x=19$

#### 5.4.2. WALL DEFORMATION MODE

In Figure 5.34 is displayed the shape of the wall along the loading phases. There is the tendency for a rotation along the tip of the wall, similarly to what was observed in the NR case. However, the wall shape is different along the depth.

It is possible to observe that below depth -15 m, the wall is in a sub-vertical position, different from NR case (dashed line). This is resultant of the presence of the KC Piles behind the wall. Although these are present up to depth -11 m, the effect of earth pressures above the monolith is obviously observed some meters below the top of the monolith. However, above -9 m, the depth of the lower level of ties, the bending shape of the wall is similar to the case NR, though with less deformation.

Moreover, comparing wall deformation in the NR case with KC case, it is possible to conclude that the presence of KC Piles reduces displacement on top almost 30%.

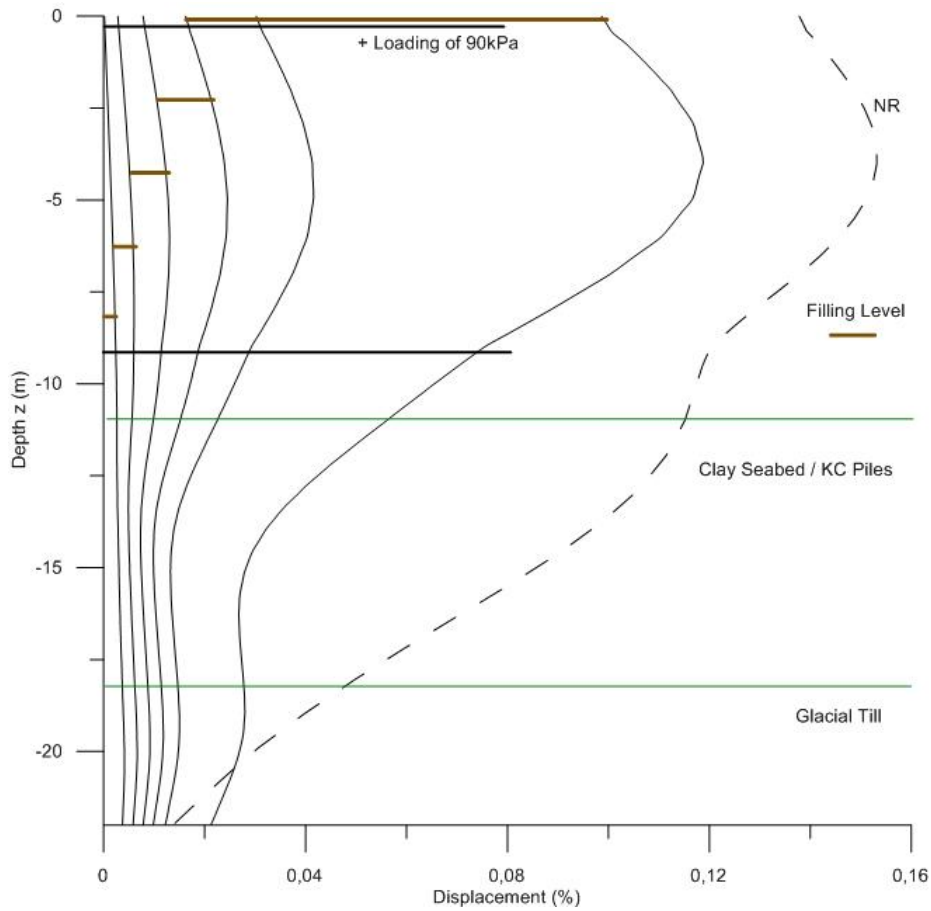


Figure 5.34 - Normalized wall deformation (s/H) at CSB along loading phase for KC, in percentage of wall height

In Figure 5.35 it is observable the lower deformation in comparison with NR case. Yet, the shape of the wall at depths -0.4 m and -9 m is similar to those in Figure 5.13, though at -9 m the variation of displacement in the transition zone (i.e. between anchored wall and mutually supported wall) is less abrupt for the KC case.

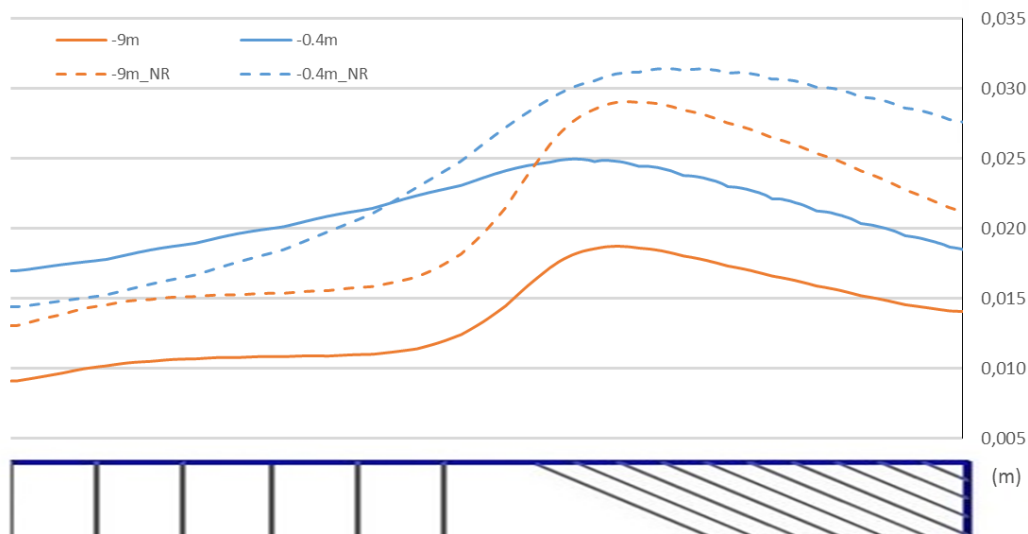


Figure 5.35 - Lateral displacement of wall in Y-direction at depth -0.4 m and -9 m, for KC

Another interesting aspect is the wall displacement at -0.4 m. In fact, it is higher for the KC case than for the NC case, described in Figure 5.13, in the area where the wall is multi-anchored. It is a rather strange situation, as the application of KC Piles is expected to reduce deformations. However, it is possible that the more rigid KC Piles mitigate the difference of stiffness along the wall, leading it to have a more uniform displacement.

#### 5.4.3. DEFORMATION OF CORNER

In Figure 5.36 and Figure 5.37 is possible to observe the deformation of wall 2 in Y- and Z- direction. As explained in section 5.3.3, rotation of the wall results from the combination of movement in these two directions, simplified by the black arrows. Similarly to the NR case, wall system rotates outwards, though with lower values, as it can be seen by the colour scale. This is an obvious consequence of the application of KC Piles.

Still in Figure 5.36 is possible to observe the maximum horizontal displacement due to bending, occurring in the area between upper and lower tie levels.

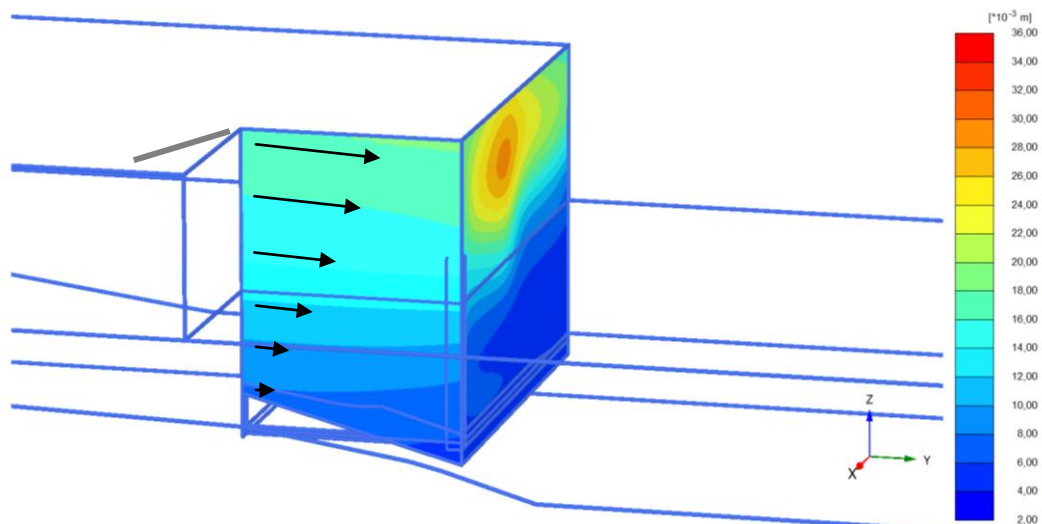


Figure 5.36 - Wall displacement in Y-direction (Horizontal displacement) for KC

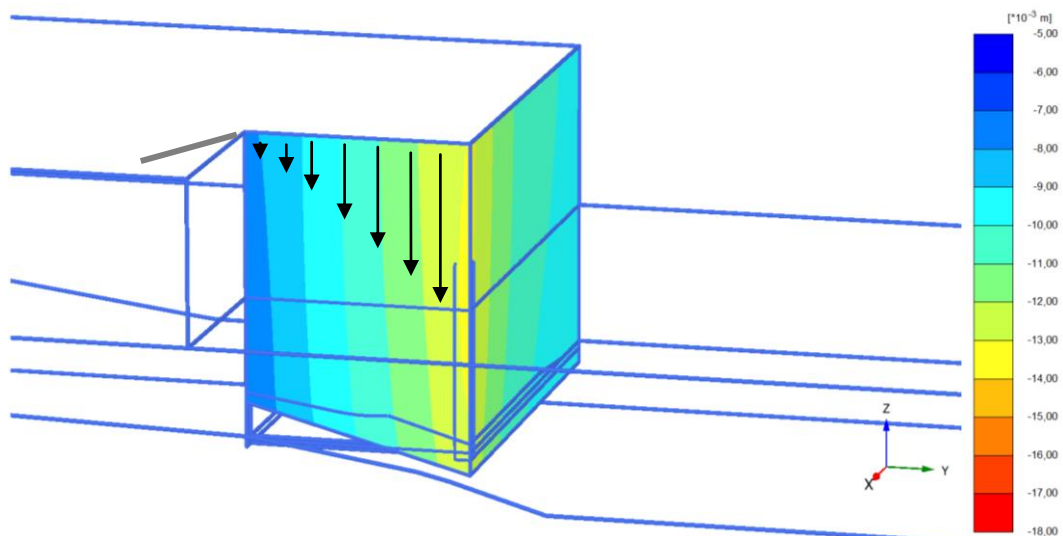


Figure 5.37 - Wall displacement in Z-direction (Vertical displacement) for KC

Similar to the observed for the NR case, the opening of wall system is not prevented with soil reinforcement using KC Piles, as it can be verified in Figure 5.38. In fact, displacement in wall 2 is not effectively reduced by the application of KC Piles, even having at some depths displacements higher than in the case with no reinforcement. This can be noticed in Figure 5.39, where wall shape at CSC for last loading stage in NR case is represented by a dashed line.

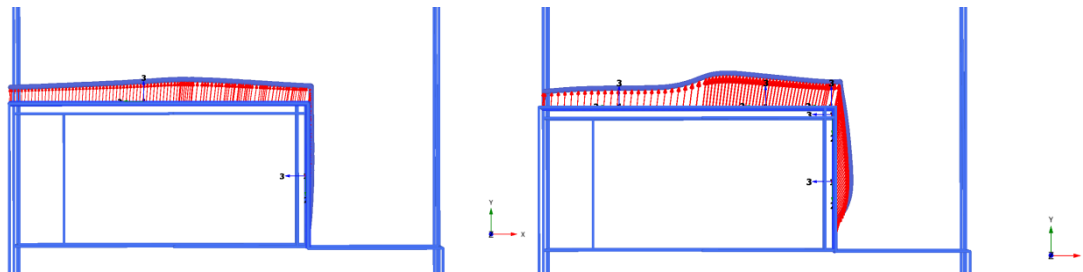


Figure 5.38 - Horizontal wall displacement at depth -0.4 m (left) and -9 m (right) for KC

Though maximum displacement is higher than in NR case, at depths below lower ties level is noticeable the influence of KC Piles. Another interesting aspect, also visible in Figure 5.34, is a slight increase of deformation at depth -20 m. This can be related with a rotation-translation movement of the monolith that pushes the soil and consequently the wall at the bottom.

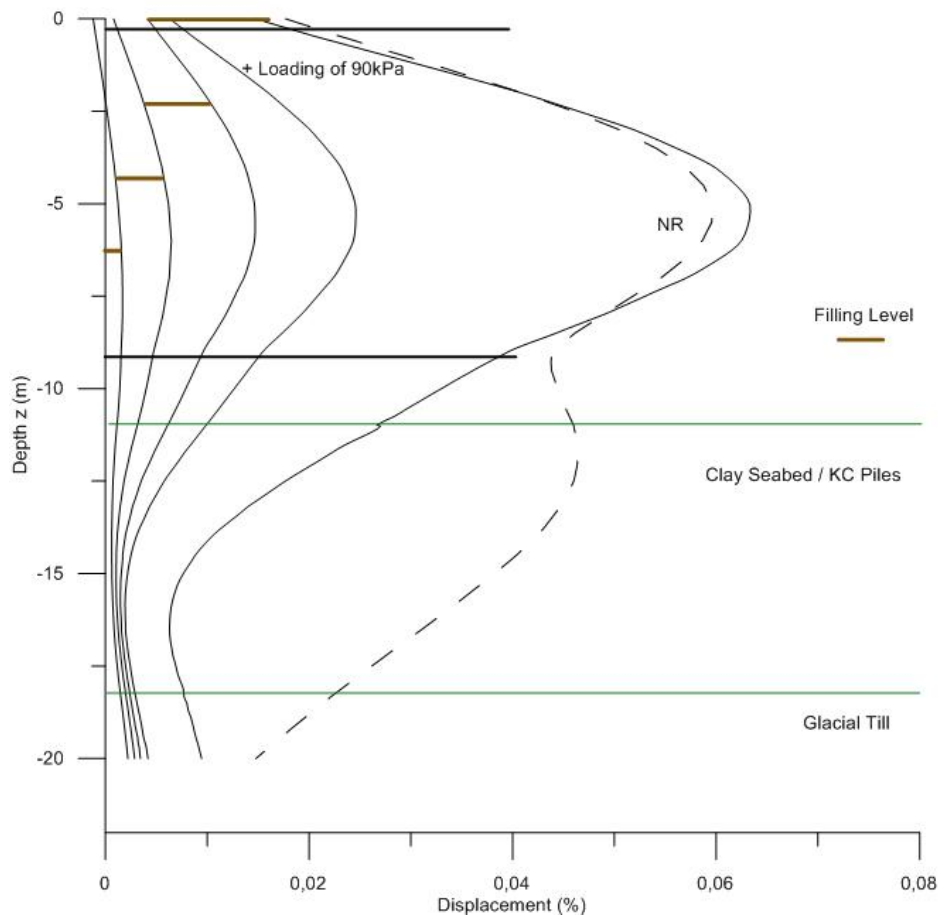


Figure 5.39 - Normalized wall deformation (s/H) at CSC along loading phases for KC, in percentage of wall height

#### 5.4.4. STRUCTURAL FORCES

##### 5.4.4.1 Anchors and Ties

The forces in anchors and ties are shown in Figure 5.40. It is possible to note the reduction in the value of maximum force to 510 kN and 290 kN in lower and upper levels of support, respectively. Similar tendency that was observed in the NR case is verified in this situation, though with lower values.

However, it is relevant to note the following differences:

- Forces in upper level remain practically the same, while force in lower levels decrease up to 30%;
- Differences of forces from anchors to ties are less pronounced.

Such observations lead to the conclusion that KC Piles have high influence in the lower support levels, but few influence in the upper levels. Furthermore, it is possible that the reduced difference of forces from anchors to ties is associated with lower lateral earth pressure redistribution due to arching effect, as relative displacements are smaller (Figure 5.35).

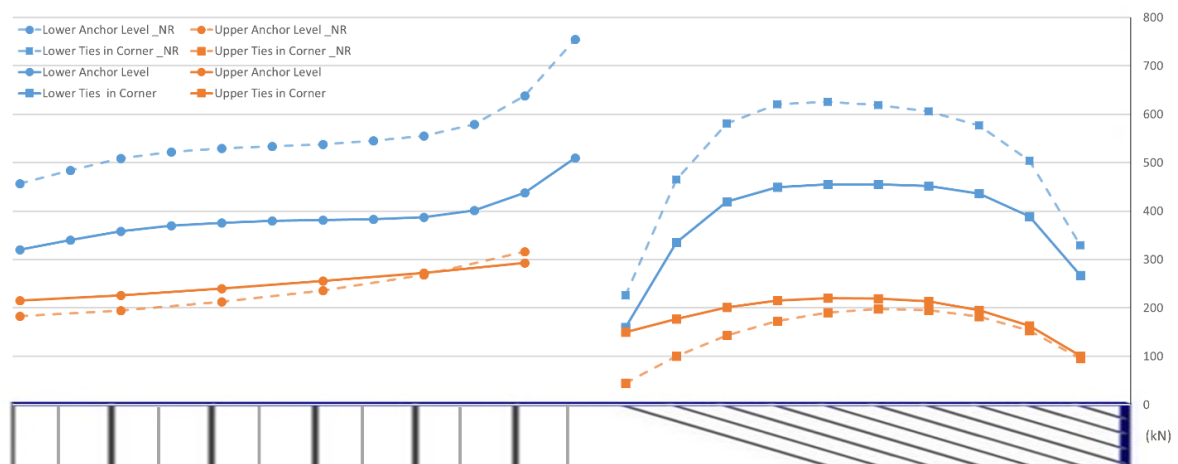


Figure 5.40 - Axial forces in anchors and ties at upper (-0.4 m) and lower (-9 m) levels, for KC (kN)

The anti-rotation anchor, located at the top of wall 2, shows, as expected, a reduced axial force of 1227 kN. However, it is still a high value in comparison with the other anchors and is close to the yielding value of 1312 kN.

##### 5.4.4.2 Waling and Capping Beam

The axial forces in the waling beam for KC are shown in Figure 5.41. It is possible to notice a reduction of approximately 25% at PSD section and 35% of the maximum axial force. However, in wall 2, the force at the waling can drop 50%.

The tendency of reduction of axial forces in the area of mutually supported wall and closer to the corner, as observed for the NR case, is clear. This variation of axial force might represent relevant information for the design of the waling, as it could be helpful to optimize the beam's dimensions, thus reducing costs in material.

In the capping beam, however, the reduction of axial force is almost none. In Figure 5.42 is verified that the existent reduction of axial forces is mainly in the anchored part of the wall, which is

practically insignificant. So, it can be concluded that the distribution of axial forces in the capping beam remains the same, thus leading again to the idea that soil reinforcement does not affect structural elements closer to the top.

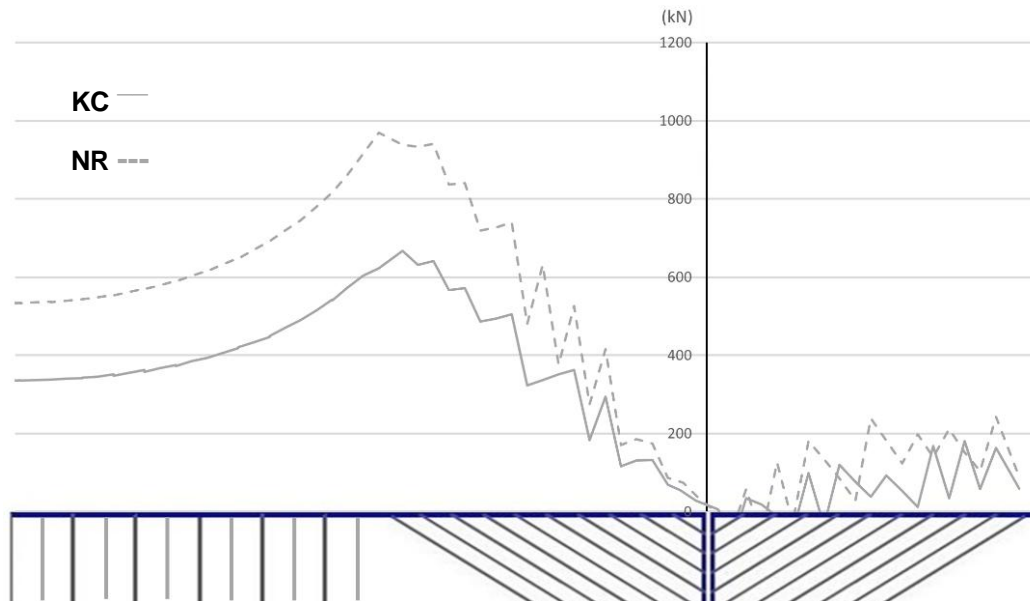


Figure 5.41 - Axial force in waling at -9m, for KC (kN)

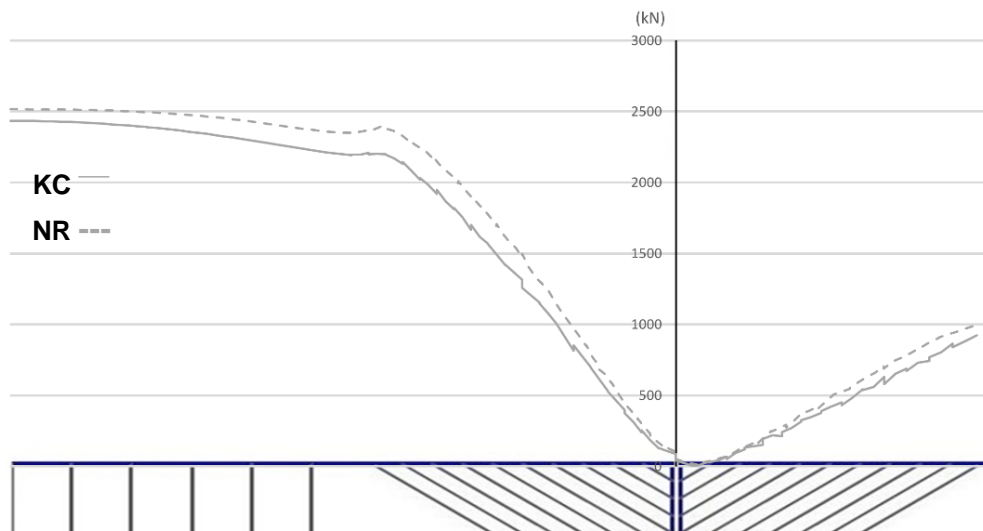


Figure 5.42 - Axial force in capping beam, for KC (kN)

The bending moment in the waling beam, shown in Figure 5.43, has a similar shape and distribution in comparison with NR case. However, maximum and minimum bending moment values are (as expected) lower, associated with reduction of earth pressures and consequent lower acting forces.

In capping beam, maximum value of bending moment is close to obtained in NR, but minimum value is much lower. Actually, these take place in the connection between wall 1 and 2. Therefore, the connecting system of the sheet piles in this location is critical and should be subject of detailed study.

Also, bending moment diagram does not follow the same shape as in NR case, as visible in Figure 5.44. In fact, in the multi-anchored part of the wall the positive bending moments (in blue) show a triangular shape, in opposition to the same diagram in the NR situation. Again, as in other parameters evaluated, the application of KC Piles has not much influence in forces of upper structural elements.

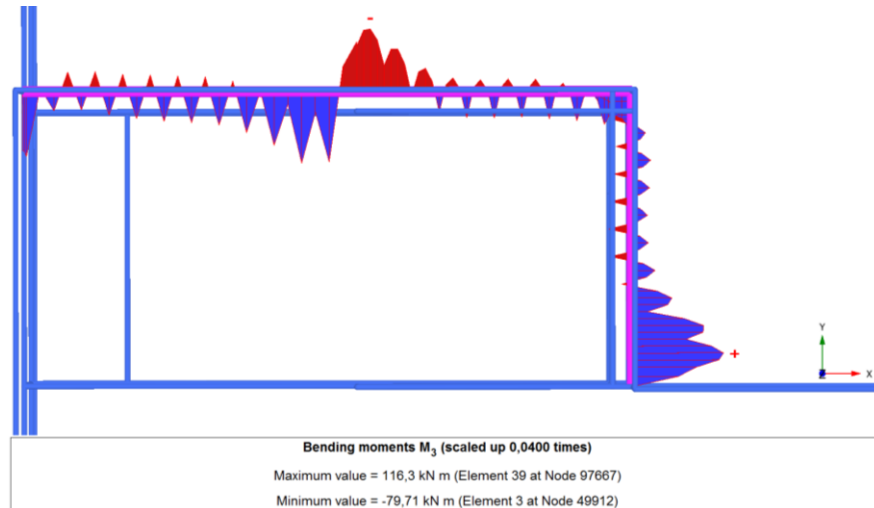


Figure 5.43 - Bending moments in waling beam at -9 m (kN.m)

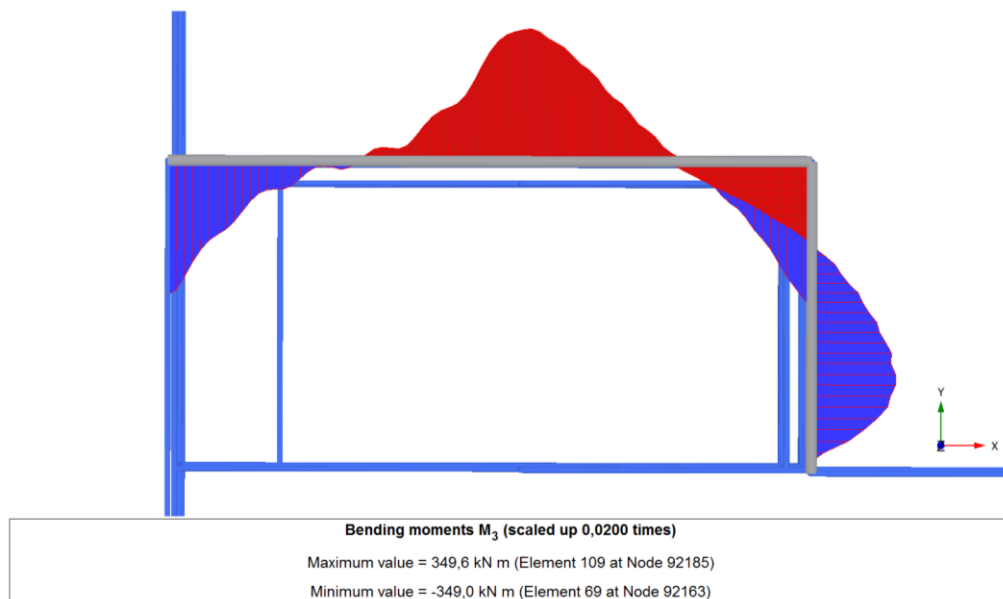


Figure 5.44 - Bending moments in capping beam (kN.m)

#### 5.4.4.3 Sheet Pile Wall

Bending moments in the sheet pile wall are represented in Figure 5.45 for section CSB and CSC. In comparison with the diagram obtained for NR case, represented by dashed line, it is possible to note that the maximum bending moment is in fact higher for the KC scenario. This can be due to the slight increase of earth pressures that can be seen above -11 m in Figure 5.30, but also associated with a reduced arching effect.

An interesting result is the inversion of bending moments that is verified below the monolith depth (-11 m). This is a rather strange effect but can be in part explained by observation of lateral earth pressures in the back and in the front of the wall. The presence of higher earth pressures in front of the wall than in the back at depth -15 m, as highlighted in Figure 5.46, are probably responsible for generating negative bending moments. In the tip of the wall, however, exist positive bending moments, revealing the embedment of the wall in the till layer.

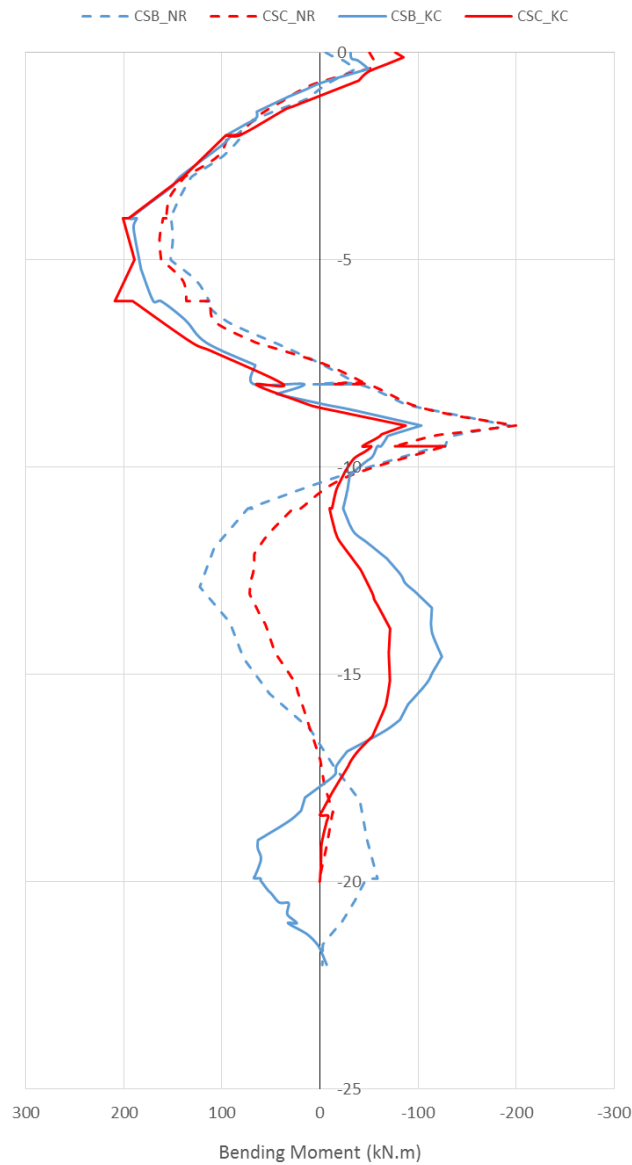


Figure 5.45 - Bending moment diagram at CSB and CSC, for KC (kN.m)

In Figure 5.47 is shown the vertical axial force in the sheet pile at cross section CSB. As expected, it is possible to see that there is a reduction of axial force at the depths of the monolith. Also, above -11 m the axial load is lower than in NR case, in dashed line. It is not an expected result as supposedly above the monolith there are no relevant changes in vertical earth pressures. Therefore, it is not explainable such reduction of axial force in the sheet pile, though this aspect is not significant.

At the till layer the axial force is again taken by mobilizing shear strength of the soil, but in this case no load is observed at the tip, as axial force is 0 kN. This is consistent with the fact that it is required more displacement to mobilize tip resistance than shear resistance, therefore the non existence of axial force at the wall tip. Besides, it is normal to obtain no tip resistance as the cross section area of the sheet pile wall is low.

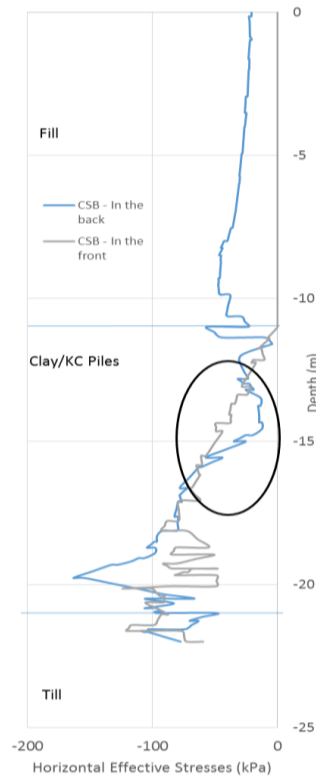


Figure 5.46 - Effective horizontal stresses in front and back of the sheet pile wall (kPa)

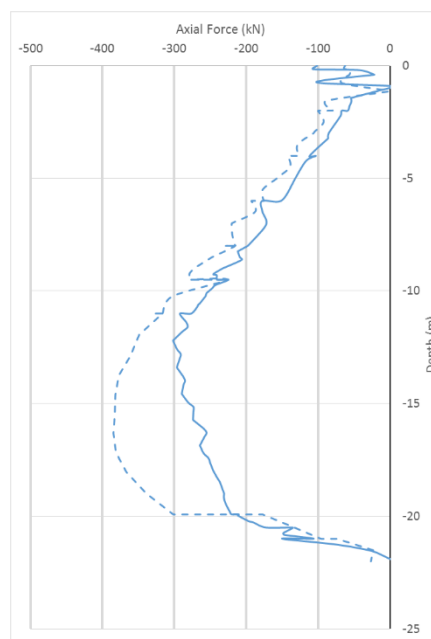


Figure 5.47 - Vertical axial force in sheet pile wall at CSB, for KC (kN)

## 5.5. KC PILES AND JET GROUTING (KC&JG)

### 5.5.1. EARTH PRESSURES

The KC&JG scenario differs from KC scenario just by introducing a jet grouting block in the corner, as explained in the previous chapter. The extraction of earth pressures is the same as used for NR and KC scenarios and the 1 m thick spacing soil layer described in Figure 5.28 is present as well.

The effective horizontal and vertical stresses at section CSB and PSD are shown in Figure 5.48. It is important to note that PSD and CSB are not in the same soil conditions. In fact, PSD is located in an area reinforced with KC piles, while CSB is in the jet grouted zone. Therefore, the dissimilarities observed in Figure 5.58 are normal, as distribution of earth pressures is expected to be different.

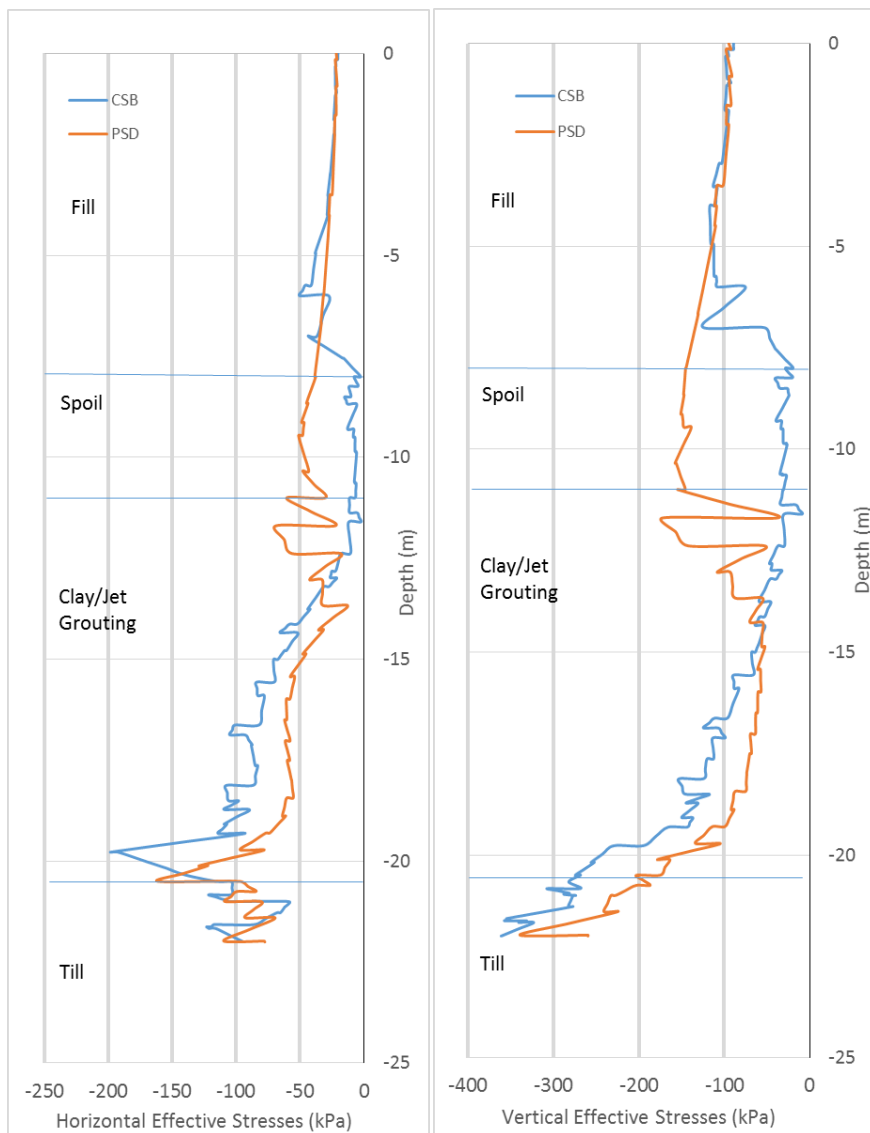


Figure 5.48 - Effective horizontal (left) and vertical (right) stresses at CSB and PSD, for KC&JG

As in the previous scenario, the diagram of earth pressures has some numerical fluctuation due to difficult meshing in the space between the monolith and the wall.

### 5.5.1.1. Coefficient of Earth Pressure

Figure 5.49 shows the variation of earth pressures in comparison with horizontal earth pressures in NR scenario (Figure 5.6). It is clear the effect of the jet grouting spoil in the horizontal earth pressures, reducing down these pressures to almost 25%. This reduction is practically constant until -13m, disregarding numerical peaks originated by change of stiffness between two layers. Below this depth, earth pressure ratio increases showing a gain of stresses in the lower 5 m of jet grouting layer. This gain is similar to the one observed and explained in section 5.4.1.1. However, it is important to say that in this situation it is more remarkable as occurs at wider depth.

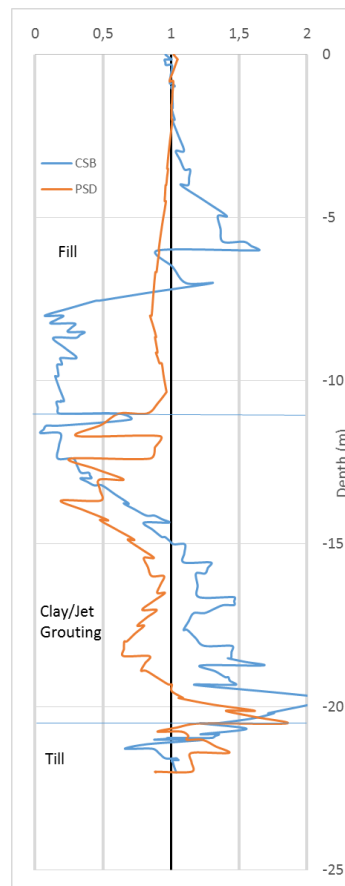


Figure 5.49 - Coefficient of lateral earth pressures

Another interesting effect, in similarity to the KC case, is the reduction of vertical earth pressures in the soil layer between the monolith and the sheet pile wall due to *silo effect*. Figure 5.50 shows the effective vertical stresses. It is clear the remarkable reduction of vertical earth pressures not only in the soil layer between the monolith and sheet pile wall but also in the back of the monolith due to roughness. Such reductions result in almost null effective earth stresses and are observed before reaching the spoil layer, as also observed in Figure 5.58, meaning the *silo effect* has influence in the soil mass above the constrained area (i.e. the spacing layer).

In contrast, the effective vertical stresses in the monolith increase along the depth, especially in the corner. Yet, it is important to note that jet grouting has a higher unit weight, so it is expected that vertical stresses are higher inside the monolith compared with, for example, at rest stresses in the edge of the cross section in Figure 5.50. But the increase in the edges is higher than in the middle of the

monolith, which can be then associated with load transfer from the soil to the monolith due to surface roughness of the jet grouting.

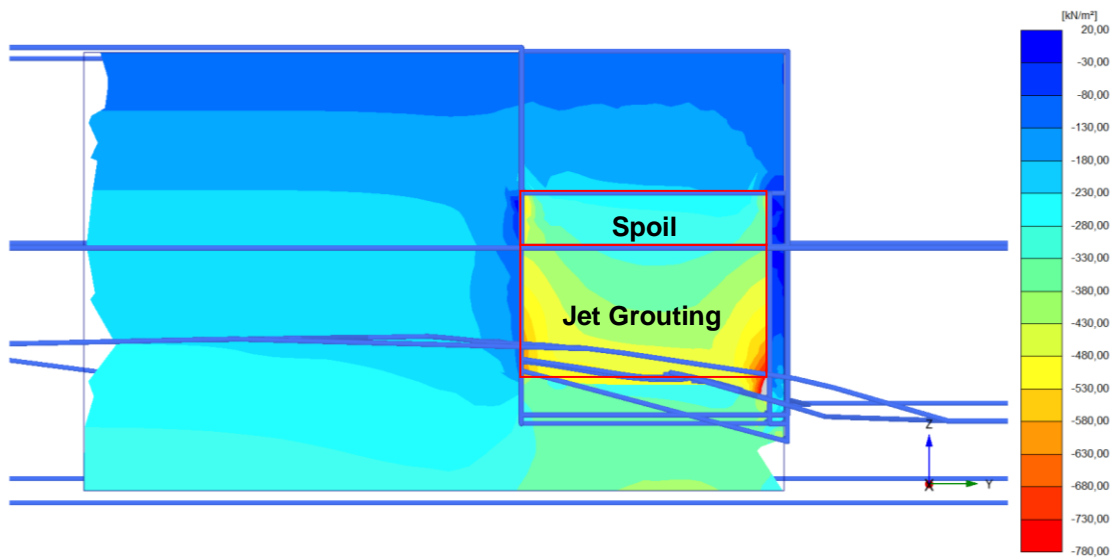


Figure 5.50 - Effective vertical stresses in cross section at x=19 m

#### 5.5.1.2. Transfer of Loads through the Monolith

To verify the loading mechanism inside the monolith it is necessary to verify the direction of principal stresses and the path the loading is taking. In Figure 5.51 are represented the principal directions at a cross section at x=19 m.

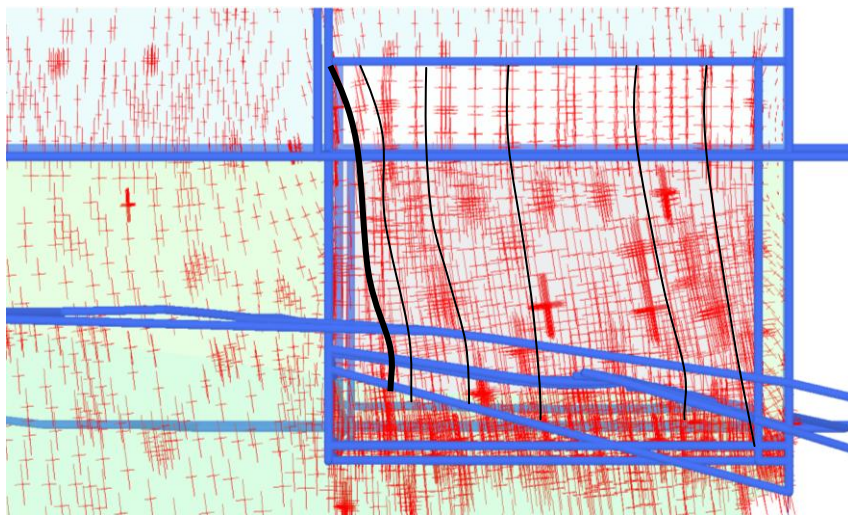


Figure 5.51 - Principal directions in a cross section at x=19 m

It is possible to observe that the loads behind the monolith are effectively transferred to the bottom of the monolith and consequently to the bearing layer.

An interesting detail when studying the monolith behaviour is the deformation mode. In fact, as described in Figure 5.52, the monolith deforms in Y-direction with small translation combined with

rotation around an oblique axis, between X and Z axis. This movement is a combination of earth pressures behind the monolith and the existent slope of the glacial till layer. Consequently, it can result in a push of the wall at lower depth in the areas close to the corner.

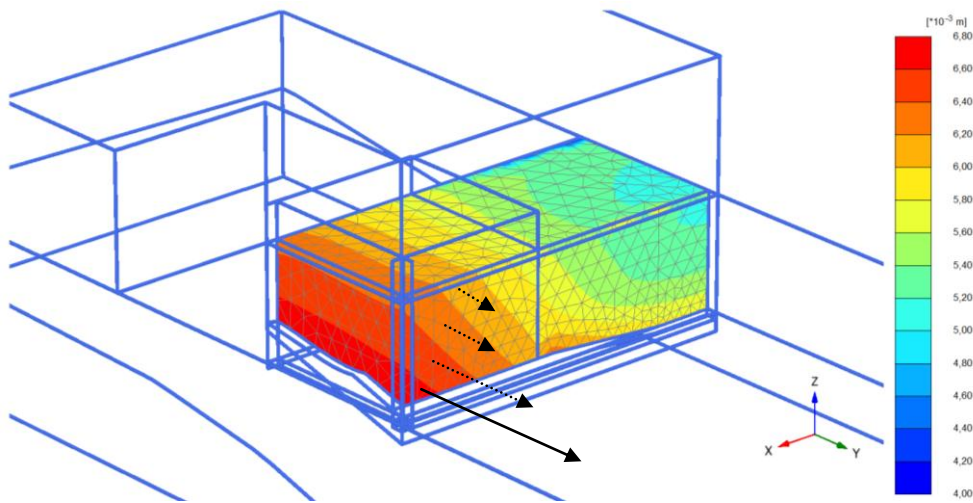


Figure 5.52 - Displacement in Y-direction of monolith composed by Jet grouting and KC Piles

#### 5.5.2. WALL DEFORMATION MODE

In Figure 5.53 is represented the wall displacement relative to total height for all loading phases, at cross section CSB. It is significant the reduction of deformation level in comparison with no reinforcement case, in discontinuous line. The reduction of almost 25% in the deformation level is obviously due to the application of jet grouting and consequent reduction of earth pressures acting on the wall. However, wall tip deformation due to translation is higher for the reinforced scenario, which is understandable as jet grouting transfers more loads to the stratum below.

It is interesting the small increase of deformation observed in the lower part of the wall, around -18 m. This deformation can be a consequence of the monolith displacement observed in Figure 5.52, but also bending due to residual earth pressures generated by the spacing soil layer between the monolith and the wall.

Another relevant aspect is that the wall shape is similar to the equivalent scenario analytically analysed in Chapter 3 for  $K_0$  and  $K_a$  scenarios (Figure 3.14). However, maximum displacement verified using PLAXIS (1.98 cm) is higher than the maximum calculated in  $K_a$  scenario (1.6 cm), but lower than the calculated in  $K_0$ . Therefore, using earth pressures calculated with  $K_0$  coefficient leads to higher (and conservative) deformation levels.

By observation of Figure 5.54 it is possible to get a wider view of wall displacement at depths -0.4m and -9m. The reduction in horizontal deformation is clear for the mutually supported wall as seen before, but for the anchored wall the deformation is in fact higher in comparison with no soil reinforcement scenario.

Also, at -9 m the displacement of the wall is more uniform and the abrupt difference of deformation observe in NR case is much lower. This in fact can be associated with the higher increase of stiffness in the corner provided by the jet grouting in comparison with stiffness provided by the KC Piles.

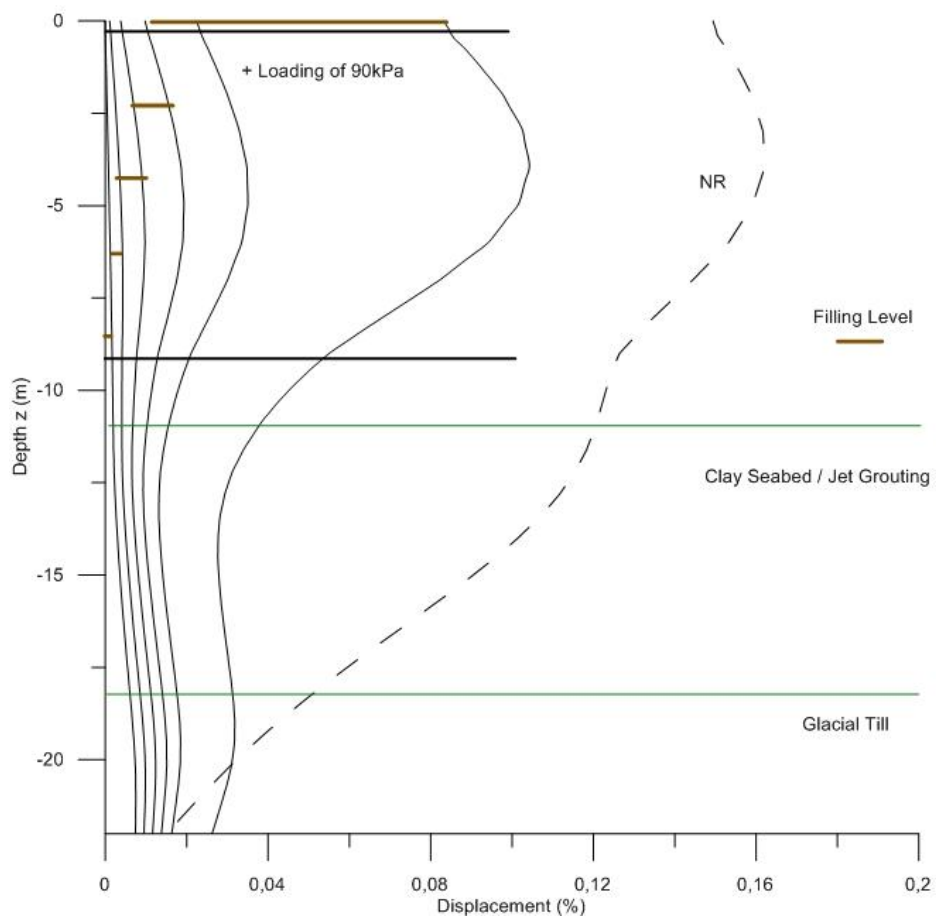


Figure 5.53 - Normalized wall deformation ( $s/H$ ) at CSB along loading phases for KC&JG, in percentage of wall height

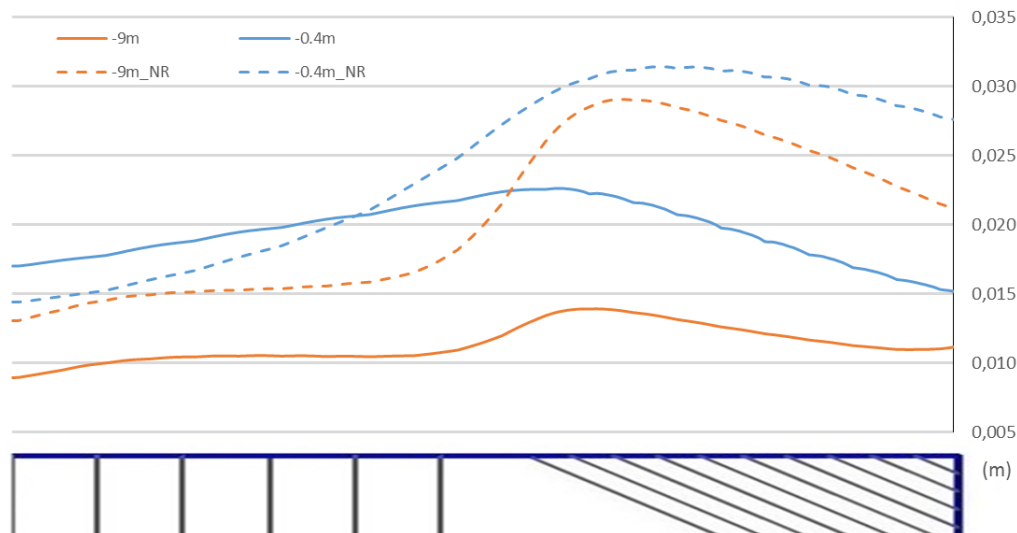


Figure 5.54 - Lateral displacement of wall in Y-direction at depth -0.4 m and -9 m

### 5.5.3. DEFORMATION OF CORNER

Figure 5.55 and Figure 5.56 represent the wall displacement in Y- and Z-direction, respectively. It is clear the rotation around the tip of wall 1, which is lower than the observed in the no reinforcement case. Also it is possible to observe that closer to PSD section the displacements are lower in comparison with the corner, though the differences are not pronounced.

The uplift of wall 2 is observed if extracting the relative vertical displacements from Figure 5.56, which means a lift of approximately 4 mm at the back of wall 2 due to rotation.

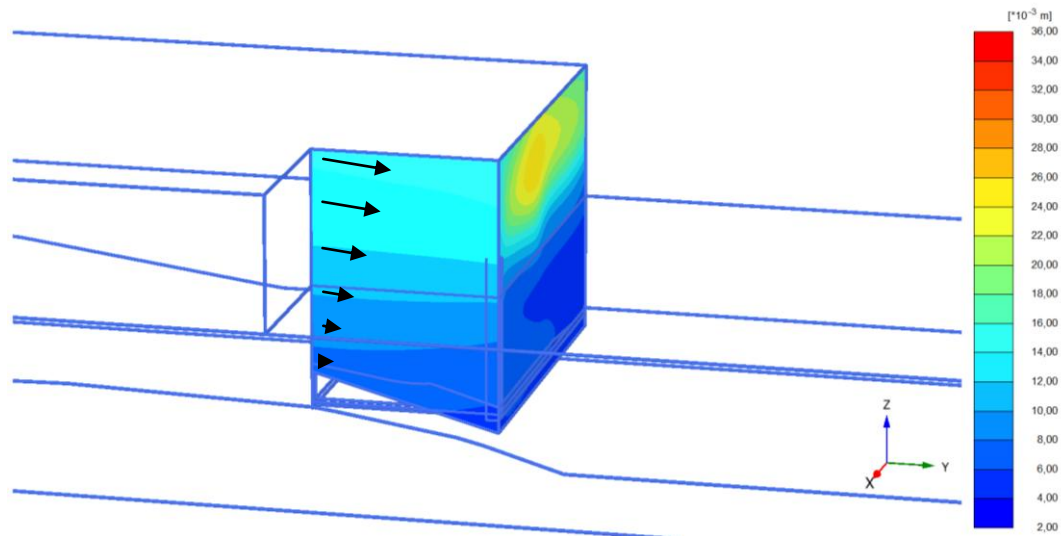


Figure 5.55 - Wall displacement in Y-direction (Horizontal displacement), for KC&JG

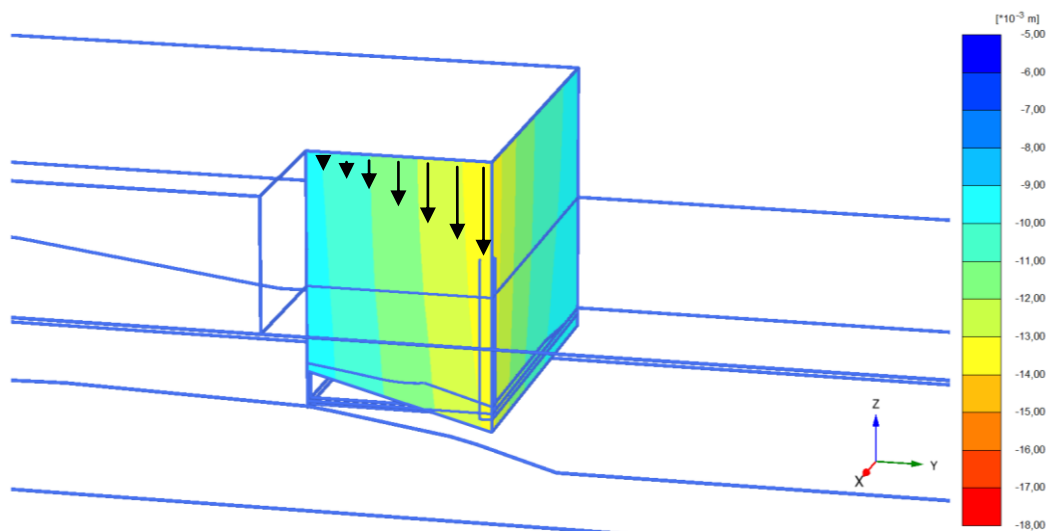


Figure 5.56 - Wall displacement in Z-direction (Vertical displacement), for KC&JG

In Figure 5.57 are displayed the horizontal wall displacement at depth -0.4 m and -9 m. At -0.4 m the wall displacement is mainly in Y-direction and there is a slight opening of the corner, though not significant. At -9 m the opening effect of the corner is significant and wall moves in both Y- and X-direction.

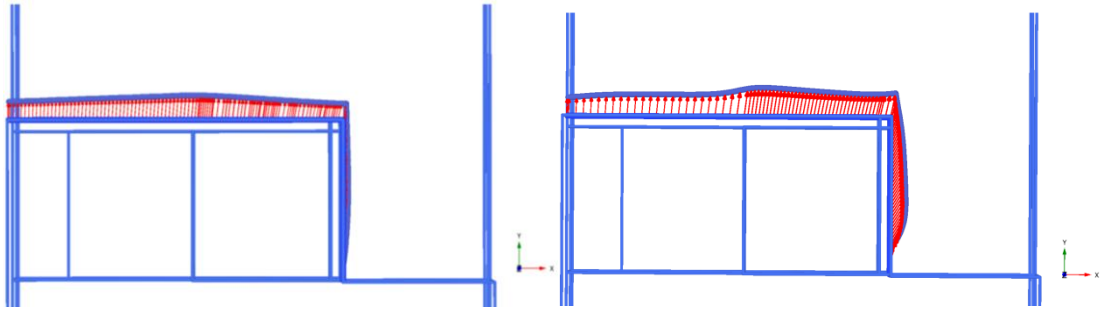


Figure 5.57 - Horizontal wall displacement at depth -0.4 m (left) and -9 m (right), for KC&JG

In Figure 5.58 the wall deformation at CSC shows the less evident of pulling of top of wall 2. Displacement is reduced at lower depths, due to jet grouting monolith. However, maximum displacement, located between upper and lower support levels, is in fact higher than the case with no soil reinforcement, in dashed line.

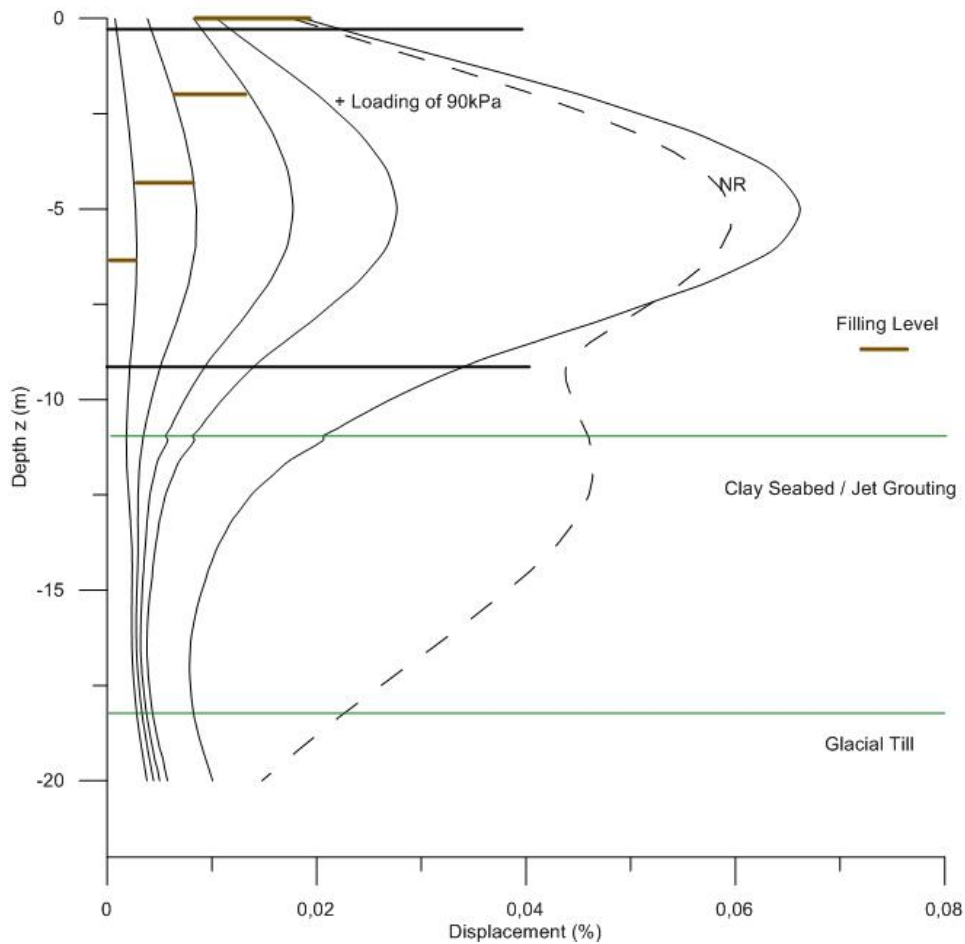


Figure 5.58 - Normalized wall deformation ( $s/H$ ) at CSC along loading phases for KC&JG, in percentage of wall height

## 5.5.4. STRUCTURAL FORCES

### 5.5.4.1 Anchors and Ties

In Figure 5.59 are displayed the axial forces in the anchors and ties. It is possible to observe a general decrease of forces, with a reduction to 430 kN and 280 kN in lower and upper anchors respectively. The anchor/tie forces in lower levels approximate to the forces in upper levels, while these last maintain close to initial case. Again here is verified the fact that the application of soil reinforcement has low influence in structures in the upper part of the wall.

Axial forces in the lower level reduce in all supports, resulting from the reduction of horizontal earth pressures especially in the location of the lower corner ties, that are covered by spoil from jet grouting. However, in the upper level there is an increase in the corner ties. There is a tendency to achieve a more uniform distribution of forces along the supports. This is associated with the fact that the deformation of the wall in the top also has a more uniform shape.

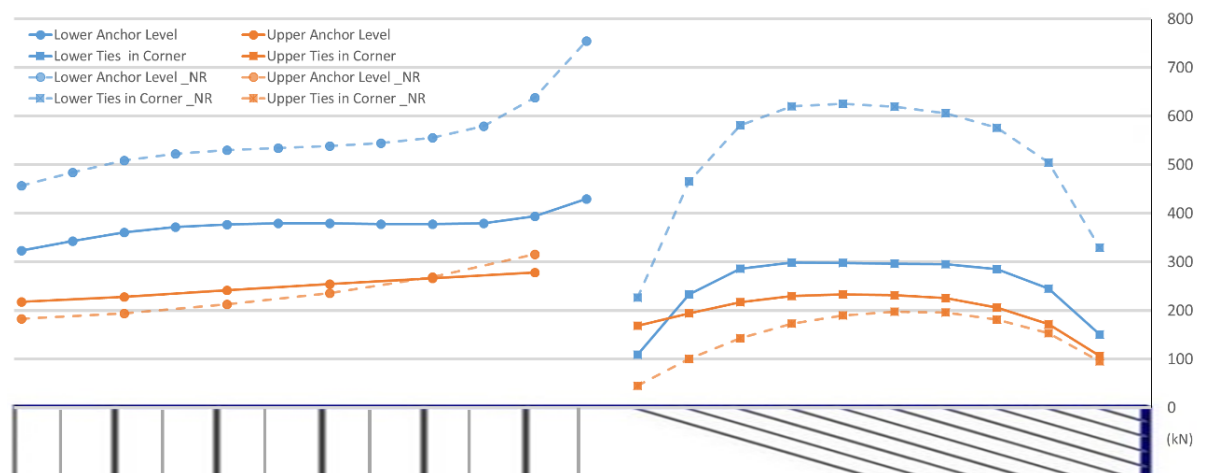


Figure 5.59 - Axial forces in anchors and ties at upper (-0.4 m) and lower (-9 m) levels, for KC&JG (kN)

These results show similar tendency with what was obtained in the analytical analysis, in section 3.5.3, for the  $K_a$  and  $K_0$  case scenario (see Table 3.3). The anchor forces are higher for lower supports and lower in the upper supports. In comparison with  $K_a$ , the case  $K_0$  shows more conservative values of anchors forces for the lower level (491 kN), even though in the upper level anchors forces are slightly lower than what was obtained with 3D analysis (228 kN).

On the other hand, T&P diagrams provide much different results. In fact, the anchors forces are higher in upper level than in the lower level, in opposition to what was observed in this analysis. This means that T&P diagrams may not be applicable for calculation of support forces when performing 2D plane strain analysis of this situation.

The anti-rotation anchor, in the top of wall 2, gives much lower forces of 990 kN. This is below the yielding limit as expected, though it is a still high value for such critical element. It is suggested by the author that an extra anchor, in similarity to the anchored wall, would provide enough safety levels.

#### 5.5.4.2 Waling and Capping Beam

In Figure 5.60 and Figure 5.61 are presented the axial forces in waling and capping beam, respectively. Axial forces in waling reduce up to 50%, to a maximum of 500 kN. However, in the capping beam the reduction is minimal.

As in NR case, represented by a dashed line, there is a tendency of decrease of axial force in the beams close to the connection between wall 1 and wall 2. In the waling, in the anchored part of the wall axial forces distribution tends to a uniform shape.

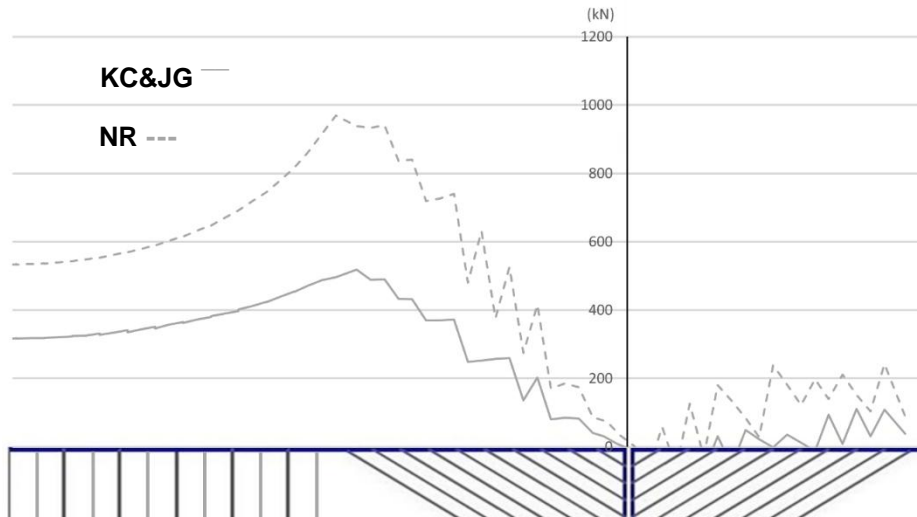


Figure 5.60 - Axial force in waling at -9m, for KC&JG (kN)

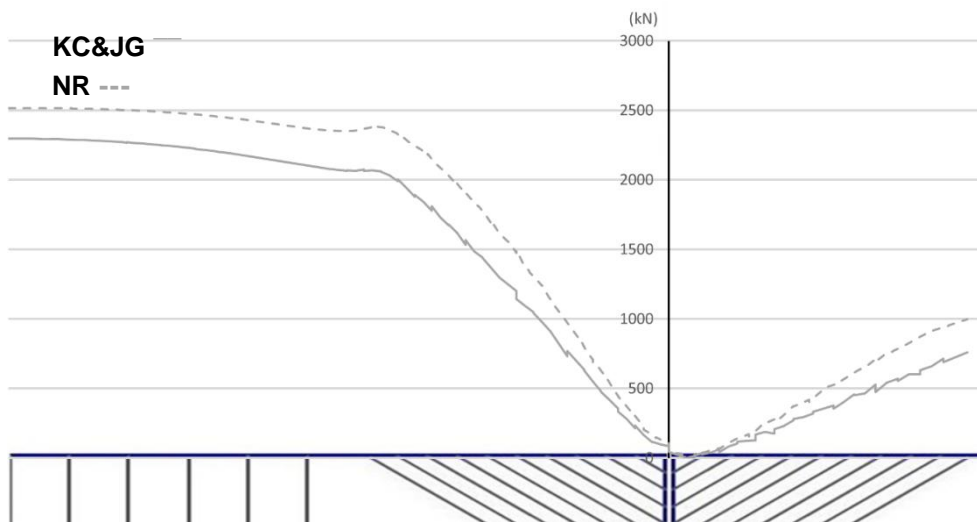


Figure 5.61 - Axial force in capping beam, for KC&JG (kN)

In Figure 5.62, the maximum and minimum bending moments in the waling beam show much variation, comparing with Figure 5.23. Maximum bending moment reduces almost 30% and minimum reduces up to 50%, which are rather relevant values. The distribution shape is similar and extreme values appear in the same sections.

In Figure 5.63 are represented the bending moments in capping beam. The maximum bending moment has insignificant reduction while minimum moment reduces up to 20%. However, the bending moments show a different shape in comparison with NR scenario. In fact, in the anchored part of the wall capping beam is subject to more negative bending moments. Moreover, the shape of positive bending moments close to PSD section shows a triangular form, in opposition to the uniform shape in NR case. The higher bending moment and the triangular shape at this section are expected, as deformation tends to be lower and more uniform, in comparison with the other sections of the wall closer to the corner, where a change of curvature is observed.

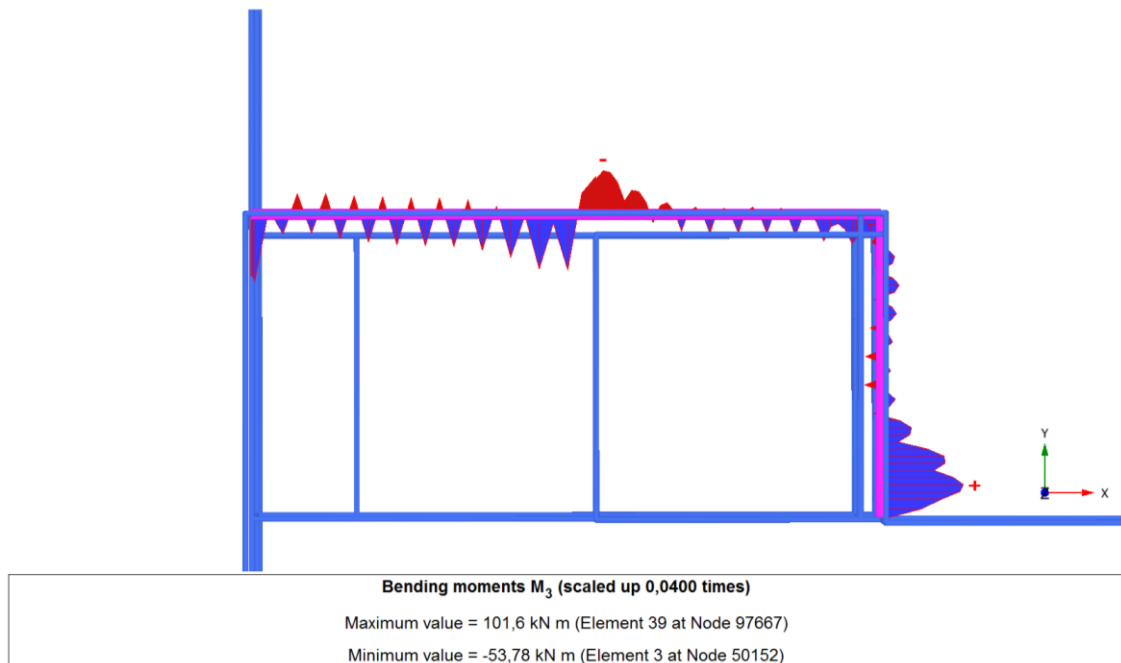


Figure 5.62 - Bending moments in waling beam at -9 m (kN.m)

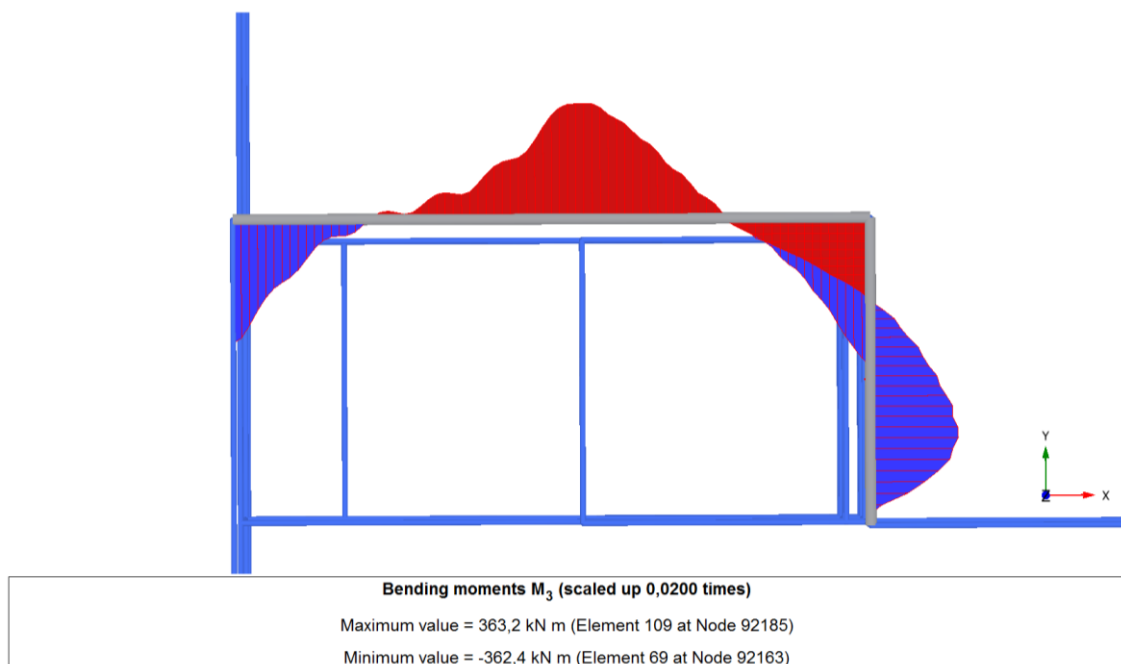


Figure 5.63 - Bending moments in capping beam (kN.m)

### 5.5.4.3 Sheet Pile Wall

Bending moments at CSB and CSC are displayed in Figure 5.64. It is clear the increase of bending moment at both section in the part of the wall above the lower anchor level (-9 m) up to 235 kN.m. However, similar to what happens in KC case, the bending moments have an inversion below the anchor level due to the almost inexistence of earth pressures on the wall.

In Figure 5.65 is represented the vertical axial force in the sheet pile wall at CSB. Again, is clear the reduction of axial force, especially through all the depth of the monolith. Like in the NR case, the axial force is then taken by the glacial till through mobilization of shear force.

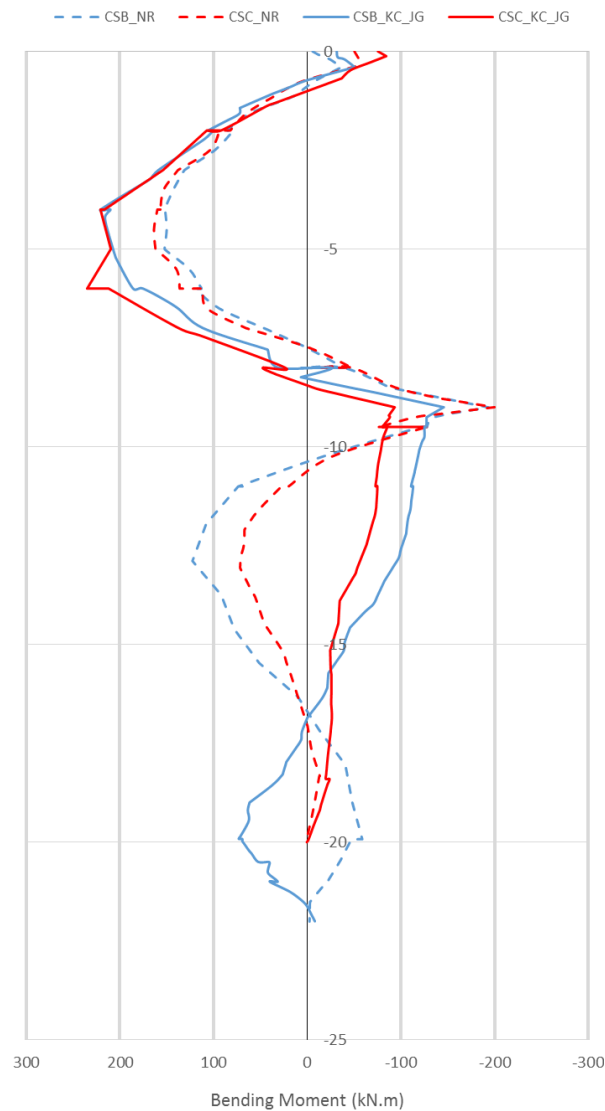


Figure 5.64 - Bending moment diagram at CSB and CSC, for KC&JG (kN.m)

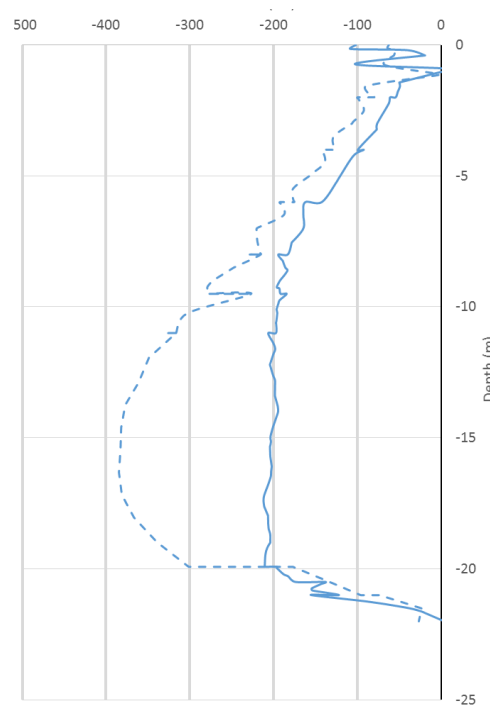


Figure 5.65 - Vertical axial force in sheet pile wall at CSB, for KC&JG (kN)

## 5.6. COMPARISON BETWEEN KC AND KC&JG

In order to evaluate the performance of the two different scenarios of soil improvement KC and KC&JG, a comparison study should be performed. In reality, the soil reinforcement with jet grouting reveals to be more expensive than application of KC Piles. Also, the block of jet grouting created may result in a too conservative solution.

Therefore, it is important to observe and compare the effects of such soil improvement techniques in the earth pressures distribution, wall displacements and variation of forces in structural elements. If such differences are relevant, especially in structural forces, it may result in the possibility of downgrading and consequent saving of costs.

Table 5.2 - Comparative cases KC and KC&JG

Case	Abbreviation	Description
KC Piles Reinforcement	KC	Model with lime-cement piles (KC Piles) reinforcement
KC Piles and Jet Grouting Reinforcement	KC&JG	Model with lime-cement piles reinforcement and jet grouting near the corner

### 5.6.1. COEFFICIENT OF EARTH PRESSURE

The first parameter to observe is the efficiency of the soil reinforcement technique in reducing the lateral earth pressures on the wall. In fact, the main objective of the ground improvement is to absorb the earth pressures and transfer them directly to the bearing till layer. This may be verified by

admitting a coefficient of earth pressures, which relates horizontal earth pressures after application of soil reinforcement with the horizontal earth pressures in the scenario with no reinforcement.

Figure 5.66 shows the coefficient of lateral earth pressures for scenario KC and KC&JG at section CSB. It is interesting to observe that as expected earth pressures are reduced up to 80% for the KC&JG case below depth -8 m, associated with the beginning of the jet grouting spoil. This reduction is constant down to -13 m, when it slowly increases reaching a "gain" of earth pressures, probably due to concentration of stresses in this area, as explained in the previous chapter.

In KC scenario is possible to observe a similar behaviour to KC&JG. However, reduction of earth pressures begins at a lower depth (-11 m), where the reinforced layer is located. At depth -19m earth pressures increase up to a peak "gain", as in KC&JG.

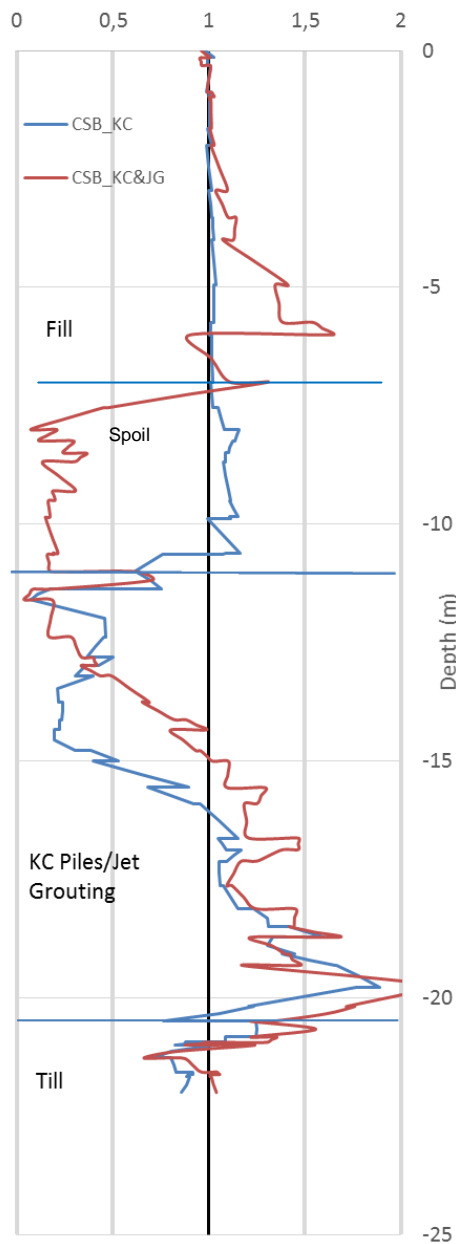


Figure 5.66 - Coefficient of reduction of lateral earth pressures at CSB, for KC and KC&JG

In both scenarios two interesting aspects can be observed:

- Reduction of lateral earth pressures is noticed before the depth of the reinforced soil layer, probably associated with soil arching effects;
- Above the depth of beginning of earth pressure reduction there is a slight gain of earth pressures.

In general, the reinforcement with jet grouting appears to cause a higher reduction of lateral earth pressures. However, the consequences of such effect are better visible in changes in deformation levels and structural forces.

### 5.6.2. WALL DEFORMATION MODE

A result of reduction of earth pressures is variation in wall deformation. In Figure 5.67 are displayed wall shapes at CSB for KC and KC&JG cases. Maximum displacement is, as expected, lower in soil reinforcement with jet grouting. Though, such reduction from KC&JG to KC scenario is up to 12%, which in absolute values corresponds to a reduction of 3 mm. Such variation may not be significant.

Although the wall shape is similar in both cases, it is interesting to note that below depth -15 m, displacements are slightly higher in KC&JG scenario. This is probably associated with higher weight of jet grouting, which combined with the ground slope, has a higher transversal displacement.

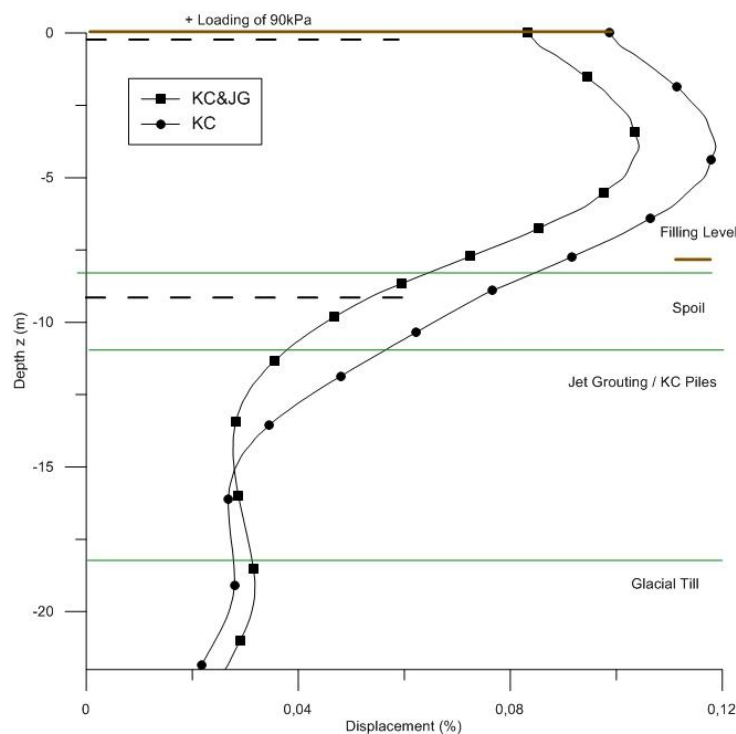


Figure 5.67 - Normalized wall deformation ( $s/H$ ) at CSB in last loading phase for KC and KC&JG, in percentage of wall height

Figure 5.68 shows the lateral displacement of the wall at depths -0.4 m and -9 m. It is clear the lower wall displacement for the KC&JG scenario close to the corner, where in fact the jet grouting reinforcement is applied. However, this reduction is mitigated closer to the PSD section. These results are not surprising as the jet grouting is only applied in the area closer to the corner, while in the zone

where the wall is multi-anchored the soil reinforcement is only executed using KC Piles. Besides, this tendency shows that the application of jet grouting in the corner practically only has local effects, which are not felt in farther areas like at PSD.

The maximum horizontal displacement is observed at both levels to be located where the longer tie is connected, i.e. close to the transition zone from anchored wall to mutually supported wall. This leads to the idea that such area should be stiffer to allow uniform wall displacement, which could be achieved by either enlarging jet grouted area or upgrading the longer anchors.

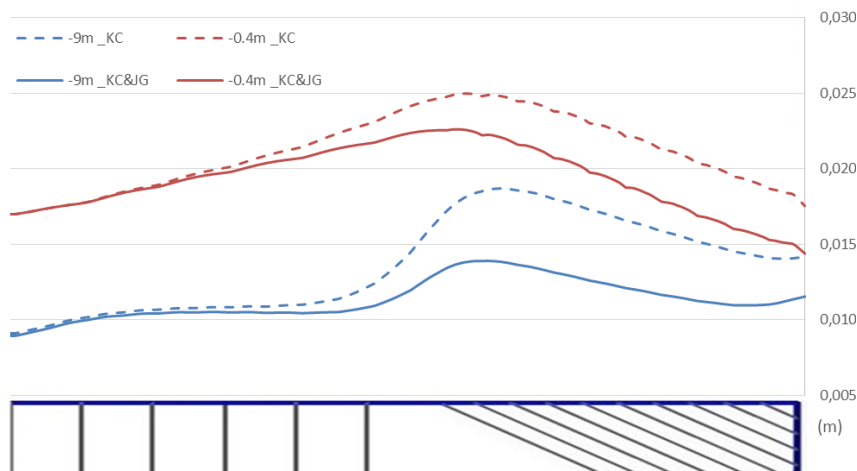


Figure 5.68 - Lateral displacement of wall in Y-direction at depths -0.4 m and -9 m for KC and KC&JG

### 5.6.3. STRUCTURAL FORCES

In Figure 5.69 are presented the axial forces in anchors and ties for both compared scenarios. It is observable a significant reduction of stresses (up to 30%) in lower corner ties. Such effect is caused by the presence of jet grouting spoil at -8 m above the depth of the lower support level, at -9 m. As a benefit, downgrading in the middle ties at lower level could be considered and further studied.

In the other elements, it is possible to observe a small reduction in anchors close to the transition zone from anchored to mutually supported wall. This variation is associated with lower deformations in this area, as observed in Figure 5.68. Closer to PSD section structural forces remain the same in both cases.

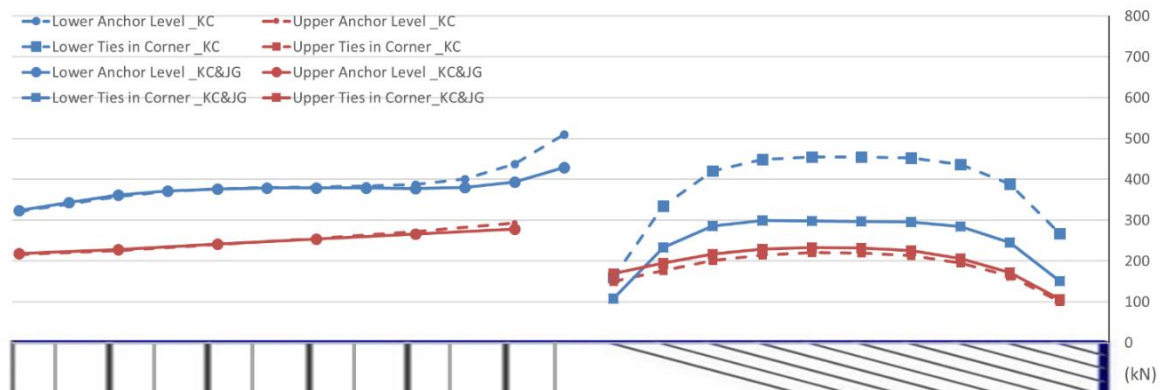


Figure 5.69 - Axial forces in anchors and ties at upper (-0.4 m) and lower (-9 m) levels, for KC and KC&JG

The anti-rotation anchor on top of wall 2 which is a critical element for the stability of the corner has significant variations. For KC anchor force is 1227 kN, while for KC&JG it is reduced to 990 kN. This represents a reduction of almost 20% in the axial stresses, locating the anchor in 75% of yielding stress.

The bending moment in the wall at CSB is presented in Figure 5.70. In general, maximum and minimum bending moment is higher for the scenario KC&JG. This is may be associated with the fact that reducing earth pressures in the back of the wall, increases the effect of generated passive earth pressures in front of the wall. This will lead to higher extreme bending moments. Therefore, this is another effect that traduces the higher reduction of earth pressures for the KC&JG scenario.

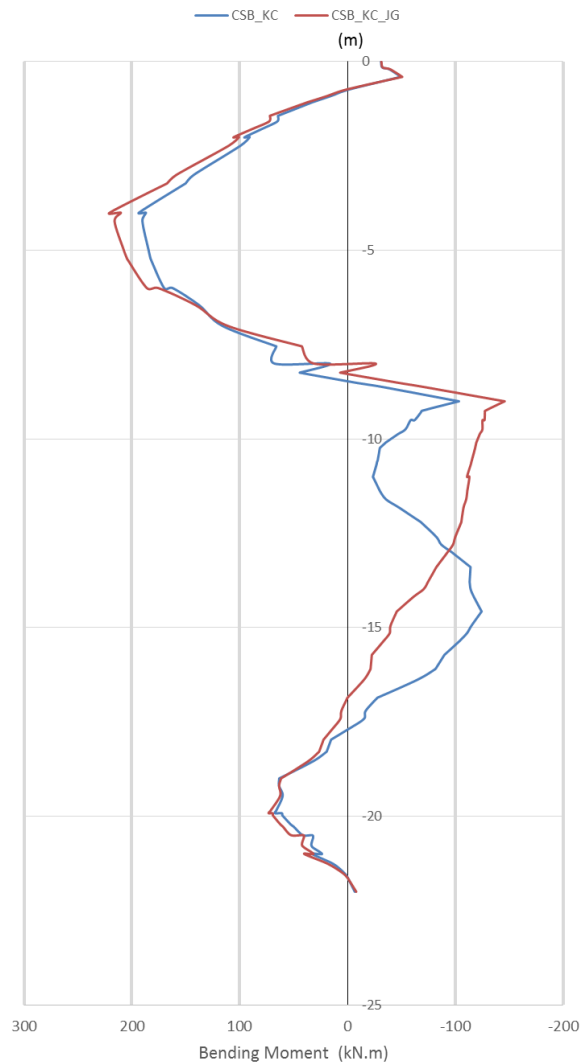


Figure 5.70 - Bending moment diagram at CSB for KC and KC&JG (kN.m)

Globally, it is noticed that the application of jet grouting reduces deformation, although not in a significant amount, and has a relevant reduction of axial stresses in the corner ties at lower level. However, the maximum and minimum bending moments can actually be slightly increased, though not significantly to justify a change of the sheet pile grade.

## 5.7. SURFACE ROUGHNESS BETWEEN SHEET PILE WALL AND SOIL

In the initial analysis performed in this chapter, the friction angle used to model the interface (surface roughness) was  $2/3$  of the soil friction angle. Such value was used as there was not enough information regarding the conditions of the material used in the sheet pile wall and, as suggested by PLAXIS (2013a), the parameter  $R_{inter}$  used was  $2/3$ . However, it is suggested in the design manual 7.02 from the Naval Facilities Engineering Command 1982 (NAVFAC 1982) that in the interface between steel sheet pile and soil, values of friction angle may vary between  $11^\circ$  and  $22^\circ$ . This is mainly dependent of the type of soil in contact with the steel sheet pile, ranging from clay to clean gravel.

So, to understand how the variation of the friction angle (surface roughness) influences the structural forces and wall deformations, it was performed a parametric analysis of the surface roughness between sheet pile wall and fill material (*Sprängsten*) for the KC&JG situation. Following NAVFAC 1982 indications, it was chosen a minimum of  $14^\circ$  and maximum of  $22^\circ$  according to the soil descriptions that could correspond to the real characteristic of the fill material, described in Table 5.3. In terms of  $R_{inter}$ , this means an approximate surface roughness of 0.3 and 0.5 respectively. However, the interface roughness between clay and sheet pile wall and the monolith remained the same, i.e.  $2/3$ .

Table 5.3 - Surface roughness chosen for the sensitivity analysis

Surface Roughness ( $R_{inter}$ )	NAVFAC 1982	Description
$2/3$	N/A	Initial assumption, suggested by PLAXIS (2013a)
0.5	$22^\circ$	Sheet pile against clean gravel, <b>gravel-sand mixture</b> , well-graded rock fill with spalls
0.3	$14^\circ$	Silty sand, <b>gravel</b> , or sand mixed with silt or clay

Observing firstly the wall deformation, in Figure 5.71, there is a remarkable difference for the various values of wall roughness. It can be verified that for lower roughness values the displacement increases at the upper part of the wall up to 40%, which in absolute values represents an increase of 9 mm. However, an inversion of this tendency is verified below -12.5 m.

Regarding effects in structural forces in anchors and ties, changes are not relevant. A small increase of axial forces for lower roughness values can be noticed, more visible in the anchors and less preponderant in the corner ties.

In Figure 5.72 are represented wall bending moments at CSB. Globally, bending moments are not much changed, although the maximum positive bending moment shows a small increase for the situation with lower wall roughness.

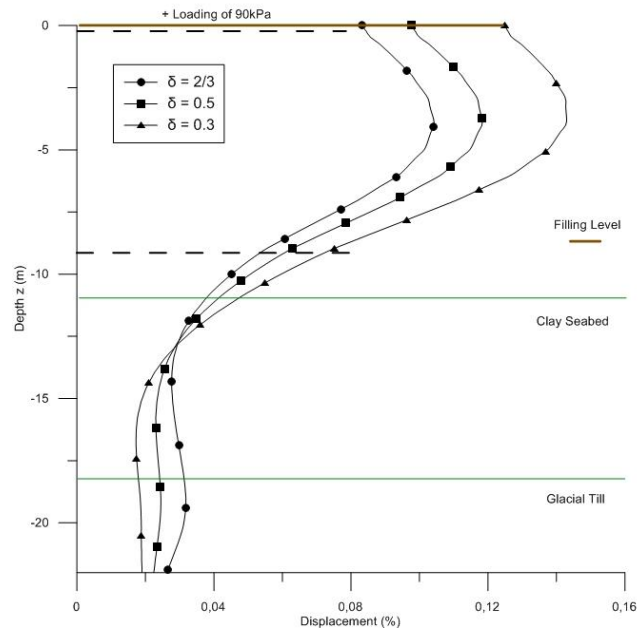


Figure 5.71 - Normalized wall deformation (s/H) at CSB in last loading phase for surface roughness 0.3, 0.5 and 2/3, in percentage of wall height

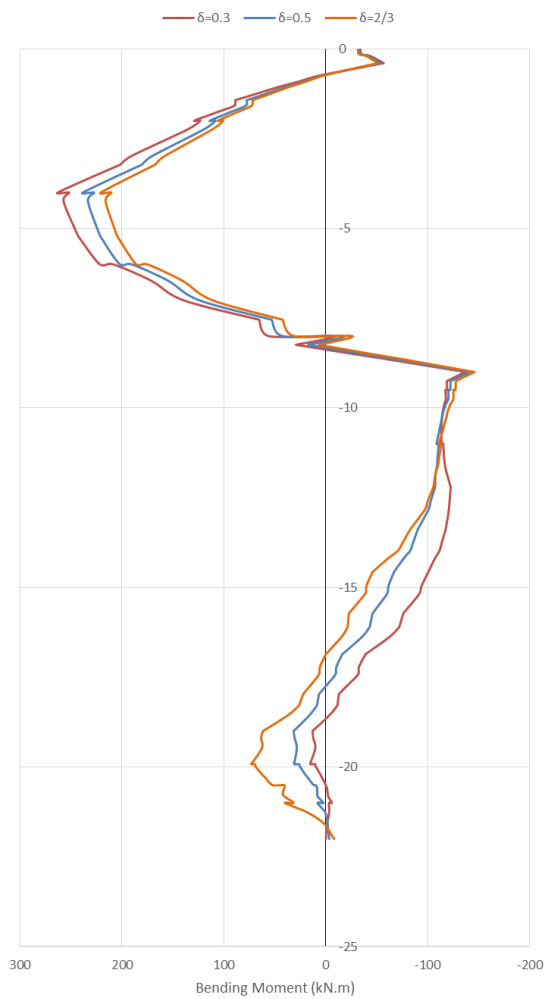


Figure 5.72 - Bending moment at CSB for surface roughness 0.3, 0.5 and 2/3 (kN.m)

Figure 5.73 shows the vertical axial force in the sheet pile wall at CSB. It is possible to verify that at upper levels the vertical axial force for surface roughness 0.5 and 2/3 are very similar, while for 0.3 there is a clear reduction in the axial force supported by the sheet pile. This is expected as a lower roughness level means that less vertical earth pressures are transferred to the sheet pile wall. However, at lower levels, for wall roughness of 0.5 the axial force is lower than for 2/3.

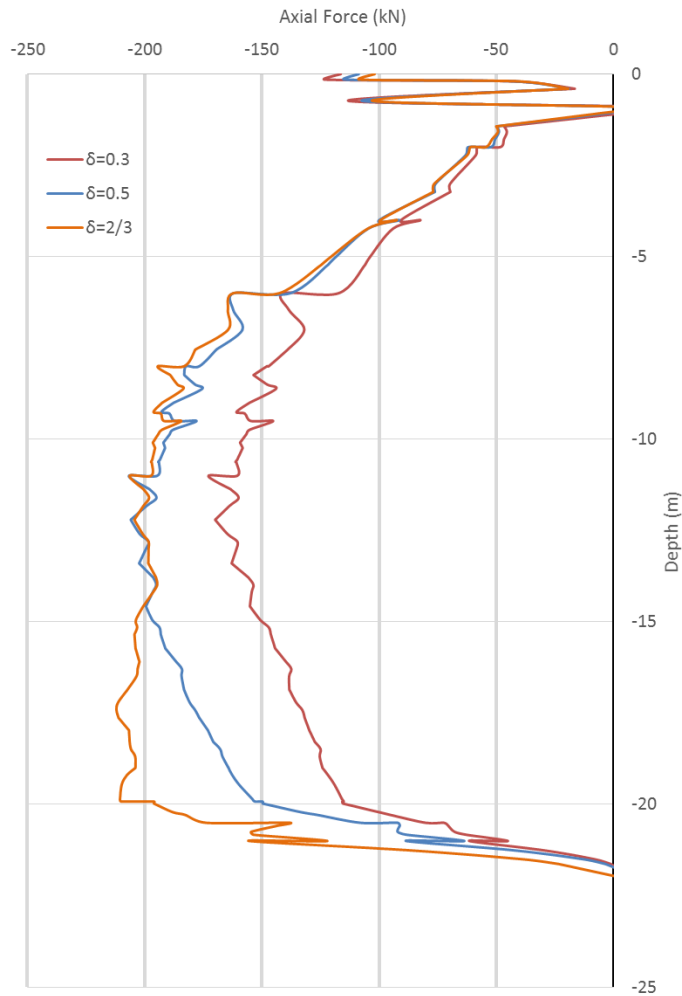


Figure 5.73 - Vertical axial force in sheet pile wall at CSB for surface roughness 0.3, 0.5 and 2/3 (kN)

# 6

## CONCLUSIONS

### 6.1. CONCLUSIONS

In this work it was developed a finite numerical model in PLAXIS 3D of a sheet pile corner, mutually supported by ties in two levels, subjected to backfilling and driven in weak soft clay. Due to the difficult ground conditions observed, soil reinforcement using jet grouting and lime-cement piles was implemented. The model was based on a real case suggested by COWI. However, it was intended that this model could be extended to other similar situations and, therefore, does not fully represent all the details in the real case.

In Chapter 3 an analytical analysis was done to understand which calculation methods would adapt better to represent a 3D problem in a 2D plane strain analysis. So, three cases for calculation of earth pressures using Terzaghi & Peck (T&P) diagrams, at rest earth pressure coefficient  $K_0$  and active earth pressure coefficient  $K_a$  were studied. The structure used was a sheet pile wall supported in two levels, representing the two levels of ties, with a monolith absorbing lateral earth pressures, representative of soil reinforcement.

It was verified that  $K_0$  case generated the highest extreme bending moments, while T&P showed more distributed bending moments, which is associated with arching effects that influence the empirical data from where T&P were developed. The global earth pressure force appeared to be higher in  $K_0$  case, although it was close to the obtained with T&P, 30% higher than  $K_a$ . Regarding deformation, T&P showed more deformation, while  $K_0$  and  $K_a$  showed lower values. The results obtained with this analysis were then used to compare with the 3D Finite Element model.

In Chapter 4 the geometry and execution of the 3D model was explained. The presented situation, a sheet pile corner, composed by two walls mutually supported in two levels of ties, subjected to backfilling and implemented in an area that showed poor soil conditions revealed to be a singular case with few related studies present in literature. It was deduced that a mutually supported wall with asymmetric conditions implies a 3D analysis, to fully understand its deformation mode and stress distribution.

To understand the 3D behaviour and effects on soil-structure interaction, three cases scenarios were planned. The first, with no soil reinforcement, would provide information regarding three dimensional effects and give a good understanding of structure behaviour. The other two, which consisted in application of soil reinforcement with lime-cement piles and after with jet grouting, intended to provide a view of the benefits of soil improvement regarding deformation modes, earth pressure distribution and global stability.

In Chapter 5 were presented the results obtained with the finite element analysis performed using PLAXIS 3D. At first, it could be verified that higher wall deformations closer to the corner, associated with different stiffness along the wall, clarified the fact that a three dimensional analysis was necessary.

The base scenario with no soil reinforcement showed that earth pressure distribution along the wall depth is not the same comparing a section in the corner with a plane strain section. Also, ratio between horizontal and vertical effective earth pressures is closer to  $K_a$  than to  $K_0$ , leading to the conclusion that soil is approaching active equilibrium limit.

Regarding deformation, the expected rotation around the tip of the wall is observed combined with small translation. However, this displacement is not the same during all loading phases, revealing to be during the initial filling levels similar to the theoretically typical movement of excavated multi-strutted walls described by Terzaghi (1941). Also, it is possible to observe that surcharges are responsible for a considerable part of the total wall displacement, up to 70%. Moreover, the wall shape is not constant in all cross sections. Such variation may be associated with the different stiffness resultant from the varying length of the ties and anchors. This effect is especially verified close to the corner. Associated with different levels of deformation and stiffness is the arching effect in the soil unit referred before.

The deformation in wall 2, the smaller wall, shows wall pulling (due to the mutual support) for the initial loading phases and opening of the corner (wall 1 and wall 2) for higher levels of filling. Also, it is possible to observe a translation movement (associated with the opening referred before) with wall bending.

Globally, the rotation mechanism observed in the corner is a combination of some characteristics of the problem:

- The ground slope does not allow the required embedment of wall 2, which is a rather important parameter to the efficient performance of the wall;
- The same ground slope contributes to the sliding (translation) of the wall;
- Reduced support at wall 2, which results in higher displacement of this wall.

The distribution of structural forces is rather interesting and not uniform, with higher loads in lower level than in the upper level. In the corner it was verified that axial force is higher for middle ties and lower for extreme ties, mainly related to shape of deformation of the wall and axial stiffness of rods. The maximum axial forces in anchors and ties were far from the yielding limit, although the anchor responsible for preventing rotation of the wall reached yielding. Therefore, soil reinforcement revealed to be necessary. Moreover, surface roughness was probably responsible for the increase of vertical axial stresses in the sheet pile wall.

The scenarios with soil reinforcement (KC and KC&JG) provide at some depths more than 50% of reduction of earth pressures, value that is more remarkable in jet grouting scenario. However, it has been verified that such reduction is not constant at all depths and at the lower parts there is a "gain" of horizontal earth pressures. This is thought to be mainly associated with concentration of stresses in the lower part of the monolith. Related to this earth pressure reduction is the considerable decrease of wall deformation down to 75% of wall displacement with no soil reinforcement. However, the rotation of the wall system is still remarkable.

Regarding the monolith behaviour, it is observable the transfer of stresses to the bearing stratum (glacial till layer) as it was expected to behave. However, there is a small displacement of the monolith to the wall due the combination of lateral earth pressures on the back of the monolith and ground slope. This movement should be better studied by modelling interfaces in all monolith surfaces.

Structural forces in scenarios with soil reinforcement are globally lower. In anchors and ties, the stresses reduce especially at the lower level and there is a tendency for a more uniform distribution of stresses. In capping and waling beams it is also visible a reduction up to 50% of the axial force in some locations and significant decrease of maximum bending moment.

However, in the sheet pile wall maximum positive bending moments increases for reinforced scenarios, associated with the reduction of earth pressures on the back of the wall at the monolith depth. Besides, vertical axial force tends to reduce with application of ground improvement.

Regarding the comparison study between both scenarios with soil reinforcement KC and KC&JG, it is possible to conclude the following:

- Jet grouting monolith provides a higher reduction of horizontal earth pressures;
- Maximum displacement is lower in KC&JG scenario, though the absolute value is not significant;
- Transversal displacement (i.e. displacement at the wall tip) is higher with jet grouting monolith;
- Jet grouting practically only influences the wall behaviour in the corner;
- Only in the lower ties corner there is a significant decrease of axial forces and anti-rotation anchor's stress is reduced 20% in KC&JG scenario, though is at 75% of yielding stress.

Taking into account the previous conclusions, it is possible to admit that jet grouting provides a better solution in terms of deformation and anchor forces in the corner. However, it would be advisable to apply an extra anchor in wall 2 and have a varying stiffness in the anchor/tie rods to obtain a constant deformation along the wall.

The sensitivity analysis performed to evaluate the influence of the surface roughness between the steel sheet pile wall and the soil was based on the recommendations of NAVFAC 1982. The results suggested the following:

- Lower surface roughness (0.3) is associated it a higher wall displacement, up to 40% more than with firstly admitted surface roughness (2/3);
- Bending moments are globally higher for lower surface roughness, though the difference is not significant;
- Forces in ties and anchors suffer low changes;
- Axial force shows a remarkable change especially when changing wall roughness from 0.5 to 0.3.

Such results reveal that the soil-structure interaction and resulting wall behaviour is particularly sensible to the wall surface roughness. Therefore, this is an important parameter to take into account when doing these types of numerical analysis.

## 6.2. SUGGESTIONS FOR FUTURE RESEARCH

Although this is a practical and very specific situation, there is not enough of literature about sheet pile wall corner behaviour and retaining walls under backfilling conditions. So, further studies on this matter should be done.

Regarding the present work, some improvements are suggested to be done in the model, namely:

- Detail modelling of the sheet pile wall, i.e. model the exact Z shape of the piles;

- Improve modelling of jet grouting and KC Piles, by creating realistic pile groups, instead of a soil unit and application of interfaces to simulate interaction with surrounding soil layers;
- Provide a study on minimum capacity of KC Piles that assures acceptable deformation and safety levels;
- Develop a sensitivity study on anchors' stiffness, to understand influence of this parameter;
- More realistic modelling of the materials.

## BIBLIOGRAPHY

- Aarsleff (2014). Presentation about Värtahamnen
- Arcelor Mittal (2014). Brochure: Extension of existing quay in Cadiz, Spain.
- Bilgin, Ö. (2010). Numerical studies of anchored sheet pile wall behavior constructed in cut and fill conditions. In *Computers and Geotechnics* 37 (3), pp. 399–407.
- Broms, B.B., Boman, P. (1975). *Lime Stabilized Columns –A New Construction Method*, XV<sup>th</sup> World Road Congress, Mexico City, pp. 22-28. Mexico
- Carrubba, P., Colonna, P. (2000). A comparison of numerical methods for multi-tied walls. In *Computers and Geotechnics* 27 (2), pp. 117–140.
- Chu, Ed. (2010). *A Self-Learning Manual. Mastering Different Fields of Civil Engineering Works*.
- COWI (2015). Internal Document.
- Eskandari, L., Kalantari, B. (2011). Basic types of sheet pile walls and their application in the construction industry - a review. In *EJGE*, pp. 1533-1541, EJGE
- Finno, R. J., Blackburn, T., Roboski, J. F. (2007). Three-dimensional effects for supported excavations in clay. In *Journal of Geotechnical and Geoenvironmental Engineering*, 133 (1), pp. 30-36
- Gui, M., Han, K. (2009). An investigation on a failed double-wall cofferdam during construction. In *Engineering Failure Analysis* 16 (1), pp. 421–432.
- Jaky, J. (1944). The coefficient of earth pressure at rest. In *Journal for Society of Hungarian Architects and Engineers*, pp. 355-358.
- Lambe, W. T., Whitman, R. V. (1969). *Soil Mechanics*. Wiley, New York.
- Lee, F., Yong, K., Quan, K., Chee, K. (1998). Effects of corners in strutted excavations: Field monitoring and case histories. In *Journal of Geotechnical and Geoenvironmental Engineering* 124 (15145), pp. 339-349.
- Matos Fernandes, M. (1990). *Estruturas de Suporte de Terras*. Porto, FEUP.
- Michalowski, R. L. (2005). Coefficient of Earth Pressure at Rest. In *Journal of Geotechnical and Geoenvironmental Engineering*. 131 (11), pp. 1429–1433.
- Moseley, M. P., Kirsch, K. (2004). *Ground improvement*. 2nd ed. London, Spon Press, New York.
- Naval Facilities Engineering Command (1982). *Foundations and Earth Structures - Design Manual 7.02*. U.S. Army Corps of Engineers, Virginia.
- Osório, P., Odenbreit, C., Vrouenwenvelder, T. (2010). *Structural Reliability Analysis of Quay Walls with Steel Sheet Piles*. Presented at PIANC MMX Congress, 2010, Liverpool.
- Ou, C., Chiou, D., Wu, T. (1996). Three-Dimensional Finite Element Analysis of Deep Excavations. In *J. Geotech. Engrg.* 122 (5), pp. 337–345.
- Ou, C., Teng, F., Wang, I. (2008). Analysis and design of partial ground improvement in deep excavations. In *Computers and Geotechnics* 35 (4), pp. 576–584.
- Pipatpongsa, T., Heng, S. (2010). Granular Arch Shapes in Storage Silo Determined by Quasi-static Analysis under Uniform Vertical Pressure. In *JMMP* 4 (8), pp. 1237–1248.

PLAXIS (2013a). PLAXIS 3D Reference Manual 2013

PLAXIS (2013b). PLAXIS 3D Material Models Manual 2013

Rowe, P. W. (1952). *Anchored sheet-pile walls*. ICE Proceedings, pp. 27–70.

ThyssenKrupp (2010). *Sheet Piling Handbook 3rd Edition*. ThyssenKrupp, Hamburg.

Stadsledningskontoret (2013). *Stockholm Facts & Figures*

Strahler, A. N., Strahler, A. H. (1973). *Environmental geoscience: interaction between natural systems and man*. Hamilton Pub. Co, Santa Barbara.

Vieira, C. S., Matos Fernandes, M. (2000). *Cortinas com um apoio estrutural na parte superior: Dimensionamento pelos métodos tradicionais e pelo eurocódigo 7*. VII Congresso Nacional de Geotecnia, 10-13 April 2000, Porto, pp. 1247-1256, SPG, Porto.

Widisinghe, S., Sivakugan, N. (2012). *Vertical Stresses within Granular Materials in Silos*. ANZ Conference Proceedings, 2012, Melbourne, pp. 590-595, ANZ, Melbourne.

ArchiExpo (<http://www.archiexpo.com>) - access date 23rd April

C.J. Mahan (<http://www.cjmahan.com>) - access date: 23rd April

Soletanche Bachy (<http://www.soletanche-bachy.com>) - access date 23rd April

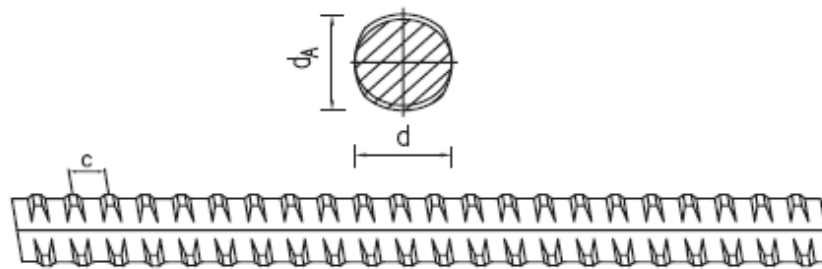
Stockholm Royal Seaport (<http://www.stockholmroyalseaport.com/en/>) - access date: 23rd April

## APPENDIX

## COMMERCIAL BROCHURE

SAS 670/800 Ø 18 - 75 mm

Adapted from Stahlwerk Annahütte



**SAS Gewindestab**  
warmgewalzt, Rippenstahl - rechtsgängig

**SAS thread bar**  
hot rolled, ribbed - right hand thread

d	[mm]	18	22	25	28	30	35	43	50	57,5	63,5	75
max d <sub>A</sub>	[mm]	21	25	28	32	34	40	48	55	63	70	82
c	[mm]	8	8	10	11	11	14	17	18	20	21	24
$f_{yk} (f_{0,2k}) / f_{tk} / A_{10}^{11}$		670 N/mm <sup>2</sup> / 800 N/mm <sup>2</sup> / ≥ 5 %										
F <sub>yk</sub> (F <sub>0,2k</sub> )	[kN]	170	255	329	413	474	645	973	1315	1740	2122	2960
F <sub>tk</sub>	[kN]	204	304	393	493	565	770	1162	1570	2077	2534	3535
A	[mm <sup>2</sup> ]	254	380	491	616	707	962	1452	1963	2597	3167	4418
G	[kg/m]	2,00	2,98	3,85	4,83	5,55	7,55	11,40	15,40	20,38	24,86	34,68

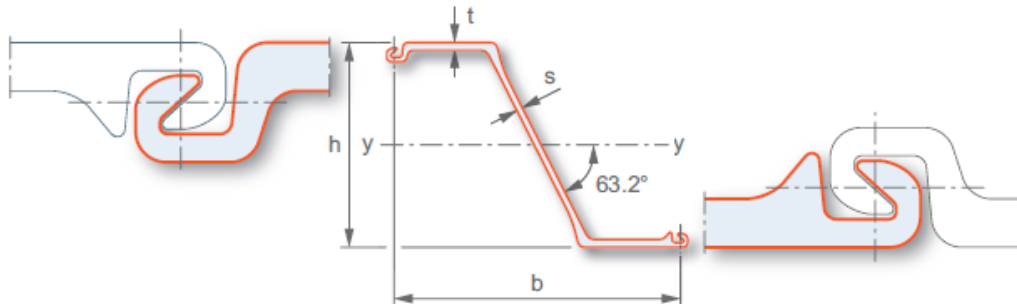
<sup>11</sup> Prozentuale Gesamtdehnung bei Höchstlast / *percentage total elongation at maximum force*

Die Gewichtsangaben sind Mittelwerte. Die tatsächlichen Gewichte können auf Grund von Fertigungstoleranzen abweichen.  
*Weight specifications are average values. The actual values may deviate due to fabrication tolerances.*

COMMERCIAL BROCHURE

AZ 46-700n

Adapted from Arcelor Mittal



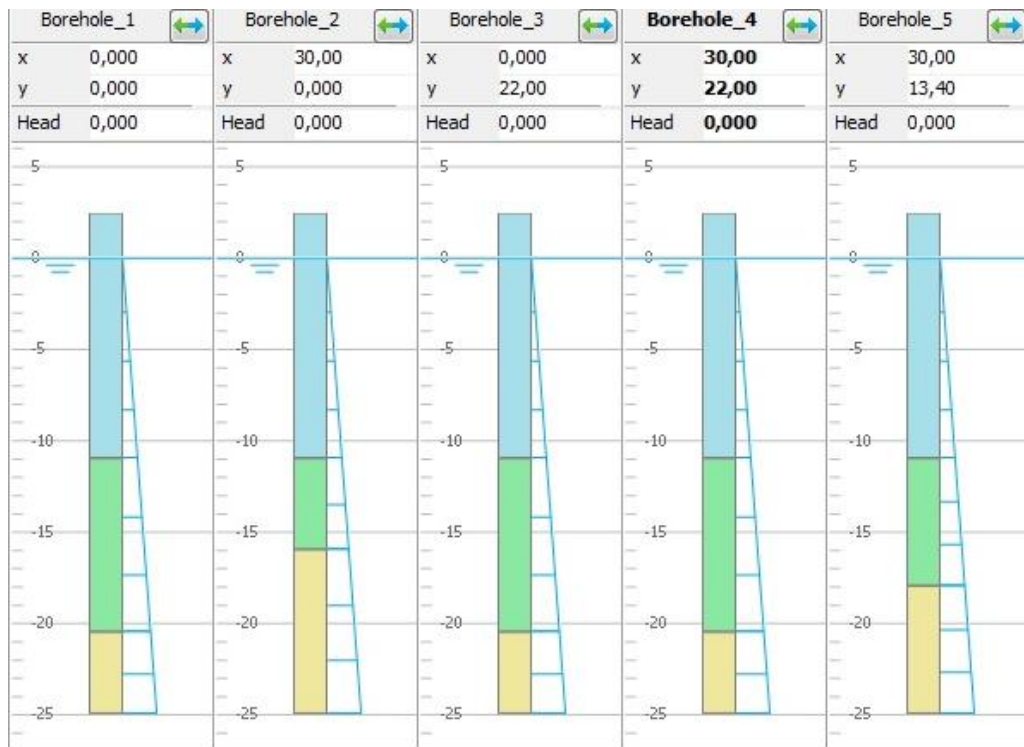
Section	Width		Height		Thickness		Sectional area	Mass		Moment of inertia	Elastic section modulus	Static moment	Plastic section modulus	Class *					
	b	h	t	s	single pile	wall		cm <sup>4</sup> /m	cm <sup>3</sup> /m					S 240 GP	S 270 GP	S 320 GP	S 355 GP	S 390 GP	S 430 GP
AZ 42-700N	700	499	18.0	14.0	259	142.1	203	104 930	4 205	2 425	4 855	2	2	2	2	2	2		
AZ 44-700N	700	500	19.0	15.0	273	149.9	214	110 150	4 405	2 550	5 105	2	2	2	2	2	2		
AZ 46-700N	700	501	20.0	16.0	287	157.7	225	115 370	4 605	2 675	5 350	2	2	2	2	2	2		

\* Classification according to EN 1993-5. Class 1 is obtained by verification of the rotation capacity for a class-2 cross-section. Steel grades S 460 AP and AMLoCor based on mill specifications, as well as ASTM A 690 are available on request.

Section properties								
Section	Diagram	S = Single pile D = Double pile	Sectional area	Mass	Moment of inertia	Elastic section modulus	Radius of gyration	Coating area *
AZ 42-700N		Per S	181.1	142.1	73 450	2 945	20.14	1.03
		Per D	362.1	284.3	146 900	5 890	20.14	2.06
		Per m of wall	258.7	203.1	104 930	4 205	20.14	1.47
AZ 44-700N		Per S	191.0	149.9	77 100	3 085	20.09	1.03
		Per D	382.0	299.8	154 210	6 170	20.09	2.06
		Per m of wall	272.8	214.2	110 150	4 405	20.09	1.47
AZ 46-700N		Per S	200.9	157.7	80 760	3 220	20.05	1.03
		Per D	401.8	315.4	161 520	6 450	20.05	2.06
		Per m of wall	287.0	225.3	115 370	4 605	20.05	1.47

\* One side, excluding inside of interlocks

LOCATION OF BOREHOLES



Layers	Borehole_1		Borehole_2		Borehole_3		Borehole_4		Borehole_5	
	Top	Bottom								
Fill	2,400	-11,00	2,400	-11,00	2,400	-11,00	2,400	-11,00	2,400	-11,00
Seabed/Soft Clay	-11,00	-20,50	-11,00	-16,00	-11,00	-20,50	-11,00	-20,50	-11,00	-18,00
Glacial Till	-20,50	-25,00	-16,00	-25,00	-20,50	-25,00	-20,50	-25,00	-18,00	-25,00

CALCULATIONS OF EARTH PRESSURES IN ANALYTICAL ANALYSIS

Water in front of wall	Water behind wall	Strata	Depth [m]	Soil pressure	Surcharges	Water	T&P		K0		Ka	
							Pressure [KPa]	Pressure [KPa]	Soil Pressure	Pressure [KPa]	Soil Pressure	Pressure [KPa]
		Top Fill	2,4	56,18	5,58	0,00	61,76	0,00	7,32	0,00	4,29	4,29
		1	1	56,18	5,58	0,00	61,76	9,02	7,32	5,28	4,29	9,57
		Compact Fill	1	50,35	5,58	0,00	55,93	9,02	7,32	5,28	4,29	9,57
		-0,36	-0,36	50,35	5,58	0,00	55,93	17,39	7,32	10,18	4,29	14,47
		-0,4	-0,4	34,85	7,73	0,00	42,58	22,81	9,61	14,12	5,95	20,07
		-0,86	-0,86	34,85	7,73	0,39	42,97	22,99	9,61	14,23	5,95	20,57
		Uncompact Fill	-8	34,85	7,73	4,91	47,48	24,96	9,61	15,45	5,95	26,30
		-9	-9	34,85	7,73	4,91	47,48	55,67	9,61	34,46	5,95	45,31
		-11	-11	34,85	7,73	4,91	47,48	59,97	9,61	37,12	5,95	47,97
		JG Spoil	-11	0,00	0,00	4,91	4,91	68,57	9,61	42,44	5,95	53,30
		-11	-11	0,00	0,00	4,91	4,91	0,00	0,00	0,00	0,00	4,91
		JG	-11	0,00	0,00	4,91	4,91	0,00	0,00	0,00	0,00	4,91
		-20,5	-20,5	0,00	0,00	4,91	4,91	0,00	0,00	0,00	0,00	4,91
		Till	-22	0,00	0,00	4,91	4,91	0,00	0,00	0,00	0,00	4,91
		Rock	-25	0,00	0,00	4,91	4,91	0,00	0,00	0,00	0,00	4,91

## PARAMETERS USED IN ANALYTICAL ANALYSIS

		Unit Weight [kN/m <sup>3</sup> ]	Friction Angle [°]	K0	Ka
<b>Earth Pressure</b>	Uncompacted Fill	21	38	0,38	0,24
	Compacted Fill	21	45	0,29	0,17
	Top Fill (above deck)	22	45	0,29	0,17
	Till	21	40	0,36	0,22

		Load [kN/m <sup>2</sup> ]	Unit Weight [kN/m <sup>3</sup> ]
<b>Surcharges</b>	Water difference	4,905	9,81
	Traffic Load	25	